CONTACT OF CLOSELY CONFORMAL SPHERICAL BODIES

BY

GEORGE IOANNOU

B.Sc.(Eng.) and B.Com.(Econ.),M.Sc., DIC.

A THESIS SUBMITTED FOR THE DEGREE OF

DOCTOR OF PHILOSOPHY

OF THE

UNIVERSITY OF LONDON

JANUARY 1984

DEPARTMENT OF MECHANICAL ENGINEERING

IMPERIAL COLLEGE OF SCIENCE AND TECHNOLOGY

UNIVERSITY OF LONDON

To my parents,
for making it all possible!

A B S T R A C T

The dry and lubricated contact problem of closely conformal spherical bodies is studied theoretically.

The models used in both cases, are the contact between an elastic sphere and either a sperical cavity in an infinite elastic medium, or a spherical elastic layer on a rigid substrate.

In modelling the lubricant, both pressure and shear-rate dependent viscosities are considered.

In the dry case, it is shown that the results depend on the degree of conformity between the two bodies, and also that Hertz's theory becomes inaccurate when the contact is larger than 30°. Further, when the available contact arc is insufficient, pressure singularities occur at the circular edge.

In the lubricated case, it is shown that for a given approach velocity of distant points on the two bodies, the rate of change of elastic deformations of the surfaces, plays a major role in determining film thicknesses. In addition, it is shown that for a pressure dependent viscosity lubricant, an entrapment starts to form, the magnitude and shape of which depend on approach velocity, lubricant viscosity, pressure viscosity coefficient, elastic properties and geometry.

ACKNOWLEDGEMENTS

The author wishes to express his sincere thanks to his supervisor, Dr Ramsey Gohar, for his invaluable guidance and assistance throughout the research period.

CONTENTS

LIST OF FIGURES

NOMENCLATURE

A	:	Matrix of size N×N, defined by equation (2.3.3).
A_n^S, A_n^L	:	Summation terms n - index s - refers to the sphere L - refers to the layer.
B	:	Matrix of size N×N, defined by equation (2.3.12).
B(N,i)	:	The ith element of the Nth row of matrix B.
B_n^S, B_n^L	:	Summation terms n - index s - refers to the sphere L - refers to the layer.
b	:	Vector of size N, defined by equation (2.3.4).
b(i)	:	The ith element of vector **b**.
c	:	Clearance (R_C-R_S).
E	:	Young's Modulus.
E_n^C, E_n^L	:	Summation terms n - index c - refers to the cavity L - refers to the layer.

e : Eccentricity.

F_n^c, F_n^L : Summation terms
n - index
c - refers to the cavity
L - refers to the layer.

F_θ : Total lubricant volumetric flow rate, at any section defined by angle θ.

$F_{\theta B}$: F_θ at the time boundary (t=0).

$F(\theta,\Phi)$: A function of θ and Φ.

G : Shear Modulus [$G = E/2(1+\nu)$].

H_n^s, H_n^c, H_n^L: Summation terms
n - index
s - refers to the sphere
c - refers to the cavity
L - refers to the layer.

H : Layer thickness ($R_o - R_i$).

h : Film thickness.

I : The unit matrix.

i,j,k : Indeces.

L : Elemental volume of lubricant in the gap.

M, M_s, M_c : Influence coefficient matrices
s - refers to the sphere
c - refers to the seat.

M_s^*, M_c^* : Same as M_s and M_c, but with the order of the elements of the rows and columns reversed.

N : Number of nodal points employed.

n : Index.

O_s, O_c : The centre of the sphere and seat respectively.

$P_n(\mu)$: Legendre polynomial of order n.

$\mathbf{p}$, $\mathbf{p}_s$, $\mathbf{p}_c$: Vector of pressure magnitudes at the nodal points.
s - refers to the sphere
c - refers to the seat.

p_j : The pressure at nodal point j.

$p_{j,new}$: The jth element of $\mathbf{p}$
old - refers to the previous iteration
$p_{j,old}$ new - refers to the present iteration.

Q : Radial load on the sphere.

q : Pressure distribution on elemental band.

q_ϵ : Constant pressure acting on the sphere.
By integrating it over its area of application, it gives Q.

R : Arbitrary radius.

R_o : The sphere or the layer outer radius.

R_i : The cavity or the layer inner radius.

R_s : The sphere undeformed radius.

R_c : The seat undeformed radius.

r : Radial coordinate.

r_s, r_c : Deformed radii of curvature of the sphere and seat surfaces respectively, measured from their respective centres.

r_1, r_2 : Deformed radii of curvature of the sphere and seat surfaces respectively, measured from the centre of the seat.

S_s, S_c : The sphere and seat surfaces respectively.

seat : Refers to either a cavity or a layer.

T_n^s, T_n^c : Summation terms
n - index
s - refers to the sphere
c - refers to the cavity.

T_1, T_2 : Time instants.

t : Time.

U_r^s, U_r^c, U_r^L: U_θ^s, U_θ^c, U_θ^L Surface displacements. Considered positive when in the coresponding positive coordinate direction.
r - denotes radial displacement
θ - denotes tangential displacement
s - refers to the sphere
c - refers to the cavity
L - refers to the layer.

$U_r(\theta_i)$: Radial displacement at node i, defined by angle θ_i.

$\mathbf{U}$: Vector of radial displacements at the nodal points.

U_s, U_c : Radial displacements of the sphere and seat surfaces respectively.

U_{so}, U_{co} : As above, but for the contact pole.

U : Total elastic deformation (U_c-U_s).

$\hat{\mathbf{U}}$: Vector of total elastic deformations at the nodal points.

V : Sphere centre velocity.

Vol : Gap volume between π and θ, see equation (3.2A.25).

v_θ : Lubricant flow velocity in the θ-direction.

W_c : Tangential displacement of the seat surface, in the θ-direction.

y : Substitute coordinate for the film thickness, see equation (3.2A.7).

α : Pressure-viscosity coefficient.

α_n, β_n, γ_n, δ_n, ε_n, ζ_n : Summation terms.

$\dot{\gamma}$: Shear strain rate.

$\dot{\gamma}_{av}$: Shear strain rate averaged across the film.

Δt : Time interval.

δ : Approach.

η : Lubricant viscosity.

η_o : Viscosity at atmospheric pressure and ambient temperature.

η_{av} : Viscosity averaged across the film.

$\eta_{j,new}$: The jth element of the viscosity vector.
$\eta_{j,old}$ old - refers to the previous iteration
new - refers to the present iteration.

θ_c : The angular extent of the contact zone.

θ_ε : The angular extent of application of q_ε.

θ, Φ : The angular coordinates.

μ : $\cos\theta$.

ν : Poisson's Ratio.

ρ : Rounoff error.

σ_r : Direct radial stress on the surface.

$\sigma(\theta)$: Radial loading on the surface.

σ_n : The nth coefficient in the series used to express the radial loading.

$\tau_{r\theta}$: Shear stress on the surface.

$\tau(\theta)$: Tangential loading on the surface.

τ_n : The nth coefficient in the series used to express the tangential loading.

ω : The exponent in the lubricant constitutive equation in the case of shear-rate dependent viscosity. When possitive the lubricant is said to be Dilatant and when negative Pseudoplastic.

Chapter 1

CHAPTER 1

THE ELASTIC EQUATIONS FOR SPHERICAL SURFACES

1.1 Introduction

Elastic contact between closely conformal spherical surfaces is frequently met in engineering structures, as well as in nature. Such contacts, however, have been given relatively little attention in the literature, and it is usually assumed that a good enough approximation of elastic behaviour is obtained by using Hertz's theory. The theoretical study reported in this thesis, was prompted by the need to test the validity of this assumption, and to investigate the dry and squeeze film lubricated behaviour of such contacts.

In general, a contact problem can be seen as presenting two distinct areas of interest; the elastic behaviour of the bodies in question, and their interaction within the contact region. However, without the use of any simplifying assumptions, it can not be treated and solved as two separate problems.

It is therefore necessary, that the equations resulting from the models describing the elastic behaviour and the contact region interaction, be in such a form as to permit their simultaneous solution.

Accordingly, taking into account the description of

the contact interactions presented in the following chapters, the requirement for the equations describing the elastic behaviour of the bodies is to give the radial displacement at a point on their surface, inside or outside the contact region, when the applied pressure is specified at a number of discrete points inside that region. Displacements outside the contact region are not essential for the solution, but are required only to complete the picture of the distorted body shapes.

Towards satisfying these requirements, Finite Elements and Boundary Integral methods were first considered. These were however, rejected for two main reasons. Firstly, the discretisation methods involved would create a large amount of information redundant to the solution of the problem in question, resulting in a possibly unnecessary waste of resources. Secondly, even if such waste were deemed acceptable in order to obtain a solution, the number of equations that would be required to model the complete problem to the required accuracy, would probably result in a system solvable by none but the most powerful of presently available computers.

A very ingenious analytical solution, by C. Weber [43b] of a single force acting normally upon the surface of a sphere, was also considered. At first sight, this appeared to satisfy the requirements of the solution, for at least the case of a sphere. However, this was also rejected, as after the calculation errors discovered in its development were rectified, it was found impossible to transform the

results into spherical polar coordinates, and thus isolate the required radial displacements.

Finally, it was decided that the general solution to the elasticity problem for bodies of revolution, presented by A.I. LUR'E [23], would be used as it permits particular solutions for a sphere, a spherical cavity and a spherical layer to be obtained in a directly usable form.

This chapter presents this general solution, and proceeds to develop the particular solutions for the three types of spherical body, and cast them into influence coefficient matrix form, as such to be used in the following chapters for the solution of the dry and squeeze film contact problems.

1.2 General Solutions

The models used in this study are based on the solution of the equilibrium equations of the theory of elasticity, for axisymmetrically loaded spherical bodies, as presented by A.I. LUR'E[1].

This solution was obtained by solving the equilibrium equations of the theory of elasticity, in their Papkovich-Neuber form[2], through the expression of displacements and stresses in terms of solid spherical harmonics.

Given below are the equations for the case of zero body forces and axisymmetric external loading, relating to an elastic sphere, to a spherical cavity in an infinite elastic

---

[1] See reference 23, chapter 6.

[2] This form of the equilibrium equations was given by P.F. Papkovich in 1932 [27], and by H. Neuber in 1934 [26].

medium, and to the inner surface of a spherical layer (hollow sphere) having a rigid substrate. The equations for the former two cases are exactly as given by LUR'E, while for the latter, they are taken a step further to include the assumption of a rigid substrate.

1.2A The equations for a sphere

The equations for the displacements on the surface of an elastic sphere, of radius R_o, are given by:

$$U_r^s(\theta)=\sum_{n=o}^{\infty}\left[A_n^s R_o^{n+1}(n+1)(n-2+4\nu)+nB_n^s R_o^{n-1}\right]P_n(\mu)$$

$$U_\theta^s(\theta)=\sum_{n=1}^{\infty}\left[A_n^s R_o^{n+1}(n+5-4\nu)+B_n^s R_o^{n-1}\right]\frac{dP_n(\mu)}{d\theta} \qquad (1.2A.1)$$

In order to obtain the constants A_n^s and B_n^s, the external loading on the surface of the sphere,

$$\sigma_r=\sigma(\theta),\ \tau_{r\theta}=\tau(\theta)\ * \qquad (1.2A.2)$$

is represented in the form of the series:

$$\sigma(\theta)=\sum_{n=o}^{\infty}\sigma_n P_n(\mu)$$

$$\tau(\theta)=\sum_{n=1}^{\infty}\tau_n\frac{dP_n(\mu)}{d\theta}=-\sum_{n=1}^{\infty}\tau_n\frac{dP_n(\mu)}{d\mu}\sin\theta \qquad (1.2A.3)$$

---

* σ and τ are assumed to be positive if the corresponding forces are directed along the positive coordinate directions r and θ respectively.

where, the coefficients of these series are determined by the formulae:

$$\sigma_n = \frac{2n+1}{2}\int_o^{\pi} \sigma(\theta) P_n(\cos\theta)\sin\theta d\theta$$

$$\tau_n = \frac{2n+1}{2n(n+1)}\int_o^{\pi} \tau(\theta) \frac{dP_n(\cos\theta)}{d\theta} \sin\theta d\theta \qquad (1.2A.4)$$

By using the above equations, the constants A_n^s and B_n^s are obtained for different values of n as follows:

For n=o

$$A_o^s = -\frac{1}{4G(1+\nu)}\sigma_o \qquad (1.2A.5)$$

note, that there is no solution relating to B_o^s.

For n=1

$$A_1^s = -\frac{1}{8GR_o(1+\nu)}\sigma_1 = \frac{1}{4GR_o(1+\nu)}\tau_1 \qquad (1.2A.6)$$

note, that the solution relating to B_1^s, represents a solid body displacement.

For $n \geq 2$, the constants A_n^s and B_n^s, are obtained from the following system of equations:

$$A_n^s(n+1)(n^2-n-2-2\nu)R_o^n + n(n-1)B_n^s R_o^{n-2} = \frac{\sigma_n}{2G}$$

$$A_n^s(n^2+2n-1+2\nu)R_o^n + (n-1)B_n^s R_o^{n-2} = \frac{\tau_n}{2G} \qquad (1.2A.7)$$

Thus, in order to obtain the displacement on the surface of the sphere at a given angle θ, the given external loading, expressed as $\sigma(\theta)$ and $\tau(\theta)$, is substituted in equation (1.2A.4), and σ_n and τ_n are obtained for a particular value of n. The corresponding values of A_n^s and B_n^s are then obtained by substituting these values of σ_n and τ_n into equations (1.2A.5) when n=o, (1.2A.6) when n=1 or (1.2A.7) when $n \geq 2$. Using these values of A_n^s and B_n^s, one term of equation (1.2A.1) is obtained. This process is repeated for up to as large a value of n as is needed to obtain the displacements $U_r^s(\theta)$ and $U_\theta^s(\theta)$ to the required accuracy.

1.2B The equations for a spherical cavity

The equations for the displacements on the surface of a cavity in an infinite elastic medium, of radius R_i, are given by:

$$U_r^c(\theta)=\sum_{n=o}^{\infty}\left[\frac{E_n^c}{R_i^{\,n}}\,n(n+3-4\nu)-\frac{(n+1)F_n^c}{R_i^{\,n+2}}\right]P_n(\mu)$$

$$U_\theta^c(\theta)=\sum_{n=1}^{\infty}\left[\frac{E_n^c}{R_i^{\,n}}(4-n-4\nu)+\frac{F_n^c}{R_i^{\,n+2}}\right]\frac{dP_n(\mu)}{d\theta} \qquad (1.2B.1)$$

In order to obtain the constants E_n^c and F_n^c, the external loading on the surface of the cavity is represented as a series, given by equations (1.2A.3) and (1.2A.4). In this case however, σ and τ are assumed to be positive, if the corresponding forces are directed along the negative

coordinate directions r and θ respectively.

Using equations (1.2A.4), the constants E_n^c and F_n^c, are obtained for different values of n as follows:

For n=o

$$F_o^c = \frac{R_i^3}{4G}\sigma_o \qquad (1.2B.2)$$

note, that there is no solution relating to E_o^c.

For n≥1, the constants E_n^c and F_n^c are obtained from the following system of equations.

$$-E_n^c \frac{n(n^2+3n-2\nu)}{R_i^{n+1}} + F_n^c \frac{(n+1)(n+2)}{R_i^{n+3}} = \frac{\sigma_n}{2G}$$

$$E_n^c \frac{n^2-2+2\nu}{R_i^{n+1}} - F_n^c \frac{n+2}{R_i^{n+3}} = \frac{\tau_n}{2G} \qquad (1.2B.3)$$

Thus, in order to obtain the displacements on the surface of a cavity at a given angle θ, the same method is used as explained for the sphere, keeping in mind the difference in the sign convention for σ and τ.

1.2C The equations for a spherical layer

The solution for a spherical layer can be obtained by superimposition of the solutions for the sphere and the spherical cavity. Thus, one obtains for the displacements at any radius R and for an arbitrary value of n, the following equations:

$$U_r^L(\theta)=\left[A_n^L R^{n+1}(n+1)(n-2+4\nu)+nB_n^L R^{n-1}\right.$$
$$\left.+\frac{E_n^L}{R^n}n(n+3-4\nu)-\frac{F_n^L(n+1)}{R^{n+2}}\right]P_n(\mu)$$

$$U_\theta^L(\theta)=\left[A_n^L R^{n+1}(n+5-4\nu)+B_n^L R^{n-1}\right.$$
$$\left.+\frac{E_n^L}{R^n}(4-n-4\nu)+\frac{F_n^L}{R^{n+2}}\right]\frac{dP_n(\mu)}{d\theta} \qquad (1.2C.1)$$

When considering a spherical layer with a rigid substrate at $R=R_o$, one set of boundary conditions, namely,

$$U_r^L(\theta)\Big|_{R=R_o} = U_\theta^L(\theta)\Big|_{R=R_o} = 0 \qquad (1.2C.2)$$

can be directly applied to equations (1.2C.1) to reduce the constants by two.

Accordingly, substituting equations (1.2C.2) into (1.2C.1), the following two equations are obtained, relating the constants F_n^L and B_n^L to A_n^L and E_n^L.

$$F_n^L=\frac{1}{2n+1}\left[E_n^L R_o^{\,2}n(2n-1)-A_n^L R_o^{\,2n+3}2(3n+1-\nu(4n+2))\right]$$

$$B_n^L=-\frac{1}{2n+1}\left[\frac{E_n^L}{R_o^{\,2n-1}}2(3n+2-\nu(4n+2))+A_n^L R_o^{\,2}(n+1)(2n+3)\right] \qquad (1.2C.3)$$

Thus substituting equations (1.2C.3) into (1.2C.1), the equations describing the displacements on the inner surface, $R=R_i$, of a spherical layer with a rigid substrate at $R=R_o$, are obtained as follows:

$$U_r^L(\theta)=\sum_{n=0}^{\infty}\Bigg\{A_n^L\Bigg[R_i^{n+1}(n+1)(n-2+4\nu)$$

$$+\frac{1}{2n+1}\Bigg[\frac{R_o^{2n+3}}{R_i^{n+2}}2(n+1)(3n+1-\nu(4n+2))$$

$$-R_o^2R_i^{n-1}n(n+1)(2n+3)\Bigg]\Bigg]$$

$$+E_n^L\Bigg[\frac{1}{R_i^n}n(n+3-4\nu)$$

$$-\frac{1}{2n+1}\Bigg[\frac{R_i^{n-1}}{R_o^{2n-1}}2n(3n+2-\nu(4n+2))$$

$$+\frac{R_o^2}{R_i^{n+2}}n(n+1)(2n-1)\Bigg]\Bigg]\Bigg\}P_n(\mu)$$

$$U_\theta^L(\theta)=\sum_{n=1}^{\infty}\Bigg\{A_n^L\Bigg[R_i^{n+1}(n+5-4\nu)$$

$$-\frac{1}{2n+1}\Bigg[\frac{R_o^{2n+3}}{R_i^{n+2}}2(3n+1-\nu(4n+2))$$

$$+R_o^2R_i^{n-1}(n+1)(2n+3)\Bigg]\Bigg]$$

$$+E_n^L\Bigg[\frac{1}{R_i^n}(4-n-4\nu)$$

$$-\frac{1}{2n+1}\Bigg[\frac{R_i^{n-1}}{R_o^{2n-1}}2(3n+2-\nu(4n+2))$$

$$-\frac{R_o^2}{R_i^{n+2}}n(2n-1)\Bigg]\Bigg]\Bigg\}\frac{dP_n(\mu)}{d\theta}$$

(1.2C.4)

In order to obtain the constants A_n^L and E_n^L, the external loading on the inner surface of the layer is represented in the form of a series as given by equations (1.2A.3) and (1.2A.4), with the same sign convention for σ and τ, as used for the cavity.

Thus, using the same method as LUR'E, but keeping in mind that the number of constants can be reduced in this particular case using equations (1.2C.3), the following equations are derived for determining the constants A_n^L and E_n^L, for different values of n.

For n=o

$$A_o^L = \left[\frac{R_o^3}{R_i^3}(4\nu-2)-(1+\nu)\right]^{-1}\frac{\sigma_o}{4G} \qquad (1.2C.5)$$

note, that there is no solution relating to E_o^L.

For n≥1, the constants A_n^L and E_n^L are obtained from the following system of equations:

$$A_n^L\alpha_n + E_n^L\beta_n = \frac{\sigma_n}{2G}$$

$$A_n^L\gamma_n + E_n^L\delta_n = \frac{\tau_n}{2G} \qquad (1.2C.6)$$

where,

$$\alpha_n = (n+1)(n^2-n-2-2\nu)R_i^{\,n}$$

$$- \frac{1}{2n+1}\left[R_i^{\,n-2}R_o^{\,2}n(n-1)(n+1)(2n+3)\right.$$

$$\left. + \frac{R_o^{\,2n+3}}{R_i^{\,n+3}}\,2(n+1)(n+2)(3n+1-\nu(4n+2))\right]$$

$$\beta_n = -\frac{1}{R_i^{\,n+1}}\,n(n^2+3n-2\nu)$$

$$- \frac{1}{2n+1}\left[\frac{R_i^{\,n-2}}{R_o^{\,2n-1}}\,2n(n-1)(3n+2-\nu(4n+2))\right.$$

$$\left. - \frac{R_o^{\,2}}{R_i^{\,n+3}}\,n(n+1)(n+2)(2n-1)\right]$$

$$\gamma_n = (n^2+2n-1+2\nu)R_i^{\,n}$$

$$- \frac{1}{2n+1}\left[R_o^{\,2}R_i^{\,n-2}(n-1)(n+1)(2n+3)\right.$$

$$\left. - \frac{R_o^{\,2n+3}}{R_i^{\,n+3}}\,2(n+2)(3n+1-\nu(4n+2))\right]$$

$$\delta_n = \frac{1}{R_i^{\,n+1}}\,(n^2-2+2\nu)$$

$$- \frac{1}{2n+1}\left[\frac{R_i^{\,n-2}}{R_o^{\,2n-1}}\,2(n-1)(3n+2-\nu(4n+2))\right.$$

$$\left. + \frac{R_o^{\,2}}{R_i^{\,n+3}}\,n(n+2)(2n-1)\right]$$

(1.2C.7)

Thus, in order to obtain the displacement on the inner surface of the layer at a given angle θ, the same method is used again as explained for the sphere, keeping in mind that the sign convention for σ and τ is the same as that for the cavity.

1.3 Particular Solutions

In this section, use is made of the relationships presented in the previous one, to obtain the equations representing the displacement at any given point on the surface of a spherical body, when the external loading is an axisymmetric variable pressure band.

The reason for obtaining this solution is that by the use of multiple such pressure bands, an arbitrary axisymmetric pressure distribution on a spherical body can be discretised and thus, the relationship between pressures and displacements can be expressed in the form of influence coefficients, as required in the following chapters for the solution of the contact problem.

The original intention was to try different functions of θ to represent the variation in pressure across the aforementioned band, in order to obtain a number of discrete models for the pressure distribution, from which the optimum one, from the point of view of accuracy versus cost, could be chosen. However, in this attempt an unsurmountable obstacle was presented by the integral in equation (1.2A.4), as the only form of the pressure variation that permits the analytical solution of this integral is a linear function of $\cos\theta$.

It should be noted here, that it is not possible to use numerical integration, because in order to obtain the value of a Legendre polynomial of order n, where n is large, a recurrence relation has to be used and started at some small value of n, where the value of $P_n(\mu)$ can be analytically obtained. Having to repeat this process a large number of times, in order to obtain the required accuracy for the numerical solution of the integral, would produce a rather large number of calculations. Further, even if numerical integration were feasible by itself, the large number of such integrations required by the overall solution would make the method completely untenable.

Only the solutions for radial displacements are derived in subsections 1.3A, 1.3B and 1.3C, because tangential displacements are not used in the following chapters. It would, however, be a very simple operation to derive them from the results presented therein, if they were required.

1.3A The solution for the sphere

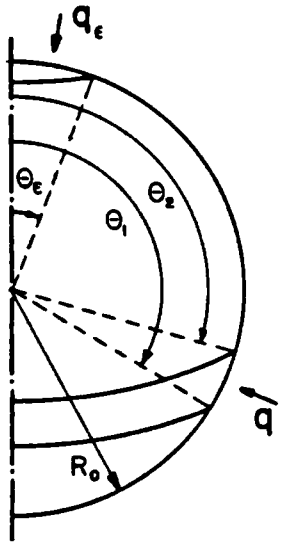

Figure 1.1 : Primary external loading on the sphere

Consider a sphere subjected to an axisymmetric loading, as shown in Figure 1.1, such that:

$$q=a+b\cos\theta \tag{1.3A.1}$$

and

$$q=q_1 \quad \text{at} \quad \theta=\theta_1$$

$$q=q_2 \quad \text{at} \quad \theta=\theta_2 \tag{1.3A.2}$$

from which

$$a=\frac{q_2\cos\theta_1-q_1\cos\theta_2}{\cos\theta_1-\cos\theta_2}$$

$$b=\frac{q_1-q_2}{\cos\theta_1-\cos\theta_2} \tag{1.3A.3}$$

and q_ε is a constant pressure acting on the angular extent θ_ε.

From static equilibrium considerations, q_ε can be expressed as a function of a and b as follows:

$$q_\varepsilon=\frac{1}{\cos^2\theta_\varepsilon-1}\left[a(\cos^2\theta_2-\cos^2\theta_1)+\frac{2}{3}b(\cos^3\theta_2-\cos^3\theta_1)\right] \tag{1.3A.4}$$

Only the applied pressure distribution q, is of direct interest to the form of the solution of the contact problem, as presented in the following chapters. However, for the existence of the elastic solution, the applied external loading should be self-equilibrating. For this reason, the pressure distribution q_ε is introduced. This equilibrating pressure distribution is used in preference to a concentrated force, because the use of the latter results in a divergent series in the solution.

For the loading shown in Figure 1.1, and following the solution as described in subsection 1.2A,

$$\tau(\theta)=0 \tag{1.3A.5}$$

and

$$\sigma(\theta)=\begin{cases} -q_\varepsilon & 0\leqslant\theta\leqslant\theta_\varepsilon \\ 0 & \theta_\varepsilon<\theta<\theta_2 \\ -q & \theta_2\leqslant\theta\leqslant\theta_1 \\ 0 & \theta_1<\theta\leqslant\pi \end{cases} \quad \text{for} \tag{1.3A.6}$$

thus, substituting equations (1.3A.1) and (1.3A.6) into equation (1.2A.4), σ_n is obtained as follows:

$$\sigma_n=\frac{2n+1}{2}\,q_\varepsilon\int_1^{\cos\theta_\varepsilon}P_n(\mu)d\mu + \frac{2n+1}{2}\,a\int_{\cos\theta_2}^{\cos\theta_1}P_n(\mu)d\mu + \frac{2n+1}{2}\,b\int_{\cos\theta_2}^{\cos\theta_1}\cos\theta\,P_n(\mu)d\mu \tag{1.3A.7}$$

In order to solve the integrals in equation (1.3A.7), use is made of the two relationships for Legendre polynomials, that are applicable for any arbitrary value of n.

These relationships are as follows:

$$P'_{n+1}(\mu)-P'_{n-1}(\mu)=(2n+1)P_n(\mu) \quad *$$

and

$$(2n+1)\mu P_n(\mu)=(n+1)P_{n+1}(\mu)+nP_{n-1}(\mu) \qquad (1.3A.8)$$

Thus, using equations (1.3A.8), equation (1.3A.7) can be rewritten as:

$$\sigma_n=\frac{q_\varepsilon}{2}\int_1^{\cos\theta_\varepsilon}\left[P'_{n+1}(\mu)-P'_{n-1}(\mu)\right]d\mu$$

$$+\frac{a}{2}\int_{\cos\theta_2}^{\cos\theta_1}\left[P'_{n+1}(\mu)-P'_{n-1}(\mu)\right]d\mu$$

$$+\frac{b}{2}\frac{n+1}{2n+3}\int_{\cos\theta_2}^{\cos\theta_1}\left[P'_{n+2}(\mu)-P'_{n}(\mu)\right]d\mu$$

$$+\frac{b}{2}\frac{n}{2n-1}\int_{\cos\theta_2}^{\cos\theta_1}\left[P'_{n}(\mu)-P'_{n-2}(\mu)\right]d\mu \qquad (1.3A.9)$$

It is now a simple matter to perform the integrations, and noting that,

$$P_n(1)=1 \qquad (1.3A.10)$$

for any arbitrary value of n, equation (1.3A.9) can be rewritten as:

---

* the (′) represents differentiation with respect to μ.

$$\sigma_n = \frac{q_\varepsilon}{2}\left[P_{n+1}(\cos\theta_\varepsilon)-P_{n-1}(\cos\theta_\varepsilon)\right]$$
$$+ \frac{a}{2}\left[\left[P_{n+1}(\cos\theta_1)-P_{n-1}(\cos\theta_1)\right]-\left[P_{n+1}(\cos\theta_2)-P_{n-1}(\cos\theta_2)\right]\right]$$
$$+ \frac{b}{2}\frac{n+1}{2n+3}\left[\left[P_{n+2}(\cos\theta_1)-P_n(\cos\theta_1)\right]-\left[P_{n+2}(\cos\theta_2)-P_n(\cos\theta_2)\right]\right]$$
$$+ \frac{b}{2}\frac{n}{2n-1}\left[\left[P_n(\cos\theta_1)-P_{n-2}(\cos\theta_1)\right]-\left[P_n(\cos\theta_2)-P_{n-2}(\cos\theta_2)\right]\right]$$

(1.3A.11)

Further, by substituting q_ε into equation (1.3A.11) from equation (1.3A.4), and a and b from equation (1.3A.3), σ_n can be written as a function of q_1 and q_2, in the following way.

$$\sigma_n = \frac{1}{2}\frac{q_2\cos\theta_1-q_1\cos\theta_2}{\cos\theta_1-\cos\theta_2}\left\{\frac{\cos^2\theta_2-\cos^2\theta_1}{\cos^2\theta_\varepsilon-1}\left[P_{n+1}(\cos\theta_\varepsilon)-P_{n-1}(\cos\theta_\varepsilon)\right]\right.$$
$$\left.+\left[P_{n+1}(\cos\theta_1)-P_{n-1}(\cos\theta_1)\right]-\left[P_{n+1}(\cos\theta_2)-P_{n-1}(\cos\theta_2)\right]\right\}$$
$$+ \frac{1}{6}\frac{q_1-q_2}{\cos\theta_1-\cos\theta_2}\left\{2\,\frac{\cos^3\theta_2-\cos^3\theta_1}{\cos^2\theta_\varepsilon-1}\left[P_{n+1}(\cos\theta_\varepsilon)-P_{n-1}(\cos\theta_\varepsilon)\right]\right.$$
$$+ \frac{3(n+1)}{2n+3}\left[\left[P_{n+2}(\cos\theta_1)-P_n(\cos\theta_1)\right]-\left[P_{n+2}(\cos\theta_2)-P_n(\cos\theta_2)\right]\right]$$
$$\left.+ \frac{3n}{2n-1}\left[P_n(\cos\theta_1)-P_{n-2}(\cos\theta_1)\right]-\left[P_n(\cos\theta_2)-P_{n-2}(\cos\theta_2)\right]\right]\right\}$$

(1.3A.12)

From equation (1.3A.12), the particular cases of σ_n for n=o and n=1, can be obtained by noting that,

$$P_{-(n+1)}(\mu) = P_n(\mu) \qquad (1.3A.13)$$

thus,

$$\sigma_o = \frac{1}{2}(q_2\cos\theta_1 - q_1\cos\theta_2)\left[1 - \frac{\cos\theta_1+\cos\theta_2}{\cos\theta_\varepsilon+1}\right]$$

$$+ \frac{1}{6}\frac{q_1-q_2}{\cos\theta_1-\cos\theta_2}\left[2\frac{\cos^3\theta_2-\cos^3\theta_1}{\cos\theta_\varepsilon+1} + \frac{3}{2}(\cos^2\theta_1-\cos^2\theta_2)\right] \qquad (1.3A.14)$$

and

$$\sigma_1 = 0 \qquad (1.3A.15)$$

It is thus possible to obtain the constants A_n^s and B_n^s in equation (1.2A.1), for different values of n, as follows:

For n=o, from equations (1.2A.5) and (1.3A.14)

$$A_o^s = -\frac{1}{8G(1+\nu)}\left[(q_2\cos\theta_1 - q_1\cos\theta_2)\left[1 - \frac{\cos\theta_1+\cos\theta_2}{\cos\theta_\varepsilon+1}\right]\right.$$

$$\left. + \frac{q_1-q_2}{\cos\theta_1-\cos\theta_2}\left[\frac{2}{3}\frac{\cos^3\theta_2-\cos^3\theta_1}{\cos\theta_\varepsilon+1} + \frac{1}{2}(\cos^2\theta_1-\cos^2\theta_2)\right]\right] \qquad (1.3A.16)$$

For n=1, from equations (1.2A.6) and (1.3A.15)

$$A_1^s = 0 \qquad (1.3A.17)$$

For n≥2, from equations (1.2A.7), noting that for the loading in question τ_n=o, for all values of n.

$$A_n^s = -\frac{\sigma_n}{4GR_o^{\,n}T_n^s}$$

$$B_n^s = \frac{\sigma_n}{4GR_o^{\,n-2}T_n^s}\,\frac{n^2+2n-1+2\nu}{n-1} \qquad (1.3A.18)$$

where

$$T_n^s = n(n-1)+(2n+1)(1+\nu) \qquad (1.3A.19)$$

and σ_n is given by equation (1.3A.12).

Finally, by substituting into equation (1.2A.1), equations (1.3A.16), (1.3A.17) and (1.3A.18), letting

$$H_n^s = \frac{2n^2(\frac{1}{\nu}-1)+n+2-\frac{1}{\nu}}{(n-1)T_n^s} \tag{1.3A.20}$$

and separating q_1 and q_2, the equation giving the radial displacement at any point, defined by θ, on the sphere, due to an axisymmetric variable pressure band, defined by q_1 at θ_1 and q_2 at θ_2, can be written as:

$$\begin{aligned}
U_r^s = {} & q_1 \frac{R_o}{4G}\left\{\frac{1-2\nu}{1+\nu}(\cos\theta_1-\cos\theta_2)\left[\frac{1}{2}-\frac{2\cos\theta_1+\cos\theta_2}{3(\cos\theta_\varepsilon+1)}\right]\right. \\
& +\nu\sum_{n=2}^{\infty}H_n^s P_n(\mu)\left\{(\cos\theta_2-\cos\theta_1)\frac{2\cos\theta_1+\cos\theta_2}{3(\cos^2\theta_\varepsilon-1)}\left[P_{n+1}(\cos\theta_\varepsilon)-P_{n-1}(\cos\theta_\varepsilon)\right]\right. \\
& +\frac{1}{\cos\theta_1-\cos\theta_2}\left[\frac{2n+1}{(n-1)(n+2)}\left[P_n(\cos\theta_1)-P_n(\cos\theta_2)\right]\right. \\
& +\left[\frac{n+1}{n+2}\cos\theta_1-\cos\theta_2\right]P_{n+1}(\cos\theta_1)+\left[\cos\theta_2-\frac{n}{n-1}\cos\theta_1\right]P_{n-1}(\cos\theta_1) \\
& \left.\left.\left.+\frac{1}{n+2}\cos\theta_2 P_{n+1}(\cos\theta_2)+\frac{1}{n-1}\cos\theta_2 P_{n-1}(\cos\theta_2)\right]\right\}\right\} \\
& +q_2\frac{R_o}{4G}\left\{\frac{1-2\nu}{1+\nu}(\cos\theta_1-\cos\theta_2)\left[\frac{1}{2}-\frac{\cos\theta_1+2\cos\theta_2}{3(\cos\theta_\varepsilon+1)}\right]\right. \\
& +\nu\sum_{n=2}^{\infty}H_n^s P_n(\mu)\left\{(\cos\theta_2-\cos\theta_1)\frac{\cos\theta_1+2\cos\theta_2}{3(\cos^2\theta_\varepsilon-1)}\left[P_{n+1}(\cos\theta_\varepsilon)-P_{n-1}(\cos\theta_\varepsilon)\right]\right. \\
& +\frac{1}{\cos\theta_1-\cos\theta_2}\left[\frac{2n+1}{(n-1)(n+2)}\left[P_n(\cos\theta_2)-P_n(\cos\theta_1)\right]\right. \\
& +\frac{1}{n+2}\cos\theta_1 P_{n+1}(\cos\theta_1)+\frac{1}{n-1}\cos\theta_1 P_{n-1}(\cos\theta_1) \\
& \left.\left.\left.+\left[\frac{n+1}{n+2}\cos\theta_2-\cos\theta_1\right]P_{n+1}(\cos\theta_2)+\left[\cos\theta_1-\frac{n}{n-1}\cos\theta_2\right]P_{n-1}(\cos\theta_2)\right]\right\}\right\}
\end{aligned} \tag{1.3A.21}$$

1.3B The solution for the cavity

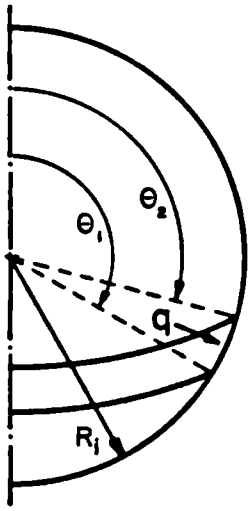

Figure 1.2 : Primary external loading on the cavity

Consider a cavity in an infinite elastic medium subjected to an axisymmetric loading as shown in Figure 1.2, such that:

$$q=a+b\cos\theta \qquad (1.3B.1)$$

and

$$q=q_1 \quad \text{at} \quad \theta=\theta_1$$

$$q=q_2 \quad \text{at} \quad \theta=\theta_2 \qquad (1.3B.2)$$

from which

$$a=\frac{q_2\cos\theta_1-q_1\cos\theta_2}{\cos\theta_1-\cos\theta_2}$$

$$b=\frac{q_1-q_2}{\cos\theta_1-\cos\theta_2} \qquad (1.3B.3)$$

For the loading shown in Figure 1.2, and following the solution as described in subsection 1.2B,

$$\tau(\theta)=0 \tag{1.3B.4}$$

and

$$\sigma(\theta)=\begin{cases} 0 & 0\leqslant\theta<\theta_2 \\ -q \quad \text{for} & \theta_2\leqslant\theta\leqslant\theta_1 \\ 0 & \theta_1<\theta\leqslant\pi \end{cases} \tag{1.3B.5}$$

thus, substituting equations (1.3B.1) and (1.3B.5) into equation (1.2A.4), σ_n becomes,

$$\sigma_n=\frac{2n+1}{2}a\int_{\cos\theta_2}^{\cos\theta_1}P_n(\mu)d\mu + \frac{2n+1}{2}b\int_{\cos\theta_2}^{\cos\theta_1}\cos\theta P_n(\mu)d\mu \tag{1.3B.6}$$

which, using the same method employed to obtain equation (1.3A.11),gives:

$$\begin{aligned}\sigma_n=&\frac{a}{2}\left[\left[P_{n+1}(\cos\theta_1)-P_{n-1}(\cos\theta_1)\right]-\left[P_{n+1}(\cos\theta_2)-P_{n-1}(\cos\theta_2)\right]\right] \\ &+\frac{b}{2}\frac{n+1}{2n+3}\left[\left[P_{n+2}(\cos\theta_1)-P_n(\cos\theta_1)\right]-\left[P_{n+2}(\cos\theta_2)-P_n(\cos\theta_2)\right]\right] \\ &+\frac{b}{2}\frac{n}{2n-1}\left[\left[P_n(\cos\theta_1)-P_{n-2}(\cos\theta_1)\right]-\left[P_n(\cos\theta_2)-P_{n-2}(\cos\theta_2)\right]\right]\end{aligned} \tag{1.3B.7}$$

Substituting a and b from equation (1.3B.3), into equation (1.3B.7), σ_n can be written as a function of q_1 and q_2, becoming:

$$\sigma_n = \frac{1}{2}\frac{q_2\cos\theta_1 - q_1\cos\theta_2}{\cos\theta_1-\cos\theta_2}\left[\left[P_{n+1}(\cos\theta_1)-P_{n-1}(\cos\theta_1)\right]-\left[P_{n+1}(\cos\theta_2)-P_{n-1}(\cos\theta_2)\right]\right]$$
$$+\frac{1}{2}\frac{q_1-q_2}{\cos\theta_1-\cos\theta_2}\left[\frac{n+1}{2n+3}\left[\left[P_{n+2}(\cos\theta_1)-P_n(\cos\theta_1)\right]-\left[P_{n+2}(\cos\theta_2)-P_n(\cos\theta_2)\right]\right]\right.$$
$$\left.+\frac{n}{2n-1}\left[\left[P_n(\cos\theta_1)-P_{n-2}(\cos\theta_1)\right]-\left[P_n(\cos\theta_2)-P_{n-2}(\cos\theta_2)\right]\right]\right] \qquad (1.3B.8)$$

and in particular for n=o, equation (1.3B.8) gives:

$$\sigma_o=(q_1+q_2)\,\frac{1}{4}\,(\cos\theta_1-\cos\theta_2) \qquad (1.3B.9)$$

It is thus possible to obtain the constants E_n^c and F_n^c in equation (1.2B.1), for different values of n, as follows:

For n=o, from equations (1.2B.2) and (1.3B.9)

$$F_o^c=\frac{R_i^{\,3}}{16G}\,(q_1+q_2)(\cos\theta_1-\cos\theta_2) \qquad (1.3B.10)$$

For n≥1, from equations (1.2B.3), noting that for the loading in question τ_n=o, for all values of n.

$$E_n^c=-\frac{R_i^{\,n+1}}{4GT_n^c}\,\sigma_n$$

$$F_n^c=-\frac{R_i^{\,n+3}}{4GT_n^c}\,\frac{n^2-2+2\nu}{n+2}\,\sigma_n \qquad (1.3B.11)$$

where

$$T_n^c=n^2+n+1-\nu(2n+1) \qquad (1.3B.12)$$

and σ_n is given by equation (1.3B.8)

Finally, by substituting into equation (1.2B.1), equations (1.3B.10) and (1.3B.11), letting

$$H_n^C = \frac{(2n^2+4n+1)(\frac{1}{\nu}-1)-n}{(n+2)T_n^C} \qquad (1.3B.13)$$

and separating q_1 and q_2, the equation giving the radial displacement at any point θ on the cavity, due to an axisymmetric variable pressure band, defined by q_1 at θ_1 and q_2 at θ_2, can be written as:

$$\begin{aligned}
U_r^C = &- q_1 \frac{R_i}{4G}\Bigg\{(\cos\theta_1-\cos\theta_2)\left[\frac{1}{4}+\frac{7-8\nu}{9(1-\nu)}\cos\theta(\cos\theta_1+\frac{1}{2}\cos\theta_2)\right] \\
&+\frac{1}{\cos\theta_1-\cos\theta_2}\sum_{n=2}^{\infty}\nu_n H_n^C P_n(\mu)\Bigg\{\frac{2n+1}{(n-1)(n+2)}\left[P_n(\cos\theta_1)-P_n(\cos\theta_2)\right] \\
&+\left[\frac{n+1}{n+2}\cos\theta_1-\cos\theta_2\right]P_{n+1}(\cos\theta_1)+\left[\cos\theta_2-\frac{n}{n-1}\cos\theta_1\right]P_{n-1}(\cos\theta_1) \\
&+\frac{1}{n+2}\cos\theta_2 P_{n+1}(\cos\theta_2)+\frac{1}{n-1}\cos\theta_2 P_{n-1}(\cos\theta_2)\Bigg\}\Bigg\} \\
&- q_2 \frac{R_i}{4G}\Bigg\{(\cos\theta_1-\cos\theta_2)\left[\frac{1}{4}+\frac{7-8\nu}{9(1-\nu)}\cos\theta(\frac{1}{2}\cos\theta_1+\cos\theta_2)\right] \\
&+\frac{1}{\cos\theta_1-\cos\theta_2}\sum_{n=2}^{\infty}\nu_n H_n^C P_n(\mu)\Bigg\{\frac{2n+1}{(n-1)(n+2)}\left[P_n(\cos\theta_2)-P_n(\cos\theta_1)\right] \\
&+\frac{1}{n+2}\cos\theta_1 P_{n+1}(\cos\theta_1)+\frac{1}{n-1}\cos\theta_1 P_{n-1}(\cos\theta_1) \\
&+\left[\frac{n+1}{n+2}\cos\theta_2-\cos\theta_1\right]P_{n+1}(\cos\theta_2)+\left[\cos\theta_1-\frac{n}{n-1}\cos\theta_2\right]P_{n-1}(\cos\theta_2)\Bigg\}\Bigg\}
\end{aligned} \qquad (1.3B.14)$$

1.3C The solution for the layer

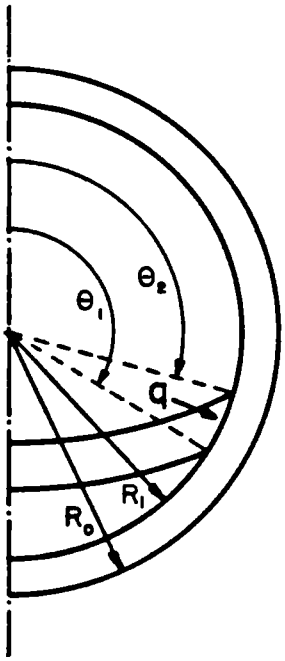

Figure 1.3 : Primary external loading on the layer

Consider a spherical layer with a rigid substrate at $R=R_o$ and subjected to an axisymmetric loading on its inner surface, at $R=R_i$, as shown in Figure 1.3, such that:

$$q=a+b\cos\theta \qquad (1.3C.1)$$

and

$$q=q_1 \quad \text{at} \quad \theta=\theta_1$$

$$q=q_2 \quad \text{at} \quad \theta=\theta_2 \qquad (1.3C.2)$$

The analysis in subsection 1.3B, up to and including equation (1.3B.9), is also directly applicable to the layer. This is because the external loading on the cavity and on the layer, as well as the method used to express it in spherical harmonics, are identical.

It is thus possible, to obtain the constants A_n^L and E_n^L in equation (1.2C.4), for different values of n, as follows:

For n=o, from equations (1.2C.5) and (1.3B.9)

$$A_o^L = \left[\frac{R_o^3}{R_i^3}(4\nu-2)-(1+\nu)\right]^{-1} \frac{1}{16G}(q_1+q_2)(\cos\theta_1-\cos\theta_2) \qquad (1.3C.3)$$

For n≥1, from equations (1.2C.6), noting that for the loading in question τ_n=o, for all values of n.

$$A_n^L = \frac{1}{2G}\frac{\delta_n}{\alpha_n\delta_n-\gamma_n\beta_n}\sigma_n$$

$$E_n^L = -\frac{1}{2G}\frac{\gamma_n}{\alpha_n\delta_n-\gamma_n\beta_n}\sigma_n \qquad (1.3C.4)$$

where, α_n, β_n, γ_n and δ_n are given by equation (1.2C.7) and σ_n is given by equation (1.3B.8).

Finally, by substituting into equation (1.2C.4), equations (1.3C.3) and (1.3C.4), letting

$$H_n^L = \frac{\delta_n\varepsilon_n-\gamma_n\zeta_n}{\alpha_n\delta_n-\gamma_n\beta_n}\frac{1}{R_i} \qquad (1.3C.5)$$

where,

$$\varepsilon_n = R_i^{n+1}(n+1)(n-2+4\nu) + \frac{1}{2n+1}\left[\frac{R_o^{2n+3}}{R_i^{n+2}}2(n+1)(3n+1-\nu(4n+2))-R_o^2R_i^{n-1}n(n+1)(2n+3)\right] \qquad (1.3C.6)$$

$$\zeta_n = \frac{1}{R_i^{\,n}}\, n(n+3-4\nu)$$
$$- \frac{1}{2n+1}\left[\frac{R_i^{\,n-1}}{R_o^{\,2n-1}}\, 2n(3n+2-\nu(4n+2)) + \frac{R_o^{\,2}}{R_i^{\,n+2}}\, n(n+1)(2n-1)\right] \tag{1.3C.7}$$

and separating q_1 and q_2, the equation giving the radial displacement at any point θ on the inner surface of the layer, due to an axisymmetric variable pressure band acting on the same surface and defined by q_1 at θ_1 and q_2 at θ_2, can be written as follows:

$$U_r^L = q_1 \frac{R_i}{4G}\left\{(\cos\theta_1-\cos\theta_2)\left[\frac{1}{2}\,\frac{(R_o^{\,3}-R_i^{\,3})(1-2\nu)}{R_o^{\,3}(4\nu-2)-R_i^{\,3}(1+\nu)} + H_1^L\cos\theta\left(\cos\theta_1+\frac{1}{2}\cos\theta_2\right)\right]\right.$$
$$+ \frac{1}{\cos\theta_1-\cos\theta_2}\sum_{n=2}^{\infty} H_n^L P_n(\mu)\left\{\frac{2n+1}{(n-1)(n+2)}\left[P_n(\cos\theta_1)-P_n(\cos\theta_2)\right]\right.$$
$$+\left[\frac{n+1}{n+2}\cos\theta_1-\cos\theta_2\right]P_{n+1}(\cos\theta_1)+\left[\cos\theta_2-\frac{n}{n-1}\cos\theta_1\right]P_{n-1}(\cos\theta_1)$$
$$\left.\left.+\frac{1}{n+2}\cos\theta_2 P_{n+1}(\cos\theta_2)+\frac{1}{n-1}\cos\theta_2 P_{n-1}(\cos\theta_2)\right\}\right\}$$
$$+ q_2 \frac{R_i}{4G}\left\{(\cos\theta_1-\cos\theta_2)\left[\frac{1}{2}\,\frac{(R_o^{\,3}-R_i^{\,3})(1-2\nu)}{R_o^{\,3}(4\nu-2)-R_i^{\,3}(1+\nu)} + H_1^L\cos\theta\left(\frac{1}{2}\cos\theta_1+\cos\theta_2\right)\right]\right.$$
$$+ \frac{1}{\cos\theta_1-\cos\theta_2}\sum_{n=2}^{\infty} H_n^L P_n(\mu)\left\{\frac{2n+1}{(n-1)(n+2)}\left[P_n(\cos\theta_2)-P_n(\cos\theta_1)\right]\right.$$
$$+\frac{1}{n+2}\cos\theta_1 P_{n+1}(\cos\theta_1)+\frac{1}{n-1}\cos\theta_1 P_{n-1}(\cos\theta_1)$$
$$\left.\left.+\left[\frac{n+1}{n+2}\cos\theta_2-\cos\theta_1\right]P_{n+1}(\cos\theta_2)+\left[\cos\theta_1-\frac{n}{n-1}\cos\theta_2\right]P_{n-1}(\cos\theta_2)\right\}\right\} \tag{1.3C.8}$$

It can be easily shown that, in the limit as $R_o \to \infty$, equation (1.3C.8) reverts to equation (1.3B.14), which gives the radial displacement for the case of the cavity.

1.4 Calculation of the influence coefficients

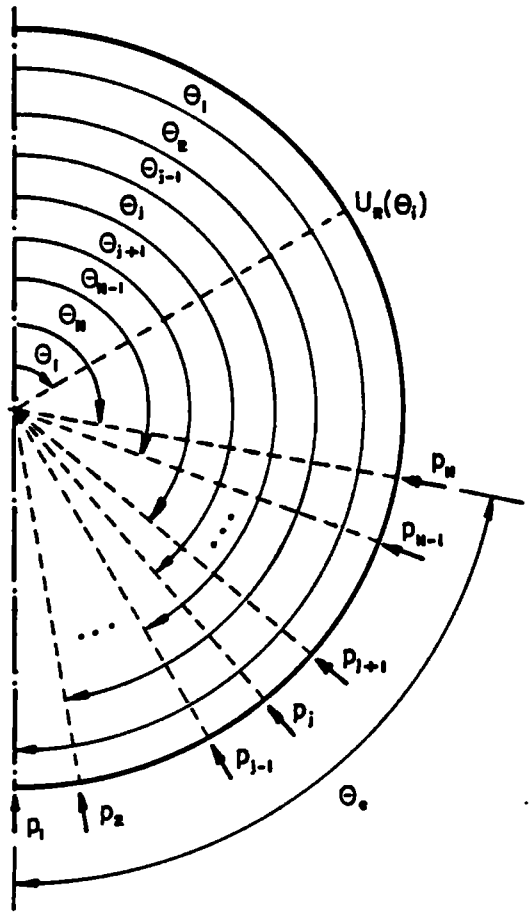

Figure 1.4 : Discretised pressure distribution on a spherical body

Consider an axisymmetric continuous pressure distribution applied to a spherical body, within an angular extent θ_c.

Such a pressure distribution can be approximated by a discretised equivalent, as shown in Figure 1.4. This model

is made up of a number of variable pressure bands, of the form used in the previous section, where the pressure p_j at the boundaries between bands is set equal to the pressure applied to the surface by the continuous pressure distribution at the particular point θ_j.

By using the principle of superposition, it is then possible to obtain the resulting displacement $U_r(\theta_i)$, on the surface of a spherical body, from the equations derived in the previous section.

It should be noted here, that the number of pressure bands used, does not affect the accuracy of the displacements obtained, resulting from the application of the discretised pressure distribution, but only the accuracy to which the actual continuous pressure distribution is approximated.

It is thus possible to express the relationship between the discretised pressure distribution and the displacements at the required points, in influence coefficient form,

$$\mathbf{U} = \mathbf{M}\mathbf{p} \qquad (1.4.1)$$

where,

U is the vector of displacements $U_r(\theta_i)$, at the required points

p is the vector of pressures p_j, at the specified points θ_j.

M is the matrix of influence coefficients.
Its elements $M_{i,j}$ give the displacement at point θ_i, due to a unit pressure at point θ_j.

In calculating the influence coefficients $M_{i,j}$, either equation (1.3A.21), (1.3B.14) or (1.3C.8) is used, when the spherical body in question is a sphere, a cavity or a layer respectively and the proceedure employed is as follows.

When calculating the influence coefficients $M_{i,1}$ or $M_{i,N}$, only one pressure band is involved, defined by p_1 and p_2 or p_{N-1} and p_N respectively, as seen in Figure 1.4. In the former case only the part of the relevant elastic equation referring to q_1 is used, with q_1 set to p_1. While, in the latter case, only the part referring to q_2 is used, with θ_1 and θ_2 replaced by θ_{N-1} and θ_N respectively and q_2 set to p_N.

When calculating the influence coefficient $M_{i,j}$, for $1<j<N$, two pressure bands are involved, as seen in Figure 1.4, and defined by p_{j-1}, p_j and p_{j+1}. Thus the relevant elastic equation is used twice and the results summed to obtain the required influence coefficient. For the pressure band defined by p_{j-1} and p_j, the part of the equation referring to q_2 is used, with θ_1 and θ_2 replaced by θ_{j-1} and θ_j respectively, and q_2 set to p_j. For the band defined by p_j and p_{j+1}, the part of the equation referring to q_1 is used, with θ_1 and θ_2 replaced by θ_j and θ_{j+1} respectively, and q_1 set to p_j.

1.5 Computer implementation

The formulation of a computer algorithm for the calculation of the influence coefficients, as described in the previous section, is a relatively simple exercise. However, two major points have to be kept in mind.

First, in the calculation of the Legendre polynomials the recurrence relationship, given by equation (1.3A.8), is used in the form:

$$P_{n+1}(\mu) = \mu P_n(\mu) - P_{n-1}(\mu) + \mu P_n(\mu) - \frac{\mu P_n(\mu) - P_{n-1}(\mu)}{n+1} \qquad (1.5.1)$$

where, $P_o(\mu)=1$

and $P_1(\mu)=\mu$ (1.5.2)

for reasons of economy and numerical stability.

Note, that for large values of n, the last term of equation (1.5.1) is negligible, giving the approximation

$$P_{n+1}(\mu) = 2\mu P_n(\mu) - P_{n-1}(\mu) \qquad (1.5.3)$$

From equation (1.5.3), it can be shown that the roundoff errors grow at worst linearly for $|\mu| \leq 1$, as follows.

If ρ_{n+k} is the error in $P_{n+k}(\mu)$, due to a single rounding error ρ in $P_n(\mu)$ the approximation gives,

$$\rho_{n+k+1} = 2\mu\rho_{n+k} - \rho_{n+k-1} \qquad (1.5.4)$$

with initial conditions

$$\rho_n=\rho \quad \text{and} \quad \rho_{n-1}=0 \qquad (1.5.5)$$

This difference equation has its maximum for $|\mu|=1$, and in this case the solutions are:

$$\rho_{n-1}=0,\ \rho_n=\rho,\ |\rho_{n+1}|=2\rho,\ldots,\ |\rho_{n+k}|=(k+1)\rho \qquad (1.5.6)$$

Second, the term H_n^L in equation (1.3C.8), given by equation (1.3C.5), has a numerator which is a function of n^4 and a denominator which is a function of n^6, which produce overflow errors when an attempt is made to calculate them directly for large values of n.

This problem was circumvented by expressing H_n^L in such a way as to only involve calculation of fractions, where the power of n is the same in the numerators and denominators, and in the worst case it is equal to 2. This was achieved through the use of recurrence relationships for all the terms of H_n^L, as follows:

H_2^L is written as

$$H_2^L = \frac{\sum_{i=1}^{i=6} C_{i,2} - C_{7,2}}{\sum_{i=8}^{i=13} C_{i,2} - C_{14,2}} \qquad (1.5.7)$$

where,

$$C_{1,2} = 4(7-10\nu)(19\nu-17)$$

$$C_{2,2} = 126\left[\frac{R_i}{R_o}\right]^3$$

$$C_{3,2} = 4(7-10\nu)(8-10\nu)\left[\frac{R_i}{R_o}\right]^3$$

$$C_{4,2} = 150(4\nu-3)\left[\frac{R_i}{R_o}\right]^7$$

$$C_{5,2} = 100(1-3\nu+2\nu^2)\left[\frac{R_i}{R_o}\right]^7$$

$$C_{6,2} = 4(8-10\nu)(7-4\nu)\left[\frac{R_i}{R_o}\right]^{10}$$

$$C_{7,2} = 252(2\nu-1)\left[\frac{R_i}{R_o}\right]^{5}$$

$$C_{8,2} = 16(7-10\nu)(7-5\nu)$$

$$C_{9,2} = 504\left[\frac{R_i}{R_o}\right]^{3}$$

$$C_{10,2} = 16(7-10\nu)(8-10\nu)\left[\frac{R_i}{R_o}\right]^{3}$$

$$C_{11,2} = 600\left[\frac{R_i}{R_o}\right]^{7}$$

$$C_{12,2} = 100(1-\nu^2)\left[\frac{R_i}{R_o}\right]^{7}$$

$$C_{13,2} = 4(8-10\nu)(7+4\nu)\left[\frac{R_i}{R_o}\right]^{10}$$

$$C_{14,2} = 1008\left[\frac{R_i}{R_o}\right]^{5} \qquad (1.5.8)$$

And letting,

$$C_{i,n+1} = C_{i,n} \times D_{i,n} \qquad (1.5.9)$$

H^L_{n+1} can be written as

$$H^L_{n+1} = \frac{\sum_{i=1}^{i=6} C_{i,n+1} - C_{7,n+1}}{\sum_{i=8}^{i=13} C_{i,n+1} - C_{14,n+1}} \qquad (1.5.10)$$

where,

$$D_{1,n} = \frac{3n+4-\nu(4n+6)}{3n+1-\nu(4n+2)} \; \frac{2n^2(\nu-1)+n(9\nu-8)+(8\nu-7)}{2n^2(\nu-1)+n(5\nu-4)+(\nu-1)}$$

$$D_{2,n} = \frac{n+2}{n} \; \frac{2n+5}{2n+3} \; \frac{2n+1}{2n-1} \left[\frac{R_i}{R_o}\right]^2$$

$$D_{3,n} = \frac{3n+4-\nu(4n+6)}{3n+1-\nu(4n+2)} \; \frac{3n+5-\nu(4n+6)}{3n+2-\nu(4n+2)} \left[\frac{R_i}{R_o}\right]^2$$

$$D_{4,n} = \frac{n+2}{n} D_{5,n}$$

$$D_{5,n} = \left[\frac{2n+3}{2n+1}\right]^2 \left[\frac{R_i}{R_o}\right]^2$$

$$D_{6,n} = \frac{3n+5-\nu(4n+6)}{3n+2-\nu(4n+2)} \; \frac{2n^2(1-\nu)+n(4-3\nu)+(1+\nu)}{2n^2(1-\nu)+n\nu+(2\nu-1)} \left[\frac{R_i}{R_o}\right]^4$$

$$D_{7,n} = D_{2,n}$$

$$D_{8,n} = \frac{n+3}{n+2} \; \frac{3n+4-\nu(4n+6)}{3n+1-\nu(4n+2)} \; \frac{n^2+3n+3-\nu(2n+3)}{n^2+n+1-\nu(2n+1)}$$

$$D_{9,n} = \frac{n+3}{n-1} \; \frac{2n+5}{2n+3} \; \frac{2n+1}{2n-1} \left[\frac{R_i}{R_o}\right]^2$$

$$D_{10,n} = \frac{n}{n-1} \; \frac{n+3}{n+2} \; \frac{3n+4-\nu(4n+6)}{3n+1-\nu(4n+2)} \; \frac{3n+5-\nu(4n+6)}{3n+2-\nu(4n+2)} \left[\frac{R_i}{R_o}\right]^2$$

$$D_{11,n} = \frac{n+3}{n-1} D_{5,n}$$

$$D_{12,n} = D_{5,n}$$

$$D_{13,n} = \frac{n}{n-1} \; \frac{3n+5-\nu(4n+6)}{3n+2-\nu(4n+2)} \; \frac{n^2+3n+3+\nu(2n+1)}{n^2+n+1+\nu(2n+1)} \left[\frac{R_i}{R_o}\right]^4$$

$$D_{14,n} = D_{9,n} \qquad (1.5.11)$$

Note that the process is started from n=2, because some of the terms $D_{i,n}$ are not defined for n=1. The value of H_1^L is of course obtained by direct substitution of n=1 into equation (1.3C.5).

Chapter 2

CHAPTER 2

DRY CONTACT

2.1 Introduction

H. Hertz [13] was first in successfully treating the contact problem between elastic bodies, and even one hundred years after its conception his theory is as widely used as ever.

Elastic contact problems can be classified as Hertzian if they satisfy the following conditions:

1) The bodies are homogeneous, isotropic, obey Hooke's law and experience small strains, (i.e. the linear theory of elasticity applies).

2) The contacting surfaces are smooth and frictionless.

3) The dimensions of the deformed contact patch remain small compared to the principal radii of curvature of the undeformed surfaces.

4) The deformations are related to the stresses in the contact zones as predicted by the linear theory of elasticity for half-spaces.

5) The contacting surfaces are continuous and may be represented by second degree polynomials prior to deformation.

Contact problems can be further classified as,

a) Counterformal (or Antiformal), where condition 3 above is satisfied.

b) Conformal, where condition 3 above can be violated.

When considering the conformal contact between a sphere and a spherical seat* of nearly the same radii, under a severe enough loading the footprint dimensions can reach the same order of magnitude as the undeformed radii of curvature, without the actual displacements of the surfaces becoming large enough to prohibit the use of the linear theory of elasticity. However, the relatively large footprint dimensions possible in this case invalidate condition 3 of Hertz's theory, thus necessitating a different solution.

In this chapter a numerical solution is presented for the problem of axisymmetric conformal contact between a sphere and a spherical seat, which presents computational time advantages over other such available solutions. The assumptions of this solution being as follows:

1) Hertzian conditions 1 and 2 apply.
2) The radii of curvature of the two bodies are almost equal.
3) The external loading is such that the resulting force acts along the line connecting the centres of the two spherical bodies and produces no rotations.

---

* seat, refers to either a spherical cavity or a spherical layer.

2.2 Geometric conditions governing the contact deformations

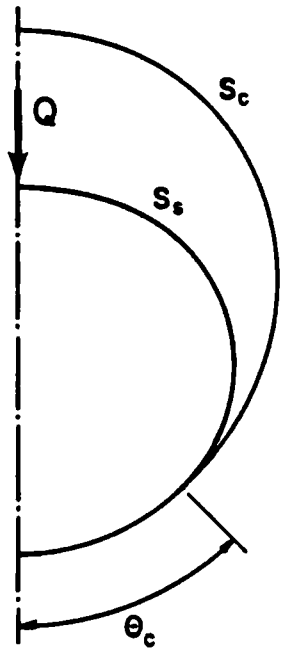

Figure 2.1 : Contact of elastic spherical bodies

Consider a smooth elastic sphere S_s and a smooth elastic seat S_c in contact along an angular extent θ_c of their boundaries, as shown in Figure 2.1. It is assumed that they are of almost equal undeformed radii ($R_s \simeq R_c$) and that the external loading Q, is non-torsional and axisymmetric about the line connecting the centres of the two bodies, permiting the consideration of only a meridional plane. It is further assumed that the displacements of the surfaces of the two bodies are of such order of magnitude as to permit the use of linear elasticity theory.

This section presents the derivation of the geometric relationships governing the deformations that characterize such a contact.

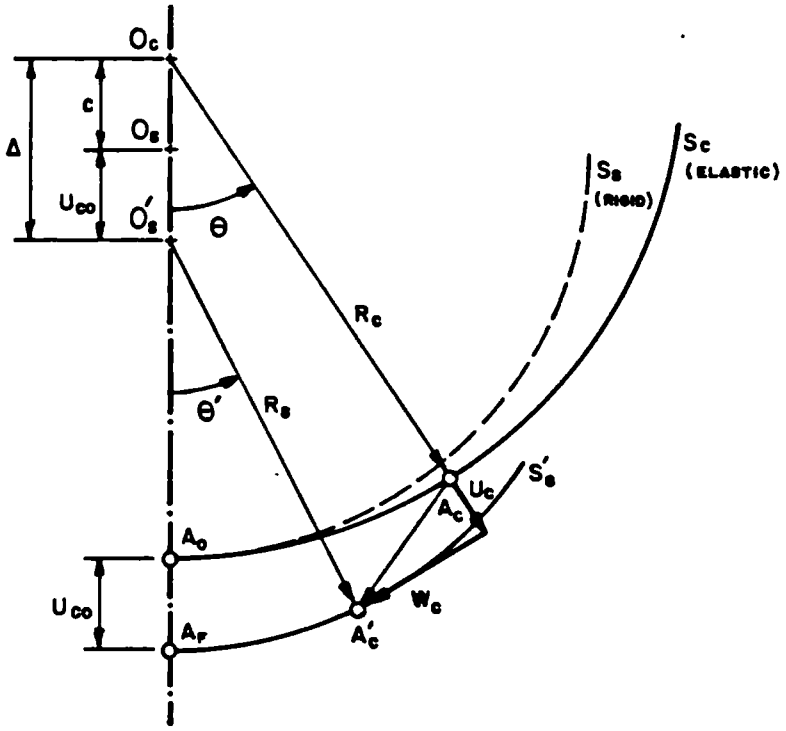

Figure 2.2 : Contact of rigid sphere and elastic seat

First, assume that the sphere S_s is rigid and the seat S_c elastic and that they are initially touching at point A_o as shown in Figure 2.2. After application of the external loading on S_s, along the O_cO_s axis, S_s penetrates S_c by U_{co}, and a typical point A_c on S_c moves to A_c', being now on the spherical surface of contact S_s', with radius R_s.

If U_c and W_c are the radial and tangential (in the θ direction) components of displacement of A_c, the following two geometric relationships can be obtained:

$$R_s\cos\theta'+\Delta = (R_c+U_c)\cos\theta-W_c\sin\theta$$

$$R_s\sin\theta' = (R_c+U_c)\sin\theta+W_c\cos\theta \qquad (2.2.1)$$

where, $\Delta = U_{co}+c$ and $c = R_c-R_s$ (2.2.2)

By eliminating θ' from equations (2.2.1) and noting that,

$$(R_c^2-R_s^2) = (R_c-R_s)(R_c+R_s) \simeq 2cR_c \qquad (2.2.3)$$

one obtains,

$$2R_c(U_c+c-(U_{co}+c)\cos\theta)+U_c^2+W_c^2+U_{co}^2+c^2+2cU_{co}$$
$$+2(U_{co}+c)(W_c\sin\theta-U_c\cos\theta) = 0 \qquad (2.2.4)$$

By neglecting second-order small quantities equation (2.2.4) can be rewritten as,

$$U_c = U_{co}\cos\theta-c(1-\cos\theta) \qquad (2.2.5)$$

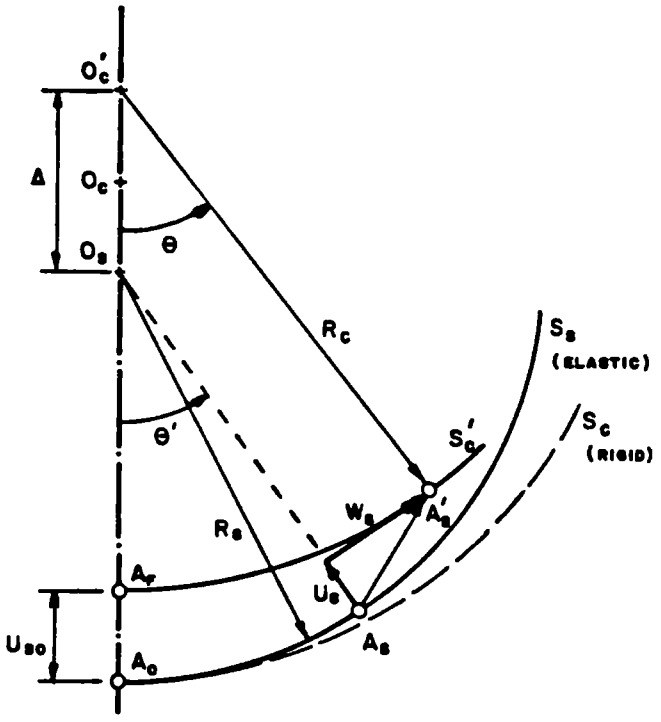

Figure 2.3 : Contact of elastic sphere and rigid seat

Next, the sphere S_s is assumed elastic and the seat S_c rigid, see Figure 2.3. By using a similar method to that employed above for the opposite case, the relationship at the

surface of contact of radius R_c, becomes:

$$U_s = U_{so}\cos\theta' + c(1-\cos\theta') \qquad (2.2.6)$$

In deriving equations (2.2.5) and (2.2.6), it was found that by neglecting second-order small quantities, the conditions of deformation in the contact region are independent of the tangential displacements. This being so in both extreme cases, when either of the two bodies is rigid, it is logical to assume that the same will apply in the case when both bodies are elastic.

The surfaces of the two bodies can be represented in spherical coordinates as,

$$S_s : \quad R_s = a_s F_s(\theta,\Phi)$$
$$S_c : \quad R_c = a_c F_c(\theta,\Phi) \qquad (2.2.7)$$

When the bodies are pressed together, the contact surface can be represented as,

$$R = \hat{a}F(\theta,\Phi) \qquad (2.2.8)$$

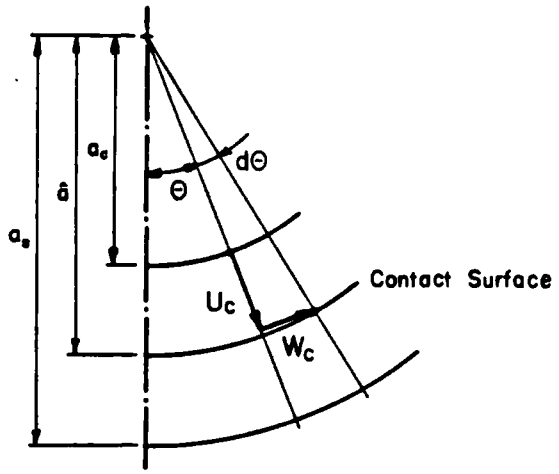

Figure 2.4 : The contact surface

From Figure 2.4, it can be seen that,

$$R_c+U_c = \hat{a}F(\theta+d\theta,\Phi) \simeq \hat{a}F(\theta+\frac{W_c}{R},\Phi) \qquad (2.2.9)$$

Expanding equation (2.2.9) as a Taylor series, it becomes:

$$R_c+U_c = \hat{a}[F(\theta,\Phi)+\frac{W_c}{R}\frac{\partial}{\partial\theta}[F(\theta,\Phi)] + \frac{W_c^2}{R^2}\frac{1}{2!}\frac{\partial^2}{\partial\theta^2}[F(\theta,\Phi)]+ \ . \ . \ .] \qquad (2.2.10)$$

In order to be able to ignore the terms in W_c,

$$\frac{\partial^n}{\partial\theta^n}[F(\theta,\Phi)] = 0 \quad \text{for all} \quad n\geq 1 \qquad (2.2.11)$$

Which leads to the conclusion that $F(\theta,\Phi)$ must be a constant, in order to conform with the assumption that the conditions of deformation in the contact region are independent of the tangential displacements; and thus the contact surface is spherical with radius R.

Thus, when both S_s and S_c are assumed to be elastic, the two extreme cases, described above, can be combined by assuming that the surface of contact is spherical with radius R.

Therefore, from equations (2.2.5) and (2.2.6) as applied to Figure 2.5, follow the relationships:

$$U_c = U_{co}\cos\theta_c'-(R_c-R)(1-\cos\theta_c')$$
$$U_s = U_{so}\cos\theta_s+(R-R_s)(1-\cos\theta_s) \qquad (2.2.12)$$

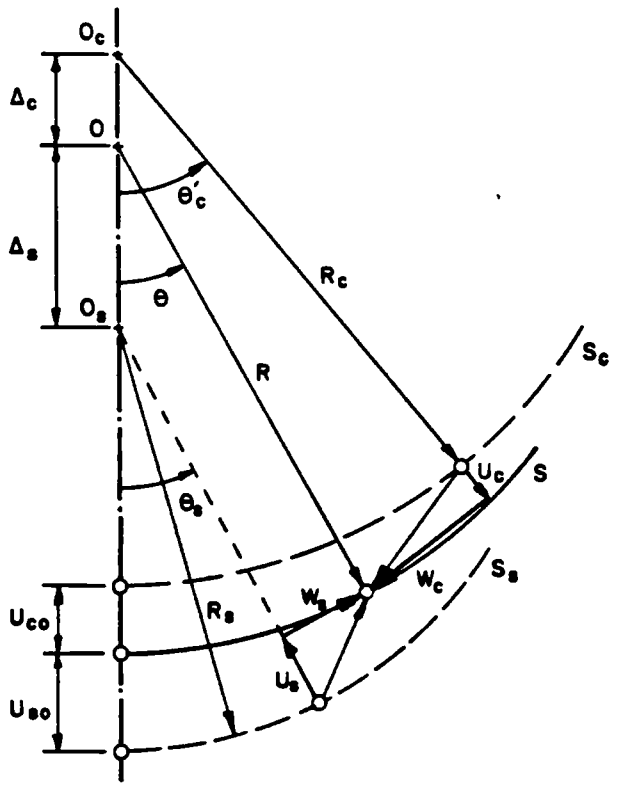

Figure 2.5 : Contact of elastic sphere and elastic seat

Now, noting that from geometrical considerations,

$$\theta_s \simeq \theta'_c \simeq \theta \qquad (2.2.13)$$

equations (2.2.12) can be combined to give:

$$U_c - U_s = (U_{co} - U_{so})\cos\theta - c(1-\cos\theta) \qquad (2.2.14)$$

Equation (2.2.14) represents the geometric relationship for the displacements within the contact region. And, of course, the relationship that holds for the displacements outside the contact region, for the two bodies not to interfere, follows directly from equation (2.2.14) and is:

$$U_c - U_s > (U_{co} - U_{so})\cos\theta - c(1-\cos\theta) \qquad (2.2.15)$$

2.3 Formulation and Solution

When considering a contact problem, the known conditions are the body geometries, the material properties and the external loading, while the unknowns are the dimensions and shape of the contact area, the approach of the two bodies and the contact pressure distribution.

By formulating the problem this way, it becomes very difficult to solve due to its non-linear nature.

One of the following two numerical methods is usually used to determine the contact area, approach and pressure distribution.

In the first method [25,28], a contact area that exceeds the expected one, as well as an approach of the two bodies is assumed. The contact area is discretised and a trial solution is obtained. If any negative pressures are present in this solution the contact area is gradually reduced until all pressures are positive or zero. Then the approach is adjusted to ensure that the bodies do not interfere outside this contact region. This process is repeated until both criteria are satisfied.

The second method [19], is based on the principle that the pressure distribution and area of contact will be such as to minimize the total elastic strain energy, subject to positive pressures within the contact region and no interference of the bodies outside it. This method can be implemented by the use of quadratic programming.

In both the aforementioned methods, the criterion of non-interference between the two bodies outside the contact region is used as a direct part of the solution, in order to provide a means by which the approach of the two bodies can be made compatible with the external loading, as well as the resulting contact area and pressure distribution. However, such interference is physically impossible, as it would require undulations of the surfaces of the two bodies, when pressed together, which are incompatible with bodies having originally smooth continuous surfaces, as is the case when a smooth sphere is contacting a smooth spherical seat.

When such a contact is stipulated, the surfaces of the deformed bodies will be expected to remain continuous, with no abrupt changes in curvature, and the resulting pressure distribution will also be continuous and dropping to zero at the contact edge. However, the non-interference criterion has still a role to play in the numerical solution of the problem in question, albeit not a direct one.

In order to be able to stipulate a smooth continuous surface for a body after the application of a given pressure distribution, it must also be smooth and continuous. However, this is not possible when the method of solution employed is numerical, as pressure and surface displacements are specified at discrete points and thus, the surface between them can take any shape compatible with the discretised pressure distribution, but not necessarily compatible with the stipulated smooth surface specified by the displacements at the discrete points.

Thus, due to the surface undulations that can be produced by the piece-wise continuous pressure distribution employed to model the expected smooth and continuous one, the discretised models of the bodies could interfere outside the contact region. Such interference however, would disappear at the limit, when the discrete points used are numerous enough to produce the theoretical continuous pressure distribution and surfaces. Therefore, the non-interference criterion, in a numerical solution of a contact problem of such form as described here, would be used only to check if the nodal point density is, at least from this point of view, satisfactory.

It is of course implied that a different way would have to be used to obtain the approach of the two bodies. Such a method is described in this section.

When considering a non-torsional axisymmetric radial loading, applied to a sphere and spherical seat in contact, such that the resulting forces act along a line connecting the centres of the two, then the contact area can be defined by a single dimension. Namely, the contact angle, as shown in Figure 2.1. This dimension characterizes the contact and is subject to a non-linear relationship with the applied external loading. The non-linearity of this relationship is the major difficulty in the solution of the problem, when formulated in the intuitively correct way described in the first paragraph of this section, and would require the use of one of the methods of solution mentioned above. However, from an engineering point of view, there is no reason why the

problem should not be formulated in the opposite way, i.e., specification of the contact angle, instead of the applied load, and upon solution, derivation of the latter.

This formulation, permits the solution of the problem, as will be seen below, without direct reference to the non-linear load-contact angle relationship; and although possibly distasteful to a mathematician, it permits comparison of results with Hertz's theory, as well as providing a design engineer with information as useful as that provided by the alternative formulation.

Accordingly, consider the contact of a smooth sphere with a smooth spherical seat as shown in Figure 2.1 and assume the contact angle to be of a given magnitude θ_c.

The first step in the solution is to discretise this contact area as shown in Figure 2.6.

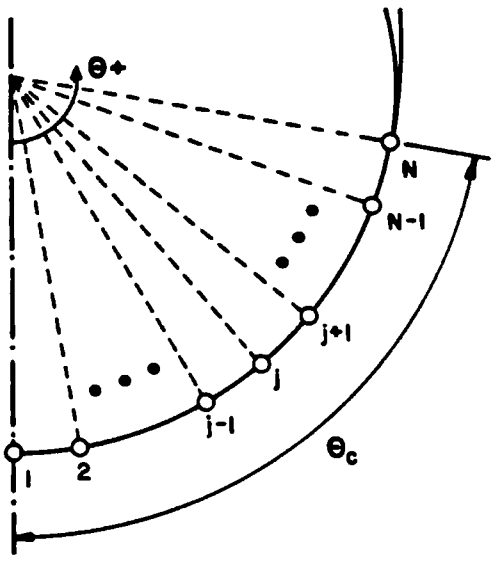

Figure 2.6 : Discretised contact area

Equation (2.2.14) is applicable to all the points in the contact area, but for point 1, when $\theta=0$, it conveys no useful information. However, at point 1 the sum of the displacements of the two bodies is equal to their approach,

$$\delta = U_{co}-U_{so} \quad * \tag{2.3.1}$$

It is thus possible, using equations (2.2.14) and (2.3.1), to write the geometric relationship governing the displacements in the contact region in matrix form,

$$A\times(U_c-U_s) = b \tag{2.3.2}$$

where,

$$A = \begin{bmatrix} 1 & 0 & \cdots & 0 & 0 & 0 & \cdots & 0 & 0 \\ \cos\theta_2 & -1 & \cdots & 0 & 0 & 0 & \cdots & 0 & 0 \\ \vdots & \vdots & \cdots & \vdots & \vdots & \vdots & \cdots & \vdots & \vdots \\ \cos\theta_{j-1} & 0 & \cdots & -1 & 0 & 0 & \cdots & 0 & 0 \\ \cos\theta_j & 0 & \cdots & 0 & -1 & 0 & \cdots & 0 & 0 \\ \cos\theta_{j+1} & 0 & \cdots & 0 & 0 & -1 & \cdots & 0 & 0 \\ \vdots & \vdots & \cdots & \vdots & \vdots & \vdots & \cdots & \vdots & \vdots \\ \cos\theta_{N-1} & 0 & \cdots & 0 & 0 & 0 & \cdots & -1 & 0 \\ \cos\theta_N & 0 & \cdots & 0 & 0 & 0 & \cdots & 0 & -1 \end{bmatrix} \tag{2.3.3}$$

---

* the minus sign is due to the sign convention used for U_s and U_c

$$b = \begin{bmatrix} \delta \\ c(1-\cos\theta_2) \\ \vdots \\ c(1-\cos\theta_{j-1}) \\ c(1-\cos\theta_j) \\ c(1-\cos\theta_{j+1}) \\ \vdots \\ c(1-\cos\theta_{N-1}) \\ c(1-\cos\theta_N) \end{bmatrix} \qquad (2.3.4)$$

and, U_s and U_c are the vector of displacements of the sphere and seat respectively, at the specified N points.

Noting that, due to the nature of matrix A,

$$A \times A \equiv I \qquad (2.3.5)$$

where, I is the unit matrix.

equation (2.3.2) can be rewritten as,

$$U_c - U_s = A \times b \qquad (2.3.6)$$

Now, using equation (1.4.1), the displacements at each specified point within the contact region can be written as a function of all the pressure magnitudes at the same points, as follows:

$$U_s = M_s \times p_s \qquad (2.3.7)$$

and

$$U_c = M_c \times p_c \qquad (2.3.8)$$

Further, at all points in the contact region the pressure magnitudes acting on the sphere and seat are equal, making it possible to write,

$$p_c = p_s = p \tag{2.3.9}$$

Thus using equations (2.3.7), (2.3.8) and (2.3.9), equation (2.3.6) can be rewritten as,

$$[M_c - M_s] \times p = A \times b \tag{2.3.10}$$

By premultiplying both sides of equation (2.3.10) with the inverse of $[M_c - M_s]$, it becomes:

$$p = [M_c - M_s]^{-1} \times A \times b \tag{2.3.11}$$

and letting

$$B = [M_c - M_s]^{-1} \times A \tag{2.3.12}$$

equation (2.3.11) can be rewritten as,

$$p = B \times b \tag{2.3.13}$$

Equation (2.3.13), specifies the pressure distribution within the contact region, but note that, the first element of **b**, namely δ, is as yet unspecified. However, using the fact that $p_N=0$, as it corresponds to the point where the contact area ends, δ can be obtained from:

$$\delta = - \frac{\sum_{i=2}^{N} B(N,i)b(i)}{B(N,1)} \tag{2.3.14}$$

Thus, **b** is now completely specified, so that all the

pressures within the contact region can be obtained from equation (2.3.13).

From the computed pressure distribution, the applied external load on the sphere, that would result in a contact angle of magnitude θ_c, can be obtained.

At this point, by using equation (1.4.1) again, but this time specifying the displacements outside the contact region, the non-interference criterion, as expressed by equation (2.2.15), can be checked and a decision made as to whether the number of nodal points used in the discretisation of the contact angle were numerous enough.

Equation (2.3.13), can also be used for the case when the seat is truncated at θ_c, i.e. for the case of a restricted contact. In this case p_N will not be equal to zero unless the specified approach is exactly equal to that obtained by setting it equal to zero. Setting the approach smaller serves no usefull purpose, as it implies a contact angle smaller than θ_c and produces negative pressures. Setting the approach larger however, implies a larger unrestricted contact angle than θ_c and thus, the pressure distribution for the case of a restricted contact is obtained. The non-interference criterion is of course irrelevant in this case, as by definition the seat does not extend past θ_c and thus, no interference is possible.

2.4 Results

The formulation of a computer algorithm for the solution of the contact problem is a very simple exercise, as the only complication presented is the requirement for matrix manipulation subroutines, which are available as software packages on most computers.

The number of nodal points used in the solution affects the accuracy of the results obtained. Figure 2.8 presents the pressure distributions obtained with different numbers of nodal points for a 10° contact, together with the resulting load, maximum pressure and approach. The choice of the optimum number of nodal points for a particular contact was made by increasing their density until the change in the results obtained was less than 1% between consecutive increases.

The non-interference criterion discussed in the previous section was checked in all cases, and was found not to be violated for all of the nodal point densities employed. Note, that the check was made at four points, with a density double that used inside the contact region.

No deformed shapes are shown as part of the results owing to the high cost that would be involved in obtaining them. This is due to the need to discretise the complete surfaces of two bodies. However, the deformed shapes within the contact region were checked and found to conform to a circular arc, as expected. As an example of deformed shapes see Figure 2.1, which is qualitatively correct.

Results were obtained for three different ratios of radii, combinations of two different materials and a range of different seat thicknesses. One material is assumed to be steel with a Young's modulus of 200 GN/m^2 and a Poisson's ratio of 0.3. The other material is assumed to high molecular weight polyethylene with a Young's modulus of 500 MN/m^2 and a Poisson's ratio of 0.38. In the case of the polyethylene, it is assumed that it behaves as alinearly elastic material by ignoring creep. Thus, the results obtained for it can be assumed to be correct only if the application of the external load is of a very short duration.

Figures 2.9 through 2.16, present the pressure distributions for different contact angles, ratios of radii, materials and seat thicknesses. It can be seen in these figures that for the case of infinite seat thickness, the shape of the pressure distributions starts by being exactly elipsoidal for small contact angles, being thus compatible with the shape assumed by Hertz. However, they deviate sharply from this shape as the contact angle reaches 90°.

By further comparing the results presented in Figures 2.9 through 2.13, it can be seen that that their magnitude is dependent on the degree of conformity of the two bodies.

Figure 2.16, presents an interesting point that was encountered, when the seat is of softer material than the sphere. In this case a limiting contact angle exists, which can not be exceeded within the confines of linear elasticity, irrespective of the magnitude of the applied load. It can be seen from equation

(2.2.14), that for a 90° contact angle to be possible, the displacements of the surfaces of the two bodies should be able to satisfy the following equation at the contact edge,

$$U_s = c+U_c \qquad (2.4.1)$$

When the material of the seat is softer than that of the sphere, equation (2.4.1) can not be satisfied even if the clearance is zero. From this, it can be surmised that the limiting contact angle is a function of the clearance and the relative material properties of the two bodies.

Figure 2.17, presents the results of truncating the seat at 10°. However, the pressure singularities involved should be considered only qualitatively correct for two reasons. First, the model used for the seat, as described in Chapter 1, becomes more inaccurate the nearer the seat is truncated to the edge of the contact zone. And second, the elements used in the region of the pressure singularity are inadequate, so some type of singularity element should be employed [25]. However, in the model used, such elements are precluded for the reason explained in Section 3 of Chapter 1.

In Hertz's theory it is assumed that both bodies can be considered as elastic half-spaces and, if they are of the same material, should undergo the same displacements at corresponding contact points. This is strongly contradicted by the results presented in Figure 2.17. This figure shows that, even for a small approach, the ratio of displacements is still not quite equal to one. However, extrapolation of the curve could

be seen to imply asymptotic equality at very small approaches, which would be as expected, because of the very localised effect of the stresses in that case.

Figures 2.19 through 2.21, present plots of dimensionless groups. It can be seen from these, that Hertz's theory overestimates the approach and the contact area, while underestimating the maximum pressure. However, for contacts angles up to about 30° it does provide a good approximation. This can be attributed to the conformity of the bodies, as despite the large contact area involved, invalidating an assumption of Hertz's theory, the actual displacements involved remain comparatively small.

Figures 2.22 through 2.24, present plots of results in the form of dimensionless groups, obtained for contacts between bodies of different materials, in an attempt to present some measure of the quality of the method of solution presented herein.

2.5 Conclusions and suggestions for further work

A numerical method has been presented for the solution of the conformal contact problem between an elastic sphere and a spherical cavity in an infinite elastic medium or an elastic spherical layer with a rigid substrate. This method presents advantages from the point of view of computational time, over other such methods, by avoiding the use of an iterative solution.

Hertz's theory was shown to provide reasonably accurate

results for an infinite seat thickness and contact angles up to 30°, even when the assumption of relatively small contact footprint dimensions has been violated. However, for the case of finite seat thicknesses no such specific statement can be made, as the difference in the results varies with seat thickness and contact angle. In this case Hertz's theory can be used, as a reasonable approximation, only when the contact arc is relatively small compared with the seat thickness.

When the seat is of softer material than the sphere, a limiting contact angle exists, which is a function of clearance and material properties and can not be exceeded, within the limits of linear elasticity theory, irrespective of the magnitude of the applied load.

When the arc available for contact is insufficient, stress concentrations result at its edge. However, in order to obtain quantitative measures of these concentrations, different models for the bodies must be employed, that permit the use of singularity elements.

The stress equations, which were used in Chapter 1 to derive the displacements, can be employed to obtain the stresses which result in the two bodies from the pressure distributions under the contacts in question.

No mention of experimental results, for the particular types of contact described, has been found in the literature and thus, any further work should first concentrate on obtaining such results, in order to validate the theory. Any discrepancies in the theory, that will be revealed by such results,

can be attributed to two major factors. First, in a real situation no frictionless contact can exist. And second, the models used for the seat are not accurate in describing any real situation in which it would be possible to load the sphere, as they involve complete cavities. In a real situation, the arrangement would be a variant of the one shown in Figure 2.7.

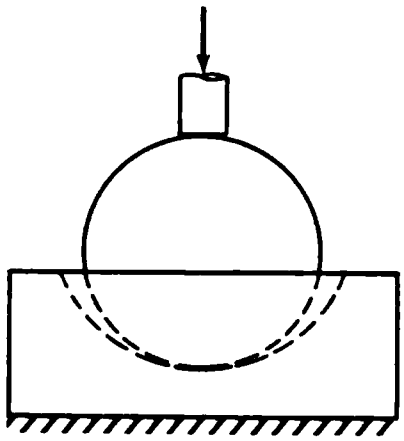

Figure 2.7 : Possible experimental arrangement

However, the method as it stands might prove adequate for design purposes, as it is more accurate, for large angle conformal contacts, than Hertz's theory.

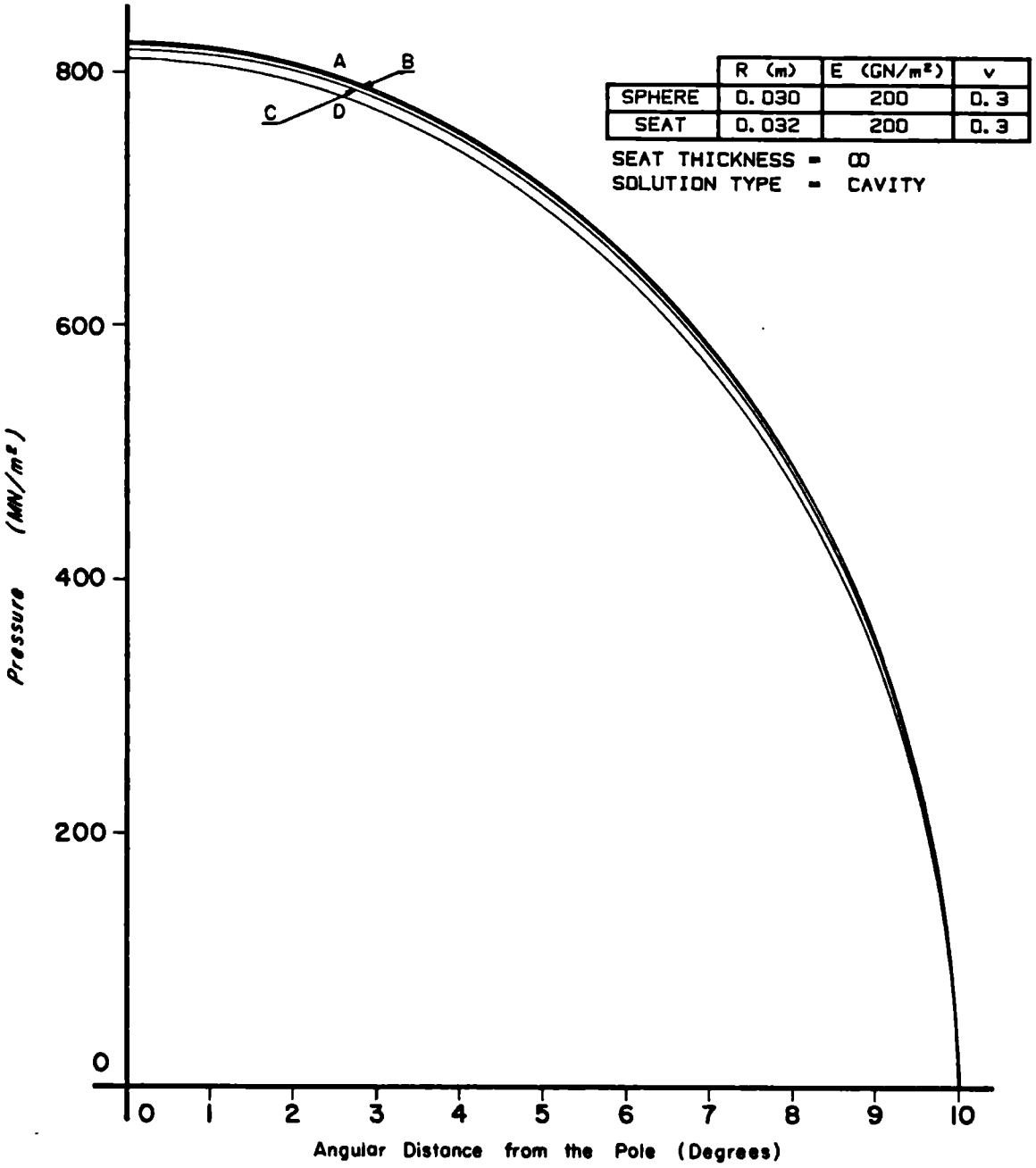

	NUMBER OF ELEMENTS	LOAD (KN)	MAXIMUM PRESSURE (MN/m²)	APPROACH (μm)
A	40	46.64	822.453	57.751
B	20	46.22	821.440	57.423
C	10	45.41	818.384	56.800
D	5	43.82	810.412	55.633

FIGURE 2.8 : Importance of Nodal Point Density

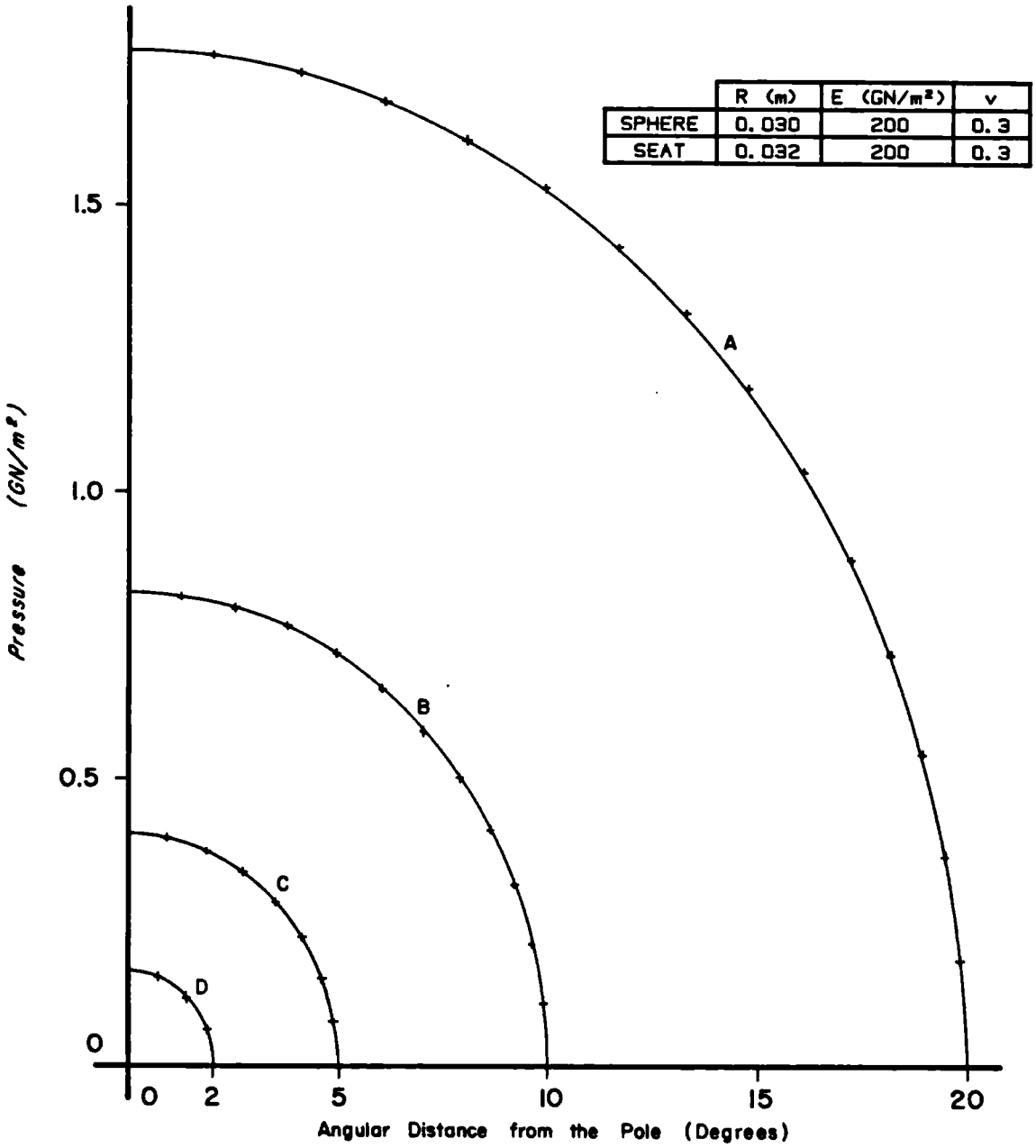

	SEAT THICKNESS	LOAD (KN)	APPROACH (μm)	CONTACT ANGLE (Degrees)	SOLUTION TYPE
A	∞	388.33	227.614	20	CAVITY
B		46.64	57.751	10	
C		5.61	14.476	5	
D		0.35	2.339	2	

FIGURE 2.9 : Unrestricted Dry Contact

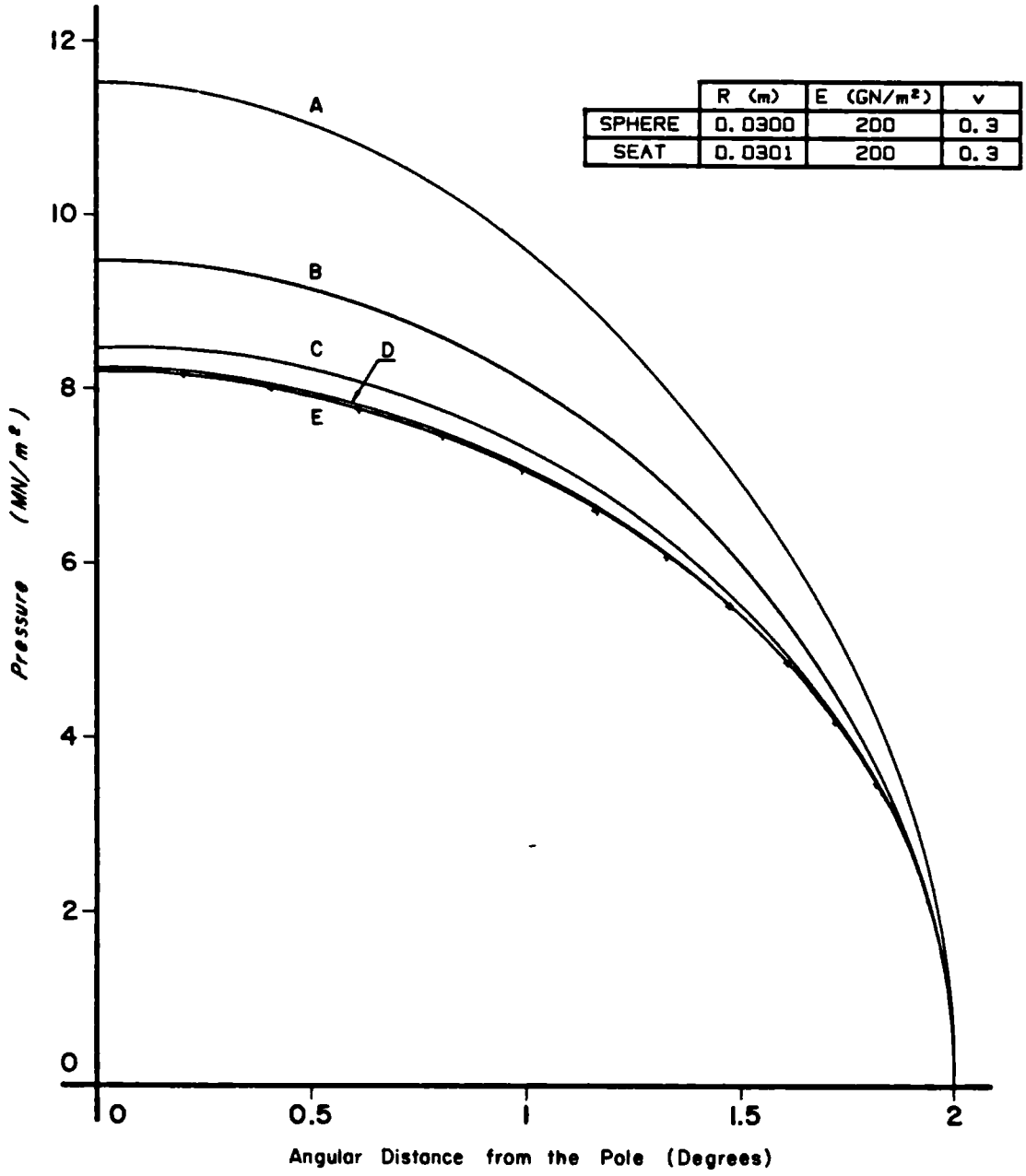

	R (m)	E (GN/m²)	ν
SPHERE	0.0300	200	0.3
SEAT	0.0301	200	0.3

	SEAT THICKNESS (m)	LOAD (N)	APPROACH (μm)	SOLUTION TYPE
A	0.0005	24.06	0.101	LAYER
B	0.0010	20.72	0.099	
C	0.0020	18.88	0.103	
D	0.0050	18.38	0.111	
E	∞	18.29	0.117	CAVITY

FIGURE 2.10 : Unrestricted 2° Dry Contact

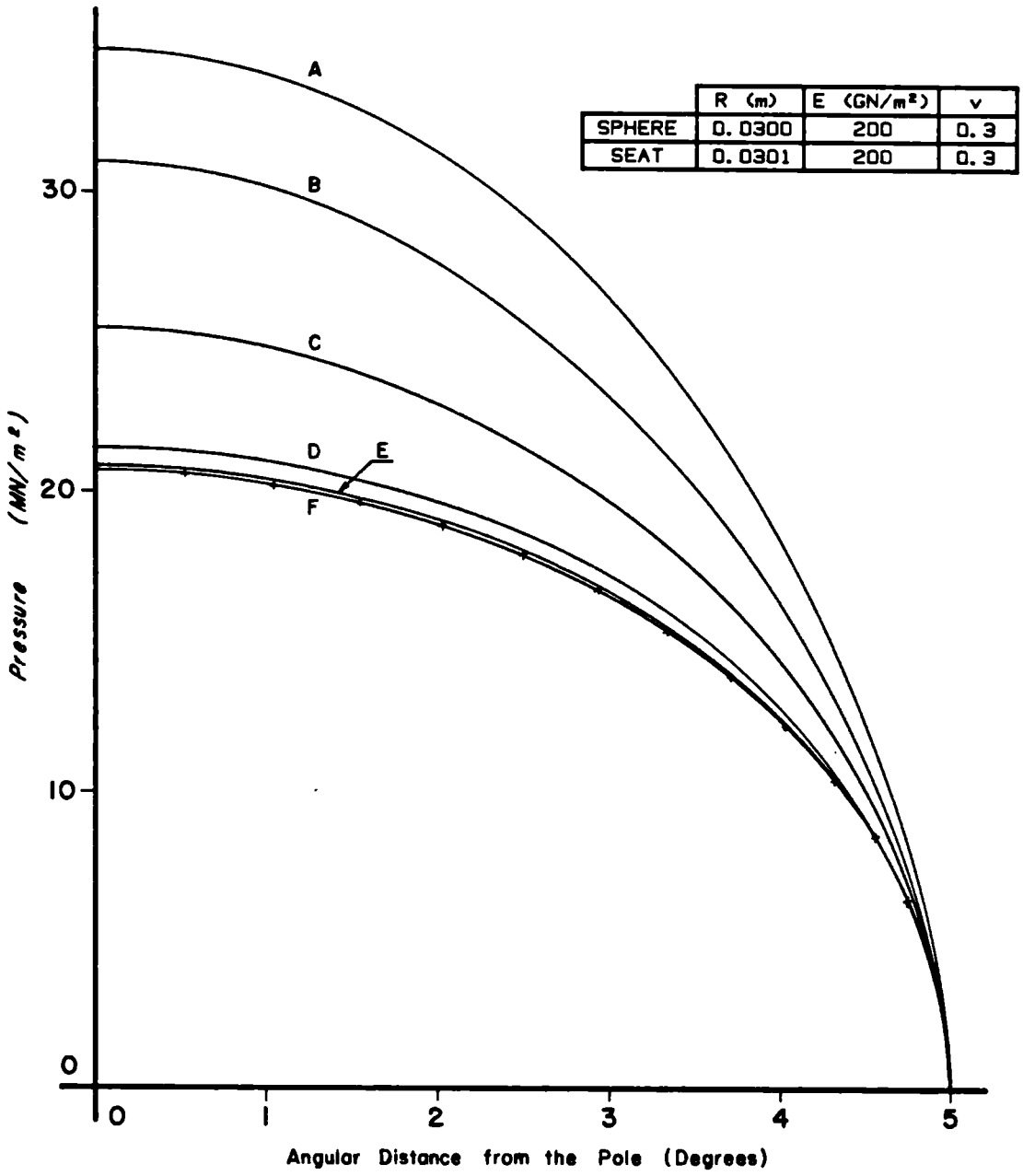

	R (m)	E (GN/m²)	ν
SPHERE	0.0300	200	0.3
SEAT	0.0301	200	0.3

	SEAT THICKNESS (m)	LOAD (N)	APPROACH (μm)	SOLUTION TYPE
A	0.0005	455.74	0.659	LAYER
B	0.0010	403.16	0.634	
C	0.0020	343.35	0.620	
D	0.0050	299.68	0.645	
E	0.0100	291.87	0.678	
F	∞	288.50	0.724	CAVITY

FIGURE 2.11 : Unrestricted 5° Dry Contact

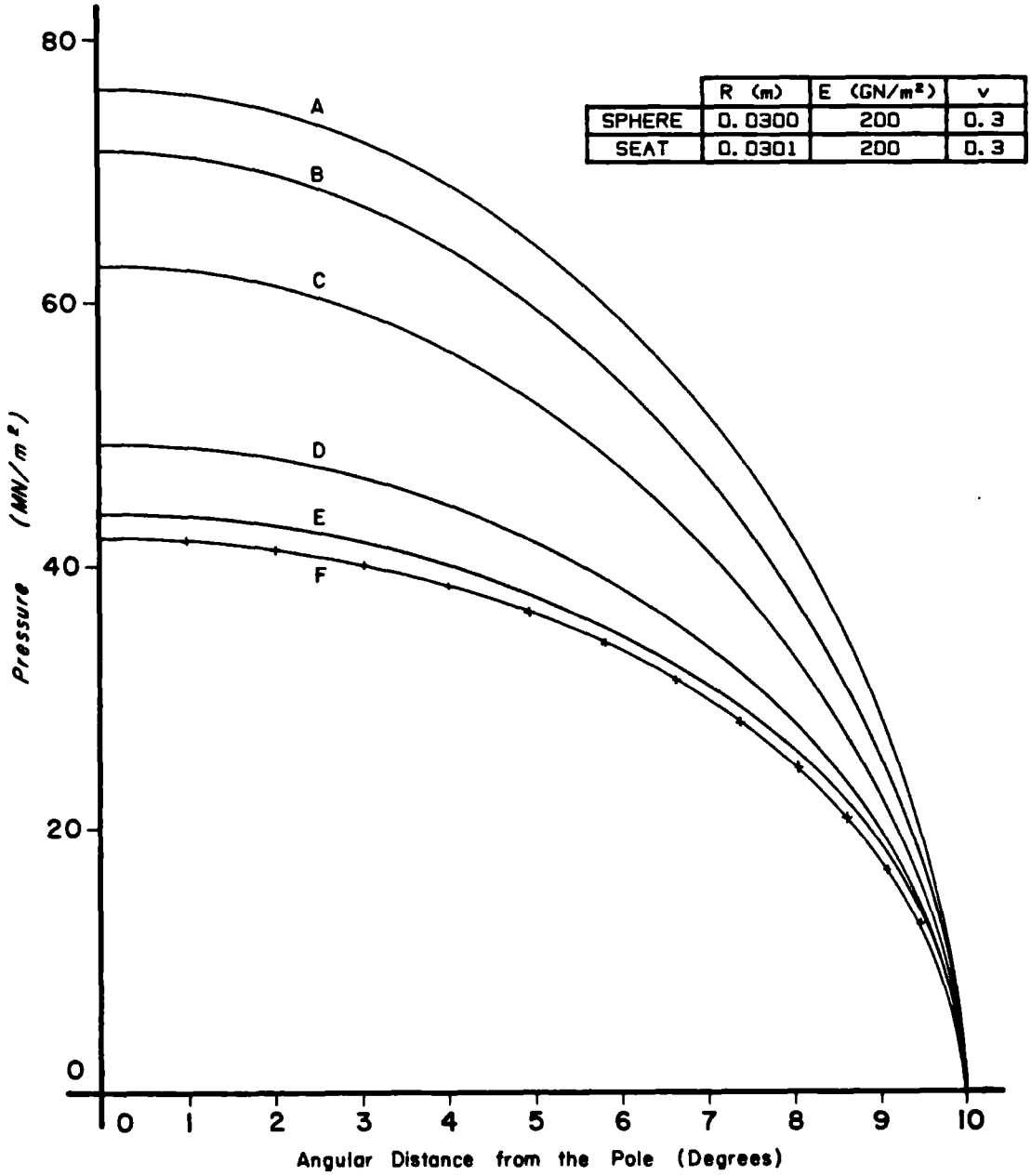

	R (m)	E (GN/m²)	ν
SPHERE	0.0300	200	0.3
SEAT	0.0301	200	0.3

	SEAT THICKNESS (m)	LOAD (KN)	APPROACH (μm)	SOLUTION TYPE
A	0.0005	4.09	2.715	LAYER
B	0.0010	3.76	2.629	
C	0.0020	3.29	2.534	
D	0.0050	2.71	2.489	
E	0.0100	2.47	2.580	
F	∞	2.38	2.872	CAVITY

FIGURE 2.12 : Unrestricted 10° Dry Contact

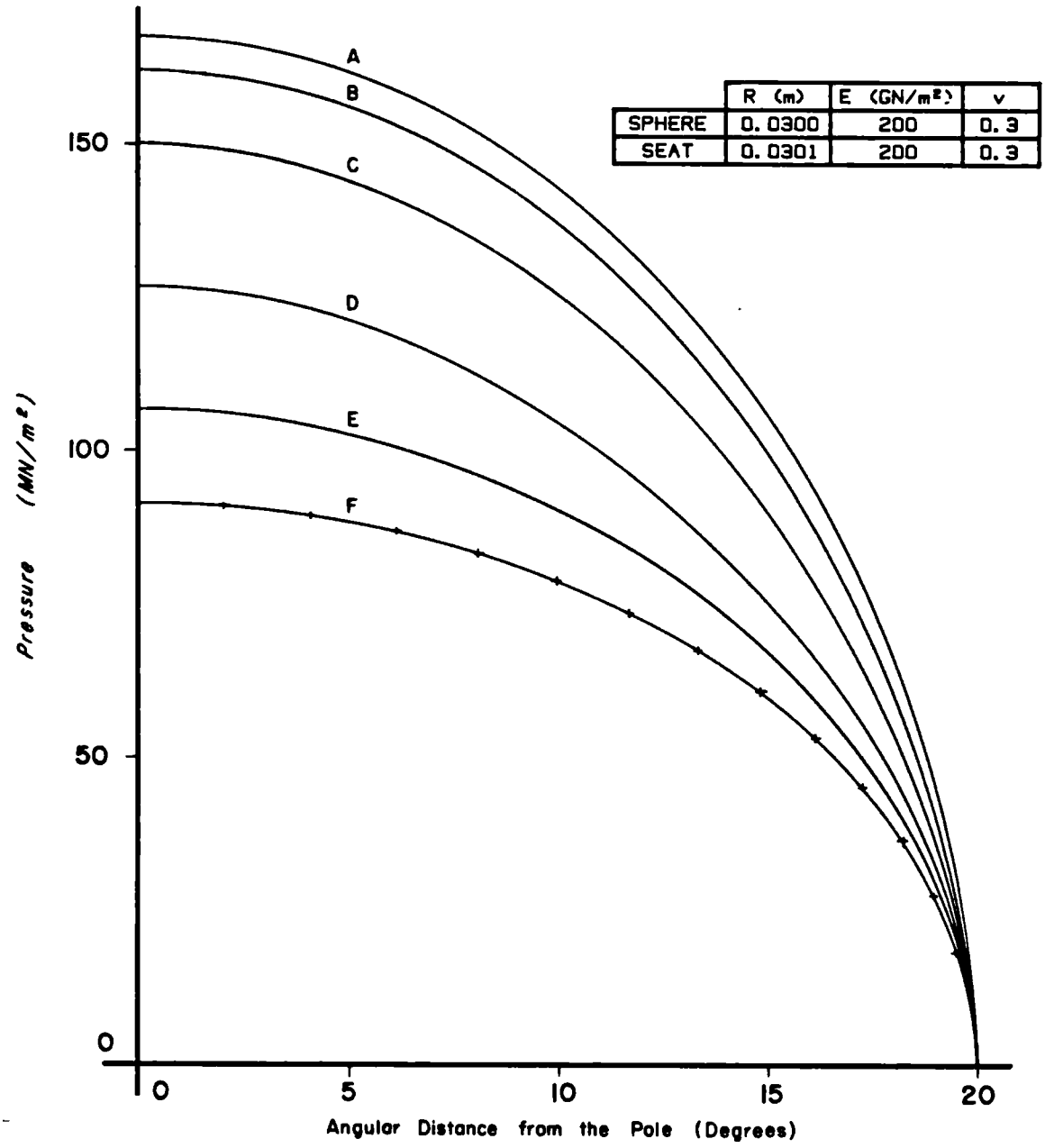

	R (m)	E (GN/m²)	ν
SPHERE	0.0300	200	0.3
SEAT	0.0301	200	0.3

	SEAT THICKNESS (m)	LOAD (KN)	APPROACH (μm)	SOLUTION TYPE
A	0.0005	35.71	10.946	LAYER
B	0.0010	33.94	10.720	
C	0.0020	30.86	10.390	
D	0.0050	26.08	10.022	
E	0.0100	22.73	10.006	
F	∞	20.01	11.381	CAVITY

FIGURE 2.13 : Unrestricted 20° Dry Contact

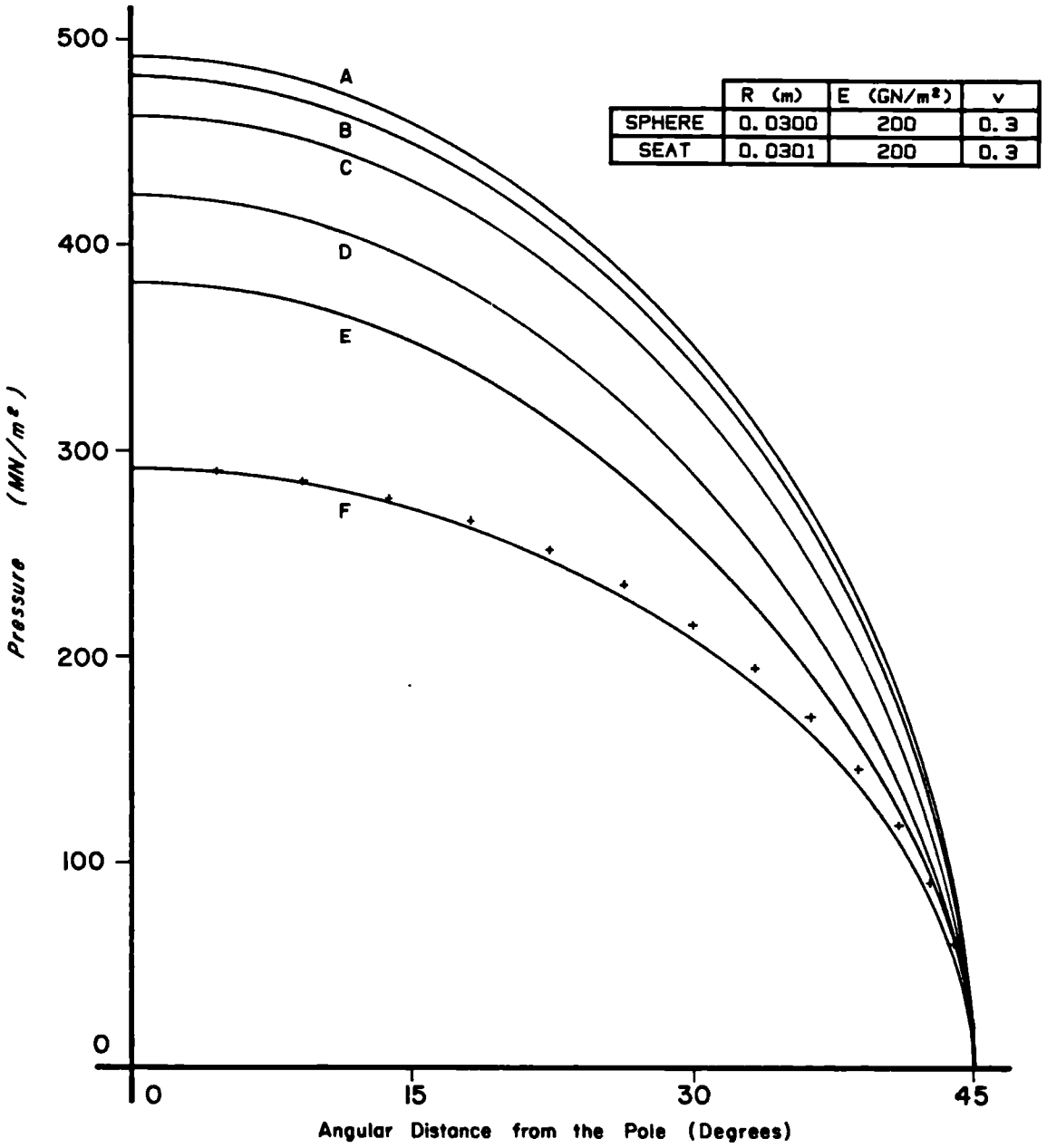

	R (m)	E (GN/m²)	ν
SPHERE	0.0300	200	0.3
SEAT	0.0301	200	0.3

	SEAT THICKNESS (m)	LOAD (MN)	APPROACH (μm)	SOLUTION TYPE
A	0.0005	0.46	55.576	LAYER
B	0.0010	0.45	55.116	
C	0.0020	0.43	54.321	
D	0.0050	0.38	53.524	
E	0.0100	0.34	53.674	
F	∞	0.27	62.929	CAVITY

FIGURE 2.14 : Unrestricted 45° Dry Contact

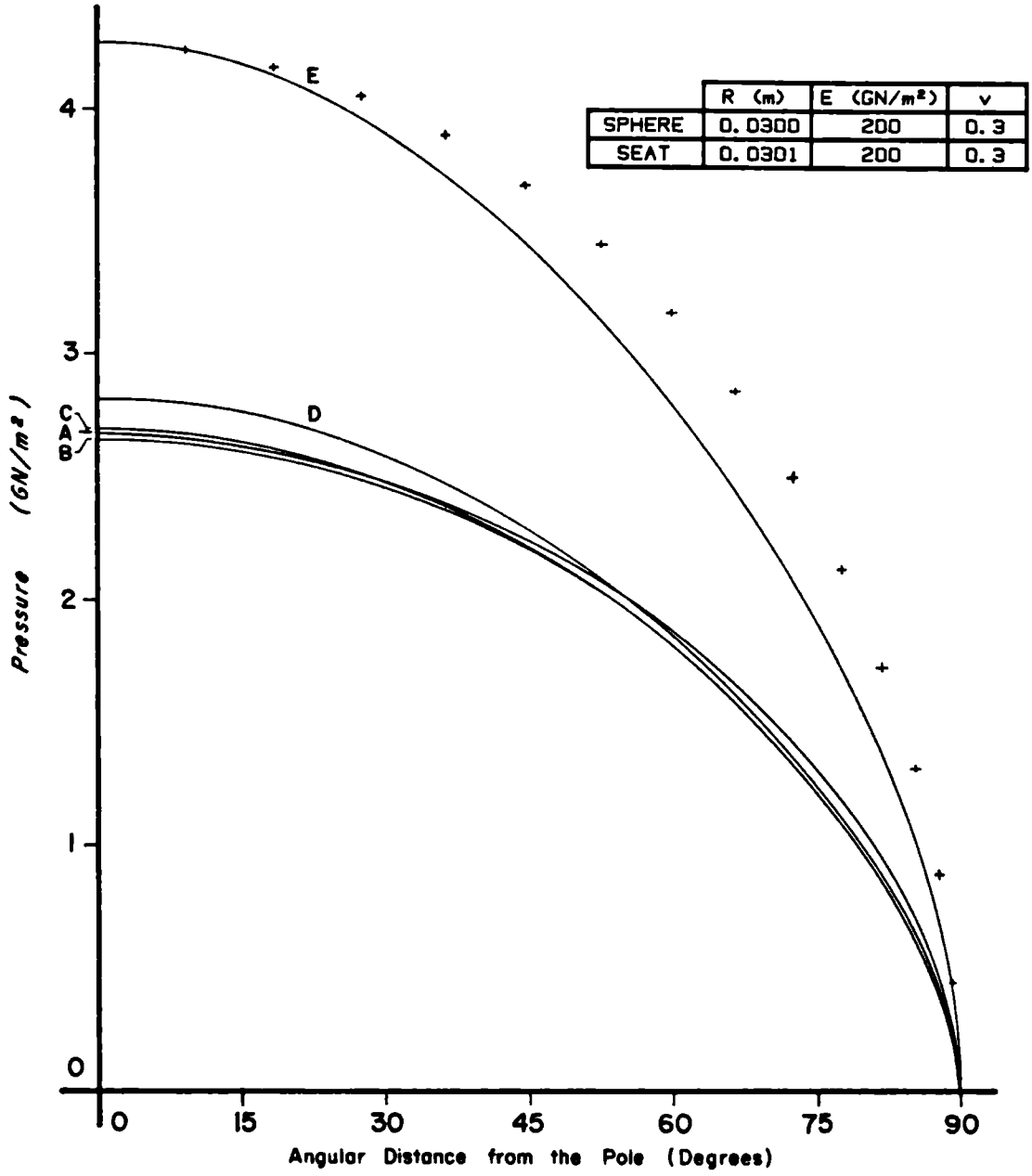

	SEAT THICKNESS (m)	LOAD (MN)	APPROACH (mm)	SOLUTION TYPE
A	0.001	6.02	0.317	LAYER
B	0.002	5.93	0.325	
C	0.005	5.92	0.355	
D	0.010	6.12	0.415	
E	∞	9.24	1.045	CAVITY

FIGURE 2.15 : Unrestricted 90° Dry Contact

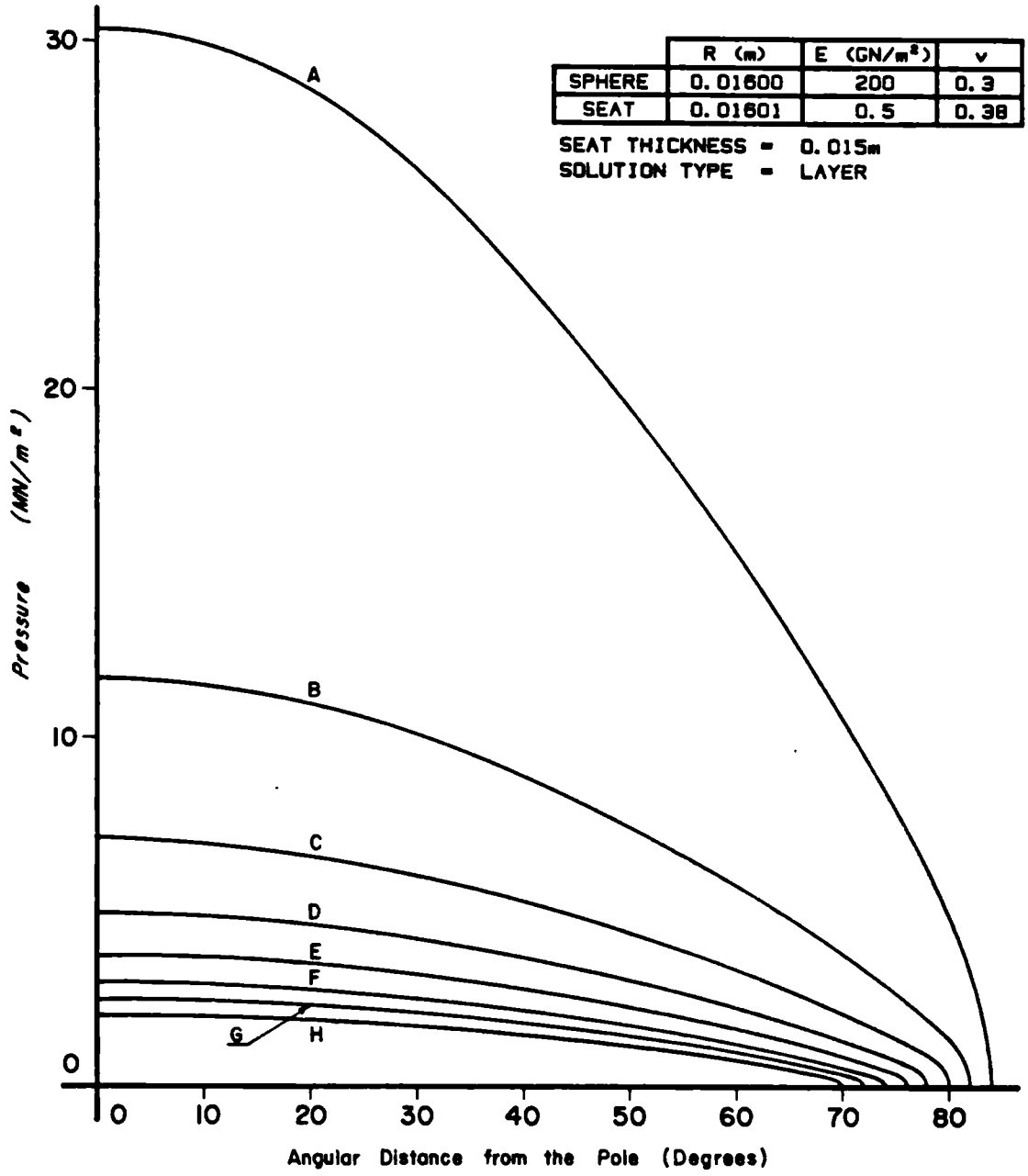

	CONTACT ANGLE (Degrees)	LOAD (KN)	APPROACH (μm)
A	84	16.28	420.055
B	82	6.18	162.552
C	80	3.65	98.014
D	78	2.50	68.682
E	76	1.85	51.938
F	74	1.43	41.121
G	72	1.13	33.565
H	70	0.92	27.995

FIGURE 2.16 : Unrestricted Dry Contact

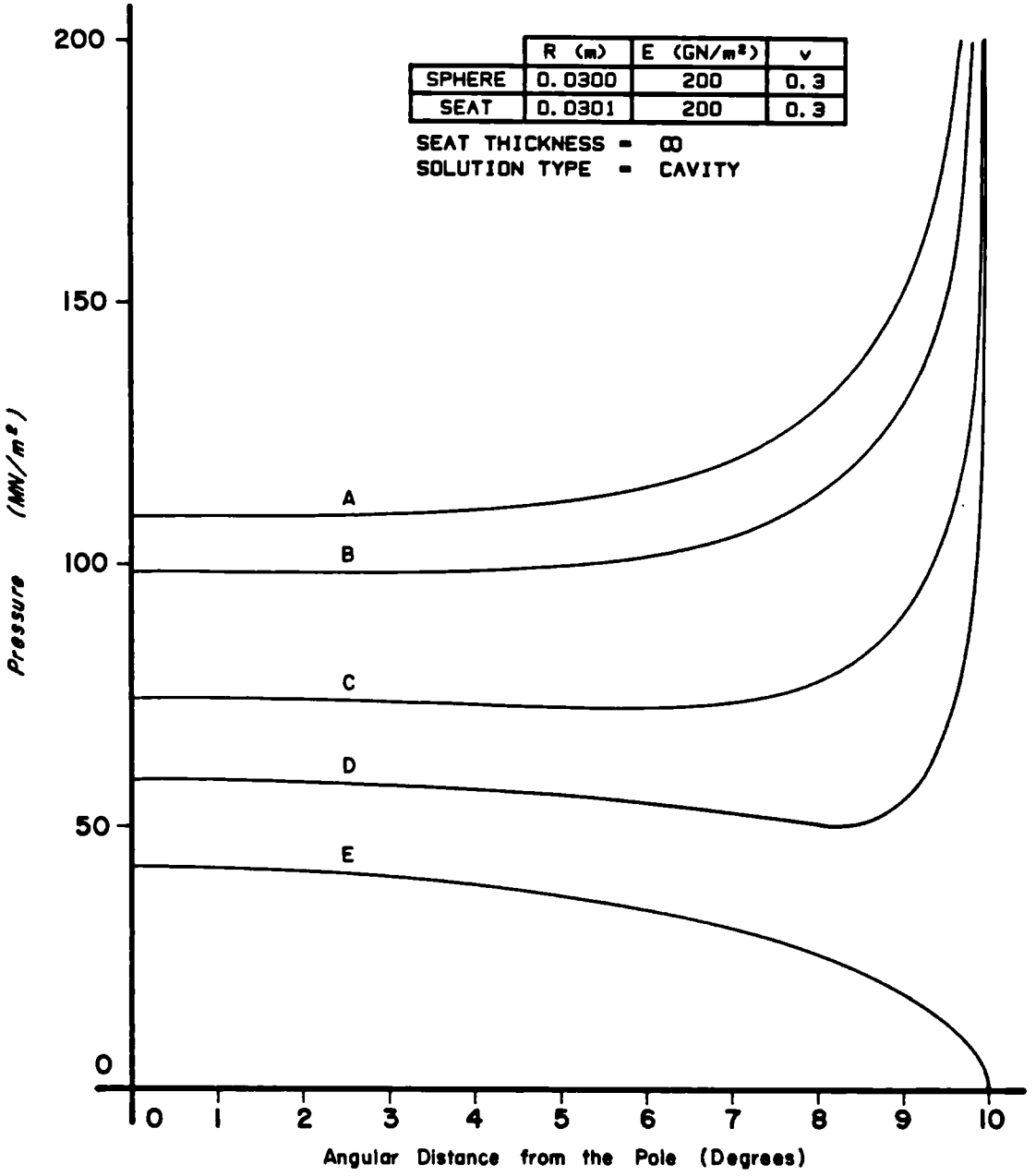

	LOAD (KN)	PRESSURE AT THE POLE (MN/m²)	APPROACH (μm)
A	13.42	109.225	11.381
B	11.63	98.457	10.000
C	7.74	74.539	7.000
D	5.14	59.007	5.000
E	2.38	42.167	2.872

FIGURE 2.17 : Restricted 10° Dry Contact

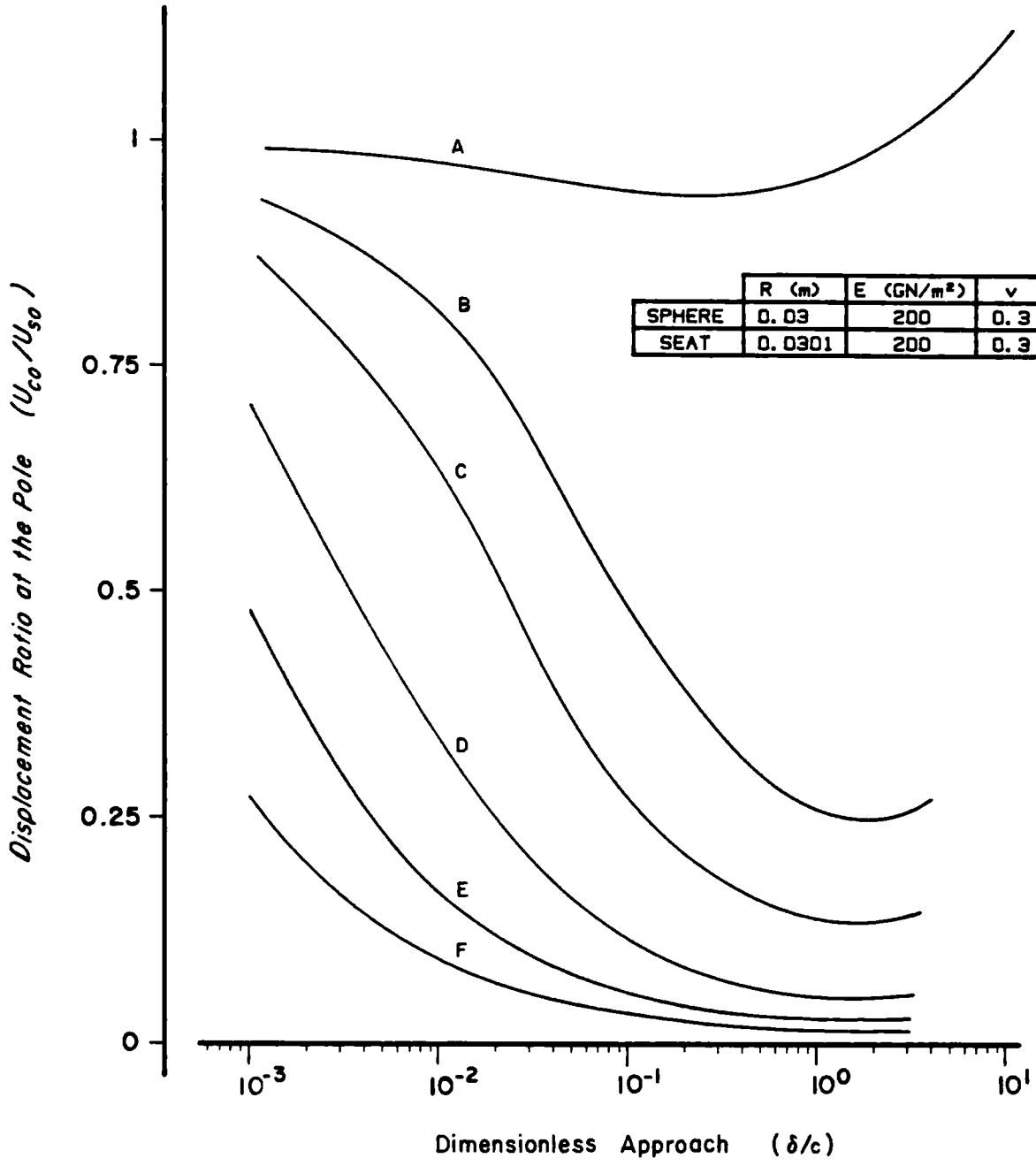

	R (m)	E (GN/m²)	ν
SPHERE	0.03	200	0.3
SEAT	0.0301	200	0.3

	DIMENSIONLESS SEAT THICKNESS (H/c)
A	∞
B	100
C	50
D	20
E	10
F	5

FIGURE 2.18 :

Variation of Displacement Ratio at the Pole with Approach

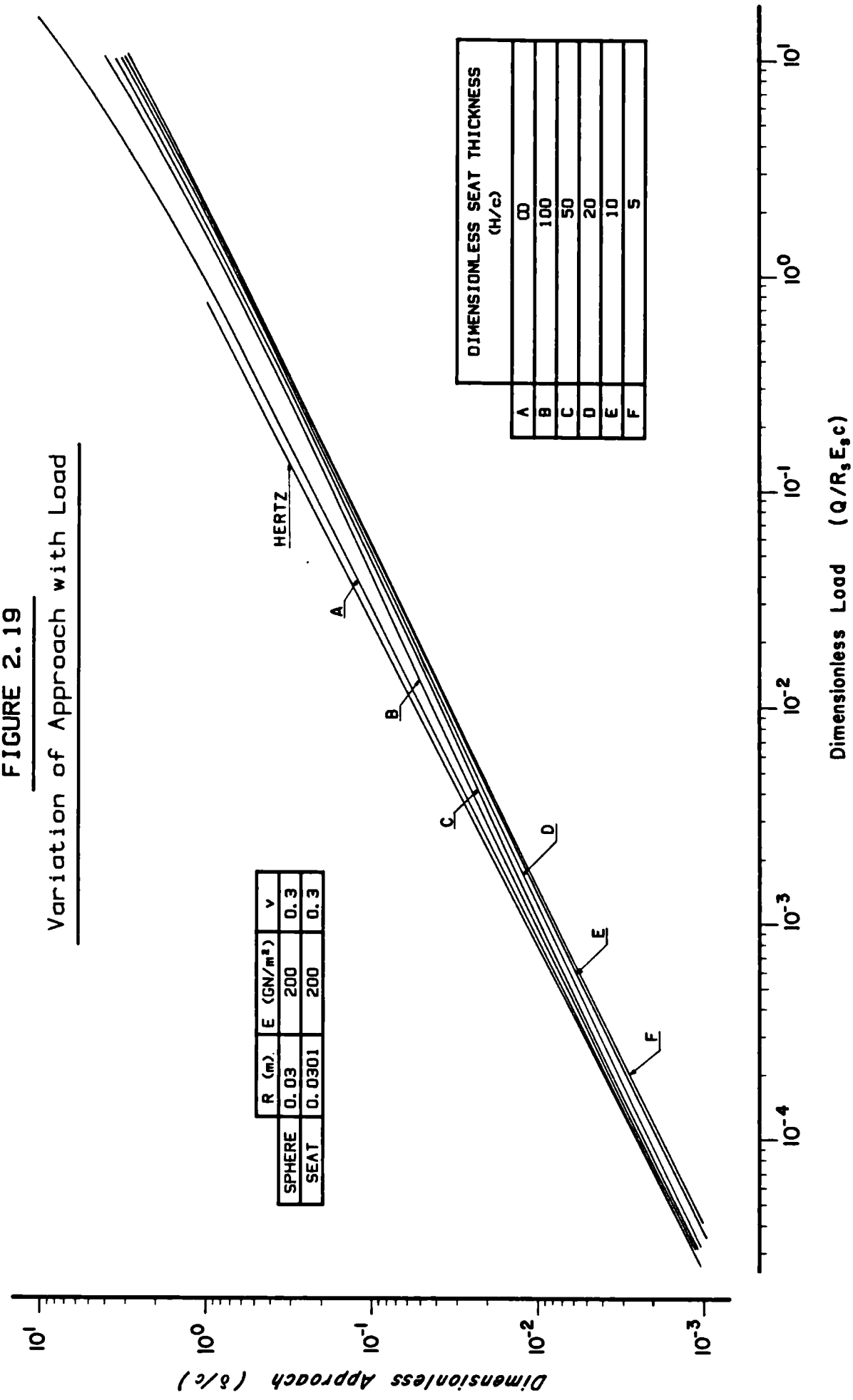

FIGURE 2.19

Variation of Approach with Load

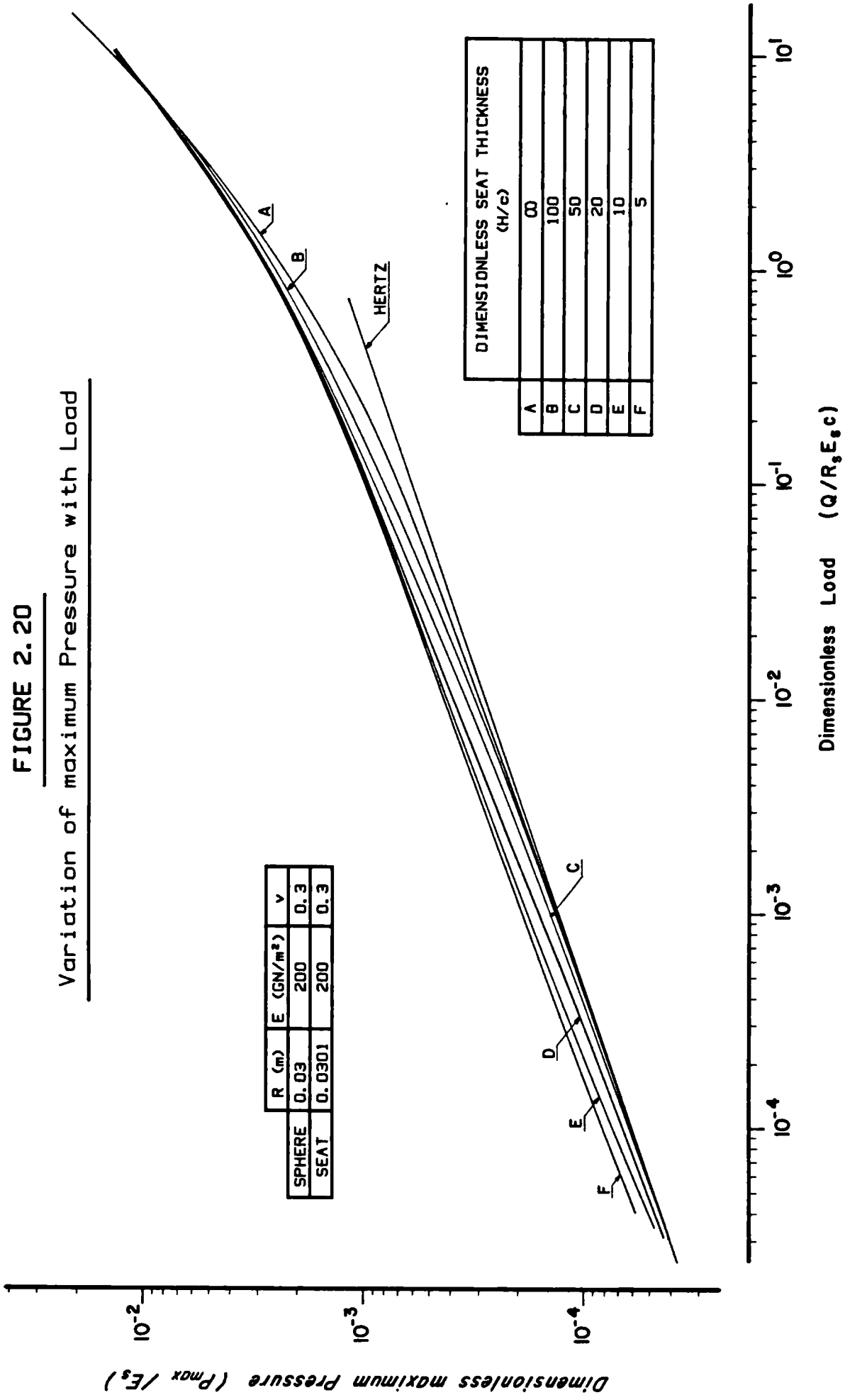

FIGURE 2.20

Variation of maximum Pressure with Load

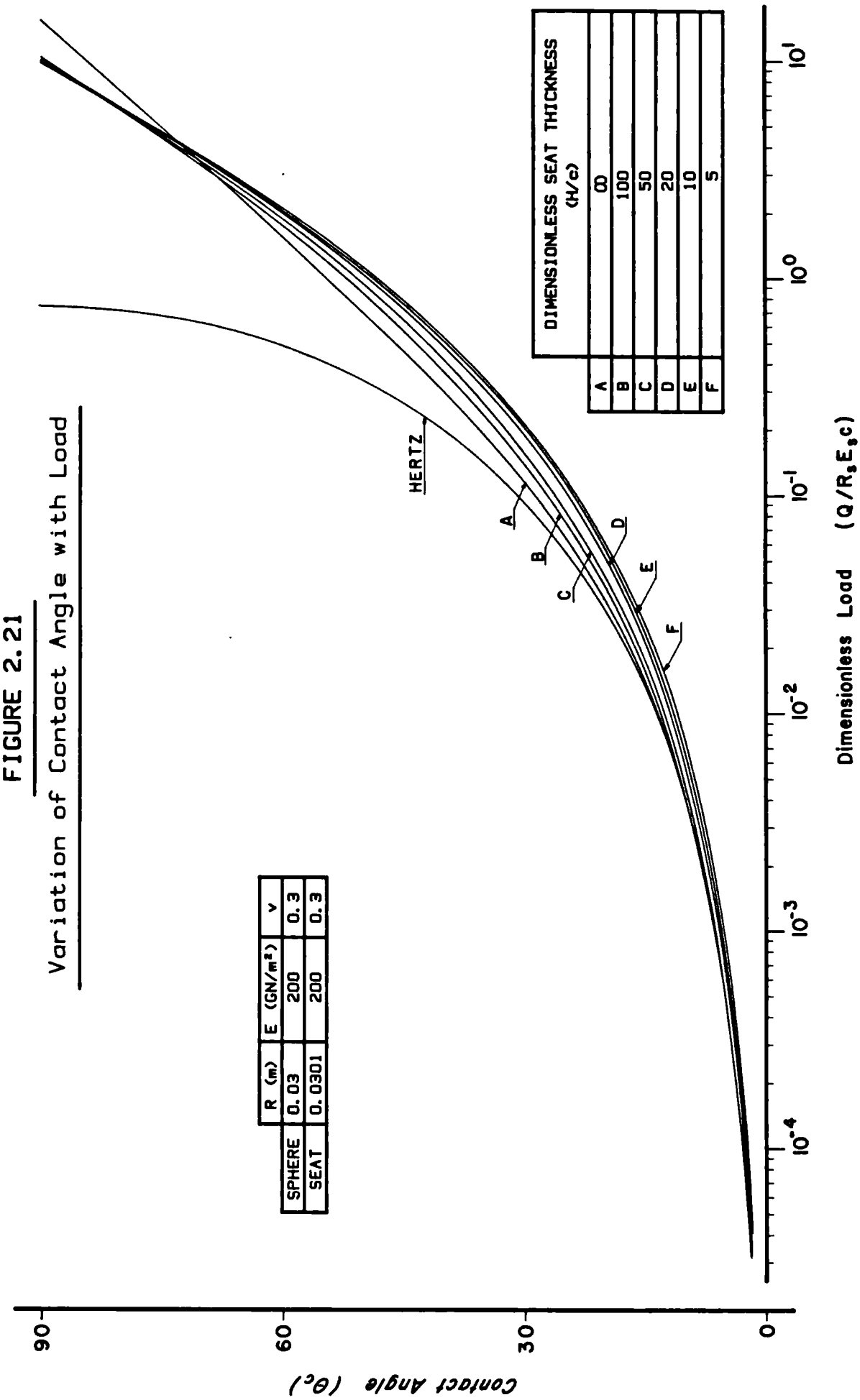

FIGURE 2.21

Variation of Contact Angle with Load

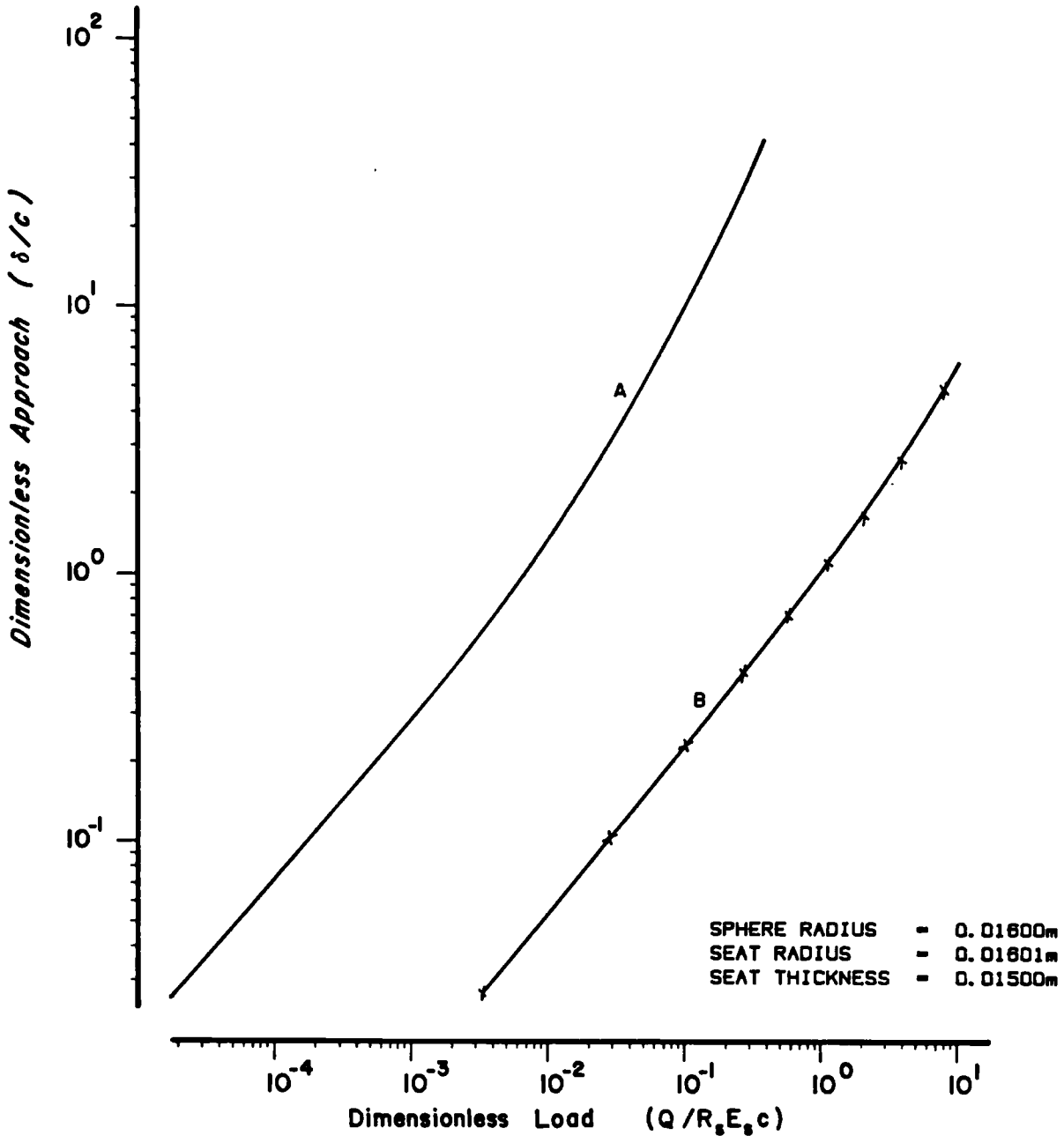

	Young's Modulus (GN/m²)		Poisson's Ratio	
	SPHERE	SEAT	SPHERE	SEAT
A	200	0.5	0.3	0.38
B	200	200	0.3	0.3
×	0.5	0.5	0.38	0.38

FIGURE 2.22 : Variation of Approach with Load

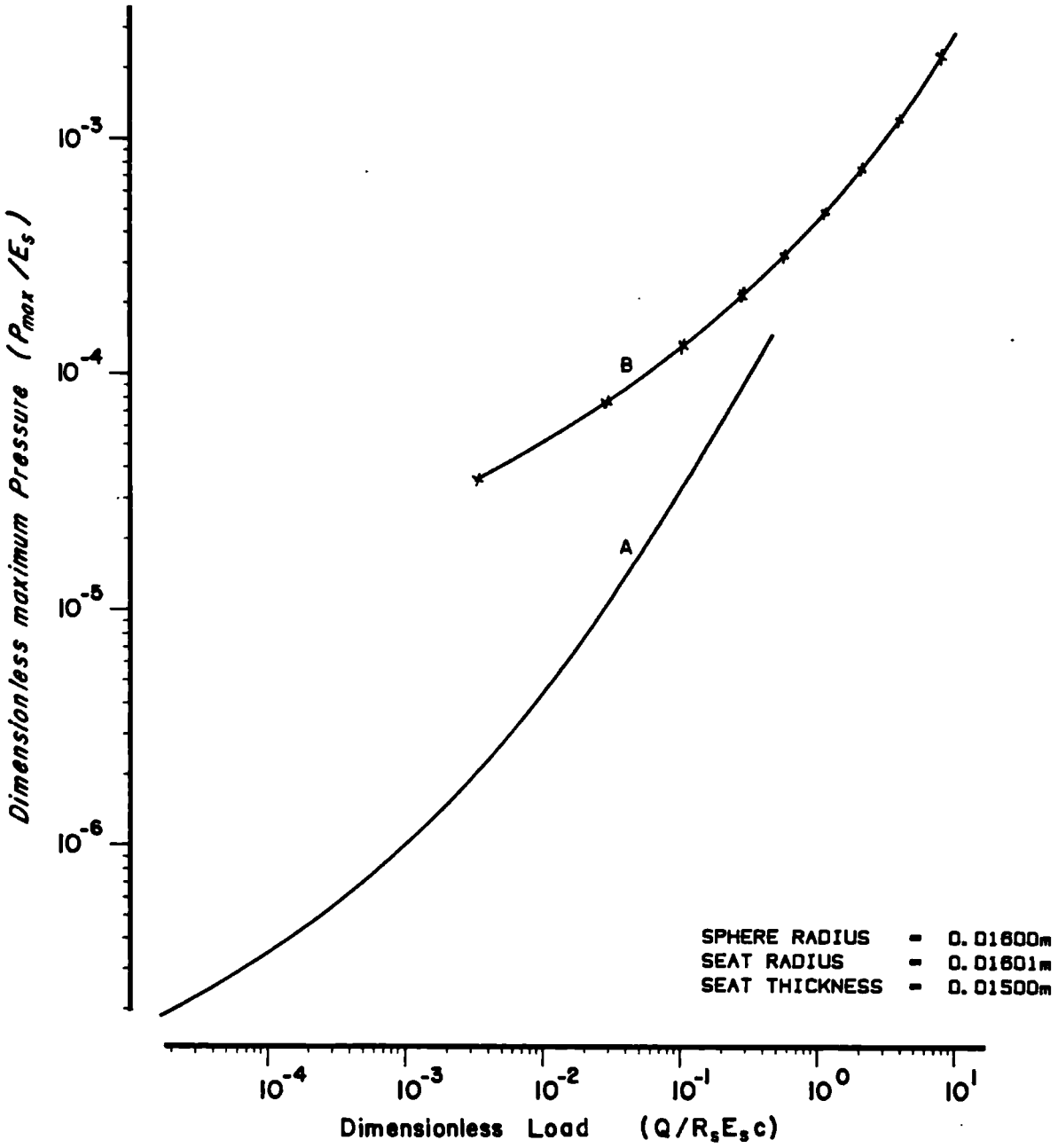

	Young's Modulus (GN/m^2)		Poisson's Ratio	
	SPHERE	SEAT	SPHERE	SEAT
A	200	0.5	0.3	0.38
B	200	200	0.3	0.3
×	0.5	0.5	0.38	0.38

FIGURE 2.23 : Variation of maximum Pressure with Load

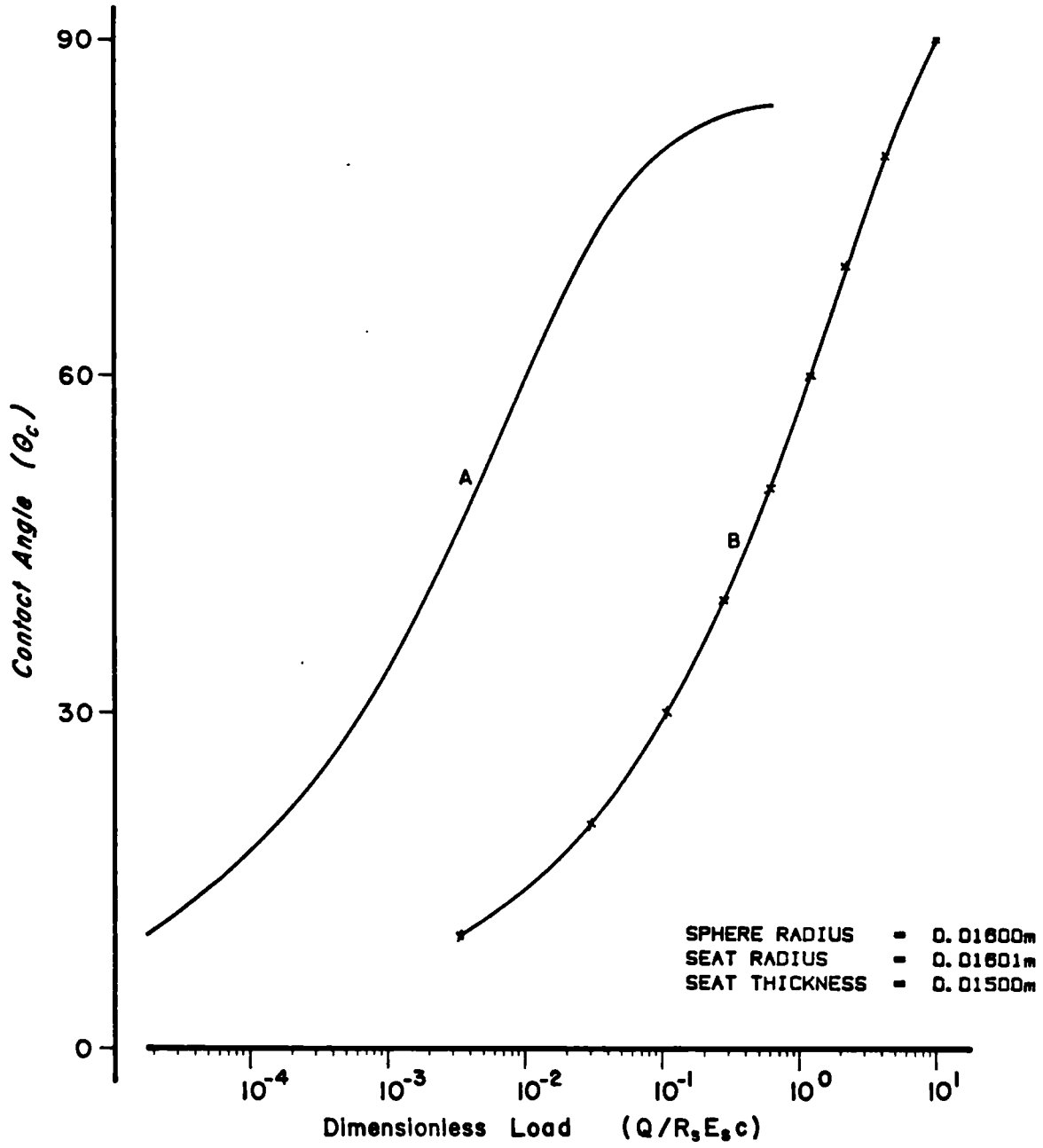

	Young's Modulus (GN/m²)		Poisson's Ratio	
	SPHERE	SEAT	SPHERE	SEAT
A	200	0.5	0.3	0.38
B	200	200	0.3	0.3
x	0.5	0.5	0.38	0.38

FIGURE 2.24 : Variation of Contact Angle with Load

Chapter 3

CHAPTER 3

LUBRICATED CONTACT

3.1 Introduction

Very little effort appears to have been concentrated on the analysis of lubricated contacts between closely conformal spherical elastic bodies. In this chapter, such contact is investigated for conditions of pure squeeze under a constant approach velocity of distant points on the two bodies.

In general, when a thin film lubricated contact is to be investigated, use is made of Reynold's equation to describe the behaviour of the lubricant. However, the analysis herein is started from the equations of motion for the lubricant and the conditions of continuity. This is because, for the particular problem in question, the continuity conditions can be explicitly stated, thus making the process a lot easier than trying to apply boundary conditions to Reynold's equation.

Two types of lubricant are considered, a paraffinic oil with pressure dependent viscosity, and synovial fluid, which is the lubricant in human joints and has shear-rate dependent viscosity.

Great interest is centred around the behaviour of natural joints, and no definite concensus exists over the lubricating

mechanisms involved. At present, a tribologist would find it extremely difficult, if not impossible, to provide a man made bearing which would operate within the body environment, occupy the same space as the natural bearing, withstand the same dynamic loads, possess the same degree of movement and low friction and have the same remarkable mean life. It would thus seem probable, that complete understanding of natural joint behaviour would revolutionize bearing design.

In this study, synovial fluid is considered as a lubricant, in a contact configuration which closely resembles an artificial hip joint replacement. The purpose of this, is to investigate whether synovial fluid per se, presents advantages over normal engineering lubricants in a bearing of such configuration.

3.2 Formulation and Solution

3.2A Pressure dependent viscosity

Consider an elastic sphere and a spherical elastic seat of almost equal undeformed radii R_s and R_c respectively, in lubricated contact, as shown in Figure 3.1.

It is assumed that:

1) The seat is stationary.
2) The sphere is subject to an axisymmetric load Q, of such varying magnitude, as to result in a constant pure squeeze velocity V for the centre of the sphere, along the line connecting the centres of the two bodies.
3) The gap between the two bodies is completely filled with

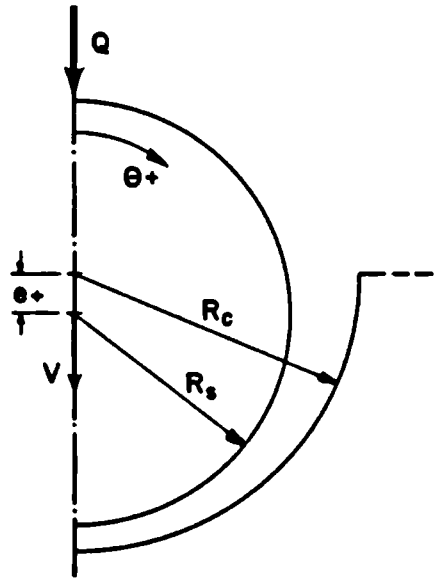

Figure 3.1 : Spherical squeeze lubricated bearing

a lubricating fluid. And further, as the gap closes, due to the movement of the sphere, the fluid is permitted to escape at the edge of the seat, in such a way as to result in a constant pressure, equal to atmospheric, at the edge.

4) The two bodies are homogenous, isotropic, obey Hooke's law, and experience small strains, permitting the use of linear elasticity theory.

5) There is no slip at the solid-fluid interface and no chemical interference.

6) The lubricant is incompressible and the process isothermal.

7) The lubricant viscosity is pressure dependent. The equation of state used for the lubricant is the one proposed by Cameron [4], and has the form:

$$\eta = \eta_o(1+\alpha p)^{16} \qquad (3.2A.1)$$

8) The inertia forces are negligible compared to the viscous ones.

9) The lubricant flow is laminar.

10) The pressure is constant across the film thickness.

Using the above assumptions, the equations of motion of the lubricant for axisymmetric flow in the gap, can be obtained from the Navier-Stokes equations and are, for spherical polar coordinates [5]:

$$\frac{\partial p}{\partial \theta} = r \frac{\partial}{\partial r} \left(\eta r \frac{\partial}{\partial r} \left(\frac{v_\theta}{r} \right) \right)$$

$$\frac{\partial p}{\partial r} = 0$$

$$\frac{\partial p}{\partial \Phi} = 0 \qquad (3.2A.2)$$

which, since the variation of r is small and the viscosity does not vary with r, can be rewritten as,

$$\frac{dp}{d\theta} \simeq \eta r \frac{\partial^2 v_\theta}{\partial r^2} \qquad (3.2A.3)$$

By integrating equation (3.2A.3), v_θ is obtained as,

$$v_\theta = \frac{1}{2\eta} \frac{dp}{d\theta} r + C_1 + \frac{C_2}{r} \qquad (3.2A.4)$$

If r_1 and r_2 are the local deformed radii of curvature of the surface of the sphere and seat respectively, measured from the centre of the seat, the film thickness can be written as,

$$h = r_2 - r_1 \qquad (3.2A.5)$$

and the boundary conditions for v_θ can be written as,

$$r = r_1 \quad : \quad v_\theta = V\sin\theta$$

$$r = r_2 \quad : \quad v_\theta = 0 \qquad (3.2A.6)$$

Using the boundary conditions (3.2A.6), equation (3.2A.5), and setting,

$$y = r - r_1 \qquad (3.2A.7)$$

equation (3.2A.4) becomes:

$$v_\theta = -\frac{1}{2\eta r}\frac{dp}{d\theta}y(h-y) + \frac{R_s}{r}\frac{h-y}{h}V\sin\theta \qquad (3.2A.8)$$

The total lubricant volumetric flow rate at any section, defined by angle θ, is given by:

$$F_\theta = \int_0^{2\pi}\int_{r_1}^{r_2} r\sin\theta\, v_\theta\, dr\, d\Phi$$

$$= 2\pi\sin\theta \int_0^h r v_\theta\, dy \qquad (3.2A.9)$$

and by substituting equation (3.2A.8) into equation (3.2A.9) and performing the integration, the flow rate due to the pressure gradient $\frac{dp}{d\theta}$ is obtained as,

$$F_\theta = \pi\sin\theta\left(-\frac{h^3}{6\eta}\frac{dp}{d\theta} + R_s h V\sin\theta\right) \qquad (3.2A.10)$$

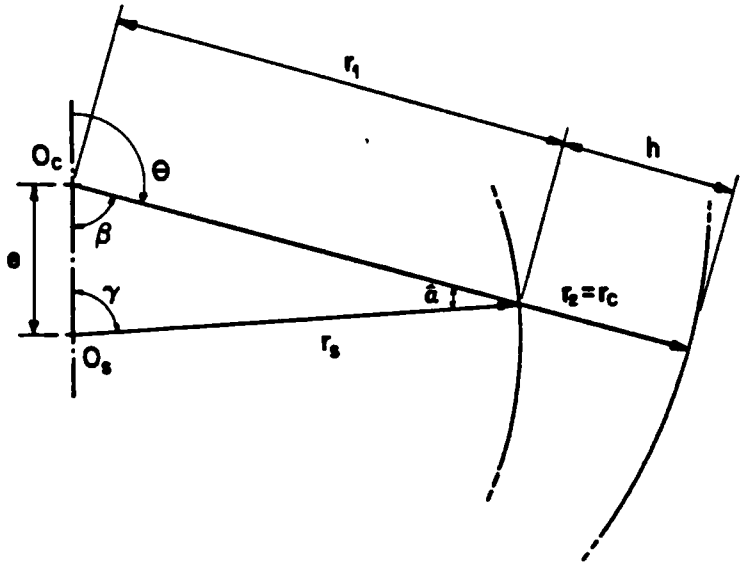

Figure 3.2 : Geometric relationships for the film thickness

Now, consider the geometrical relationships pertaining to the film thickness as shown in Figure 3.2, from which,

$$\frac{e}{\sin\hat{\alpha}} = \frac{r_s}{\sin\beta} = \frac{r_1}{\sin\gamma} \qquad (3.2A.11)$$

and

$$\hat{\alpha}+\gamma = \theta \qquad (3.2A.12)$$

From equations (3.2A.11) and (3.2A.12), r_1 is obtained as,

$$r_1 = \frac{r_s}{\sin\theta} \sin[\theta-\sin^{-1}(\frac{e}{r_s}\sin\theta)] \qquad (3.2A.13)$$

which can be rewritten as,

$$r_1 = \sqrt{r_s^2-e^2\sin^2\theta} - e\cos\theta \simeq r_s - e\cos\theta \qquad (3.2A.14)$$

Thus, using equation (3.2A.14) and noting that:

$$r_s = R_s+U_s \quad \text{and} \quad r_2 = r_c = R_c+U_c \tag{3.2A.15}$$

equation (3.2A.5), giving the film thickness, can be written as,

$$h = c+U+e\cos\theta \tag{3.2A.16}$$

where,

$$c = R_c-R_s \quad \text{and} \quad U = U_c-U_s \tag{3.2A.17}$$

Now, as the sphere approaches the seat, lubricant is displaced, and from geometrical considerations, the volumetric flow rate of the lubricant at any section specified by θ, can be calculated. Consider an element of the gap as shown in Figure 3.3.

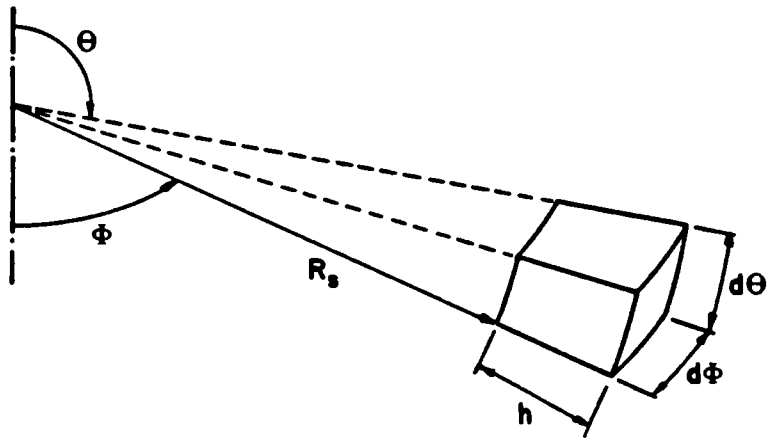

Figure 3.3 : Elemental volume of lubricant

The volume of the element is:

$$L = R_s^2 \sin\theta \; h \; d\theta \; d\Phi \tag{3.2A.18}$$

The rate of change of the volume of the element is:

$$\frac{dL}{dt} = R_s^2 \sin\theta \frac{dh}{dt} d\theta \, d\Phi \qquad (3.2A.19)$$

thus, the volumetric flow rate at any section can be written as,

$$F_\theta = 2\pi R_s^2 \int_\theta^\pi \sin\theta \frac{dh}{dt} d\theta \qquad (3.2A.20)$$

By using equation (3.2A.16) and noting that by definition $\frac{de}{dt} = V$, equation (3.2A.20) can be rewritten as,

$$F_\theta = 2\pi R_s^2 \int_\theta^\pi \left(\frac{dU}{dt} + V\cos\theta \right) \sin\theta \, d\theta \qquad (3.2A.21)$$

By equating the flow rates obtained from equations (3.2A.10) and (3.2A.21), an equation specifying the pressure gradient can be obtained, which together with the elasticity equations and the equation of state of the lubricant, would completely specify the problem and permit its solution, if somehow the term $\frac{dU}{dt}$ in equation (3.2A.21) could be specified. Indeed, in most cases it is solved in this fashion by neglecting the term in question. However, results by Herrenbruch [12], suggest that this term becomes of increasing importance, and can not be safely neglected, as film thicknesses decrease and elastic deflections increase.

This problem was circumvented by using a numerical method to calculate the flow rate resulting from continuity considerations.

At some considerable film thickness, it can indeed be assumed that:

$$\frac{dU}{dt} << V\cos\theta \qquad (3.2A.22)$$

and thus from equation (3.2A.21), the flow rate can be obtained at the time boundary as,

$$F_{\theta B} = -\pi R_s^2 V \sin^2\theta \qquad (3.2A.23)$$

Considering two consecutive time instants T_1 and T_2, separated by a small time interval Δt, and assuming that the flow rate varies linearly within the said time interval, the following relationship is obtained:

$$Vol\Big|_{T_2} - Vol\Big|_{T_1} = \frac{\Delta t}{2}\left(F_\theta\Big|_{T_1} + F_\theta\Big|_{T_2}\right) \qquad (3.2A.24)$$

where, "Vol" is the gap volume enclosed by the section in question, defined by θ, and is given by:

$$Vol = 2\pi R_s^2 \int_\theta^\pi \sin\theta \; h \; d\theta \qquad (3.2A.25)$$

Therefore, assuming that the flow rate at time T_1 is known, the one for T_2 is obtained from:

$$F_\theta\Big|_{T_2} = \frac{2}{\Delta t}\left(Vol\Big|_{T_2} - Vol\Big|_{T_1}\right) - F_\theta\Big|_{T_1} \qquad (3.2A.26)$$

It is now possible to obtain the solution to the problem numerically, by discretising the contact area as per Figure 3.4. Note, that the order in which the nodal points are numbered, is

the reverse to that employed in Chapter 1, and thus the order of the elements of the rows and columns of the influence coefficient matrices, must also be reversed.

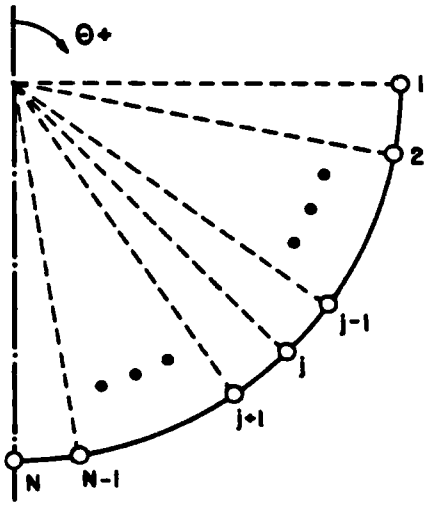

Figure 3.4 : Discretised area of contact

The algorithm employed to obtain the solution is as follows:

Part A : At time t=0, the sphere is assumed to be in a position relative to the seat, specified by a given eccentricity, while its centre is moving with velocity V.

The iteration steps are:

1) A quess is made for the pressure vector. Its element p_1 being set to zero to comply with assumption 3.
2) The vector of flow rates is obtained using equation (3.2A.23).
3) Using the pressure vector and equation (1.4.1), the elastic deflections are obtained as,

$$\hat{U} = (M_C^* - M_S^*) \times p \qquad (3.2A.27)$$

4) Using the elastic deflection vector and equation (3.2A.16), the film thicknesses are obtained.

5) Using the pressure vector and equation (3.2A.1), the viscosity vector is obtained.

6) Using equation (3.2A.10), in its finite difference form, a new pressure vector is obtained.

Steps 3 to 5 are repeated until convergence is reached. The convergence criterion employed is,

$$\frac{\left|p_{j,new} - p_{j,old}\right|}{p_{j,old}} \leq 10^{-8} \qquad (3.2A.28)$$

for all values of j, $2 \leq j < N$.

The load Q on the sphere is calculated by integrating the pressure distribution.

The volume vector is calculated using equation (3.2A.25).

The pressure, volume and flow vectors, as well as the eccentricity and sphere centre velocity, are passed on as input data for the calculation of the next time instant.

Part B : A new eccentricity is specified. Using this, together with the eccentricity of the previous time step and the sphere centre velocity, the size of the time step Δt is calculated.

The iteration steps are:

1) As a first quess for the pressure vector, the one obtained from the solution of the previous time step is used.

2) Elastic deflections are obtained.

3) Film thicknesses are obtained.

4) The volume vector is calculated using equation (3.2A.25).

5) Equation (3.2A.26) is used to obtain the volumetric flow rates.

6) The viscosity vector is obtained.

7) Using equation (3.2A.10), a new pressure vector is obtained.

Steps 2 to 7 are repeated until convergence is reached, with the same convergence criterion as in Part A.

The load Q on the sphere is calculated.

The pressure, volume and flow vectors, as well as the eccentricity and sphere centre velocity, are passed on as input data for the calculation of the next time instant.

Part B of the algorithm is repeated for as many time steps as are required.

A major problem presented, is the choice of starting eccentricity and the size of the time intervals Δt.

From the total elastic deflections obtained for the pole of the contact (nodal point N) from each time step, $\frac{dU}{dt}$ can be obtained numerically. Thus the choice of starting eccentricity can be judged as for its adequacy.

The choice of the time steps is first made by adjusting their size to produce a smooth $\frac{dU}{dt}$ curve. And finally, their size is halved repeatedly, until the change in the results between two consecutive runs is less than 1%.

3.2B Shear-rate dependent viscosity

When considering a lubricant with shear-rate dependent viscosity, in a contact configuration as described in subsection 3.2A, all assumptions made therein are applicable, except for assumption 7, which would only be applicable if the viscosity were pressure dependent as well.

For the purposes of the analysis presented here,it is assumed that the viscosity of the lubricant is only shear-rate dependent, with a constitutive equation as given below:

$$\eta = \eta_o \, |\dot{\gamma}|^{\omega} \qquad (3.2B.1)$$

However, in this case the equations of motion, equations (3.2A.2), become analytically intractable because of the variation of the viscosity with r.

Very recently Tayal et al [37], presented an analysis based on the Navier-Stokes equations, which is applicable to any form of the constitutive law for the lubricant. However, taking into account the algebraic complications involved, as well as the expensive computations resulting from the three dimensional finite element formulation employed, it appears to be rather impractical from an engineering point of view.

An alternative method was presented by Malik et al [24], the results of which compare favourably with published experimental ones [41]. In this approach, the lubricant viscosity is defined in terms of the shear strain rates averaged integrally across the film. The viscosity is thus reduced to a function which is independent of r, making it possible to

apply the method used in the previous section with the addition of a further iteration loop.

Accordingly, the constitutive equation for the lubricant is given as,

$$\eta_{av} = \eta_o \dot{\gamma}_{av}^n \tag{3.2B.2}$$

and the shear strain rate averaged across the film is defined as,

$$\dot{\gamma}_{av} = \frac{1}{h}\int_0^h |\dot{\gamma}|dy \tag{3.2B.3}$$

where, $$\dot{\gamma} = \frac{dv_\theta}{dy} \tag{3.2B.4}$$

and thus, using equation (3.2A.8) for v_θ, the average strain rate is obtained as,

$$\dot{\gamma}_{av} = \frac{1}{2h}\left\{(h-\frac{\beta'}{\alpha'})|\alpha'-\beta'-h| + \frac{\beta'}{\alpha'}|\beta'|\right\} \tag{3.2B.5}$$

where,

$$\alpha' = \frac{1}{\eta_{av} R_s}\frac{dp}{d\theta}$$

$$\beta' = \frac{1}{2\eta_{av} R_s}\frac{dp}{d\theta}h + \frac{V\sin\theta}{h} \tag{2.3B.6}$$

It is now possible to obtain the solution numerically, by discretising the contact area as in subsection 3.2A.

The algorithm employed to obtain the solution is as follows:

Part A : At time t=0, the sphere is assumed to be in a position relative to the seat, specified by a given eccentricity, while its centre is moving with velocity V.

The iteration steps are:

1) A quess is made for the pressure vector, with p_1 set to zero.
2) The flow rates are obtained from equation (3.2A.23).
3) All average viscosities are set equal to η_o.
4) Elastic deflections are obtained from equation (3.2A.27).
5) Film thicknesses are obtained from equation (3.2A.16).
6) Using equation (3.2A.10), in its finite difference form, a new pressure vector is obtained.
7) Steps 4 to 6 are repeated until convergence is reached, according to the convergence criterion (3.2A.28).
8) Using equations (3.2B.2) and (3.2B.5), new values of average viscosities are obtained.

Steps 4 to 8 are repeated until convergence is reached.

The convergence criterion employed for the average viscosities is:

$$\frac{|\eta_{j,new} - \eta_{j,old}|}{\eta_{j,old}} < 10^{-8} \qquad (3.2B.7)$$

for all values of j, $2 \leq j \leq N$.

The load Q on the sphere is calculated by integrating the pressure distribution.

The volume vector is calculated using equation (3.2A.25).

The pressure, volume, flow and viscosity vectors, as well as the eccentricity and sphere centre velocity, are passed on

as input data for the calculation of the next time instant.

Part B : A new eccentricity is specified. Using this, together with the eccentricity of the previous time step and the sphere centre velocity, the size of the time step Δt is calculated.

The iteration steps are:

1) As a first guess for the pressure and viscosity vectors, the ones from the previous time step are used.
2) Elastic deflections are obtained.
3) Film thicknesses are obtained.
4) The volume vector is calculated using equation (3.2A.25).
5) Equation (3.2A.26) is used to obtain the volumetric flow rates.
6) Using equation (3.2A.10), a new pressure vector is obtained.
7) Steps 2 to 6 are repeated until convergence is reached, according to convergence criterion (3.2A.28).
8) New average viscosities are obtained.

Steps 2 to 8 are repeated until convergence is reached, according to convergence criterion (3.2B.7).

The load Q on the sphere is calculated.

· The pressure, volume, flow and viscosity vectors, as well as the eccentricity and sphere centre velocity, are passed on as input data for the calculation of the next time instant.

Part B of the algorithm is repeated for as many time steps as required.

The choice of the starting eccentricity and of the size of the time steps is made in the same way as described in subsection 3.2A.

3.3 Results

In obtaining the results for both cases of pressure and shear-rate dependent viscosity, three interesting points were encountered.

First, the choice of starting eccentricity is not critical, as long as it is smaller than the eccentricity at which the rate of change of total elastic deformation at the contact pole versus eccentricity starts rising sharply *. It was found that two solutions with different starting eccentricities, chosen according to the above criterion, converge on each other with results differing by less than 0.1%, within about three time steps; which confirms the validity of the assumption made to obtain the flow rate at the time boundary.

Second, it was found in all cases that it was possible to obtain results satisfying the criterion of less than 1% change between consecutive runs, with only one halving of the size of the time steps used. However, this is probably because the original time steps were chosen very carefully to give a smooth curve, as seen by eye, for the rate of change of total elastic deformation at the pole versus eccentricity.

Third, the algorithms become unstable when the rate of change of total elastic deformation at the pole becomes nearly equal to the sphere's centre velocity, making it impossible to obtain results past that point.

---

* See Figures 3.5 through 3.8 and 3.10 through 3.13, for plots of $\frac{dU}{dt}$ versus eccentricity.

Results were obtained with a seat spaning a 90° angle, for two different ratios of radii, two combinations of materials, two seat thicknesses, two lubricants, and a number of different sphere centre velocities.

The two materials used are the same as the ones used in Chapter 2, and are specified in section 2.4.

One lubricant is assumed to be oil, with a constitutive equation expressed as,

$$\eta = 0.01(1 + 1.842\times10^{-9}\times p)^{16} \qquad (3.3.1)$$

The values for the viscosity and the pressure viscosity coefficient, were obtained from Cameron [ref.4, p.23, Fig.2.6, for 24° C].

The other lubricant is assumed to be normal human synovial fluid in vitro, the viscosity of which is invariant with pressure and varies inversely with shear strain rate [6]. The experimental results available for this variation do not however cover the large shear rates required here. It was therefore assumed that the viscosity of synovial fluid tends to that of water at large shear rates, and thus the constitutive equation used is,

$$\eta = 0.001 + 8.541(\dot{\gamma})^{-0.795} \qquad (3.3.2)$$

Equation (3.3.2), represents a good fit for the available experimental results [ref.6, p.113, Fig.12.7], and gives the viscosity of water when $\dot{\gamma}\rightarrow\infty$.

Figures 3.5 through 3.8, present film thickness profiles,

pressure distributions and plots of rate of change of total elastic deformation at the contact pole versus eccentricity, for the cases of pressure dependent viscosity, a steel seat of infinite thickness and a steel sphere with centre velocities of 1m/s, 1dm/s, 1cm/s and 1mm/s respectively.

Figure 3.9, presents a comparison of load carrying capacities for the above cases.

Figures 3.10 through 3.13, present film thickness profiles, pressure distributions and plots of rate of change of total elastic deformation at the contact pole, for a seat thickness of 1.5cm and a sphere centre velocity of 7.5cm/s; where,

a) the sphere and seat are steel and the lubricant is oil (Figure 3.10),

b) the sphere is steel, the seat is polyethylene and the lubricant is oil (Figure 3.11),

c) the sphere and seat are steel and the lubricant is synovial fluid (Figure 3.12),

d) the sphere is steel, the seat is polyethylene and the lubricant is synovial fluid (Figure 3.13).

Figure 3.14, presents a comparison of load carrying capacities for the above four cases.

It should be noted here, that for the case of a polyethylene seat, the results were stopped when the elastic displacements started becoming too large to safely assume the validity of linear elasticity theory.

3.4 Discussion and suggestions for futher work

It can be seen from all the results obtained, that $\frac{dU}{dt}$ rapidly reaches the same order of magnitude as the sphere centre velocity. It would thus be disastrous to the accuracy of any results obtained, to consider it relatively negligible under conditions of large elastic deformations and thin films. Further, by observing the film thickness profiles, it can be seen that $\frac{dh}{dt}$ is not uniform, thus refuting the occasional uniform velocity assumption used in the solution of ehl squeeze problems. These results are in agreement with the conclusions reached by Herrenbruch [12], for counterformal cylinders.

Entrapments of the lubricant are beginning to form in all cases of pressure dependent viscosity, and become more apparent at high sphere centre velocities and small clearances. This is in qualitative agreement with the experimental results obtained by Paul [29], for a ball falling onto a flat plate covered with oil, where small entrapments were observed when ball bounce was inhibited. The larger entrapments predicted here, can be attributed to the close conformity of the two bodies, the larger extent of the ehl contact and the constant sphere centre velocity.

From Figure 3.9, it can be seen that for the case of pressure dependent viscosity, the load carrying capacity is strongly dependent on approach velocity, lubricant viscosity and pressure-viscosity coefficient, as well as the material properties of the two bodies. However, this dependency is weakened conciderably after the entrapments start to appear,

probably because of the reduction in lubricant outflow from the region of the entrapment, which corresponds to the region of highest pressure.

A very interesting behaviour is presented for the case of a polyethylene seat and a pressure dependent viscosity lubricant (see Figure 3.11). An entrapment appears to start forming near the edge of the contact, however, no final conclusion can be reached by the present method, due to the limitations of linear elasticity theory.

No obvious entrapments appear to be generated with either a steel or a polyethylene seat when the lubricant viscosity is shear-rate dependent, despite the considerable reduction in the lubricant outflow. The film thickness profiles have similar shapes but the load carrying capacity of the polyethylene seat is considerably smaller for similar film thicknesses (see Figures 3.12 through 3.14).

From the results obtained here, synovial fluid per se, does not appear to present any advantages, except of course for lower friction, as it results in thinner films and lower load carrying capacities than a pressure dependent viscosity lubricant. Thus, nothing positive can be said to have been added to the understanding of the operation of human hip joints, however, the knowledge that more complex models will be needed for that purpose, might prove of some use to further research.

The present model could easily be extended to include porous bearing surfaces, and possibly dynamically varying velocity under a constant or a changing external load on the

sphere. Any further work should concentrate on those lines, and possibly an attempt made in reshaping the algorithms to remove the instability and thus enable results for thinner films to be obtained; which judging from the relative behaviour shown in Figure 3.14, might reverse the conclusions about synovial fluid. And of course, some experimental results would be of the utmost importance, in order to validate the theory.

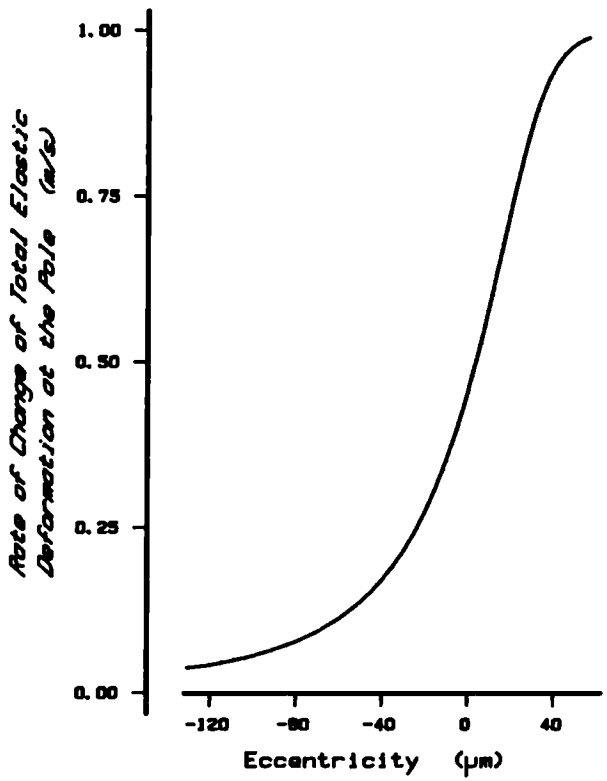

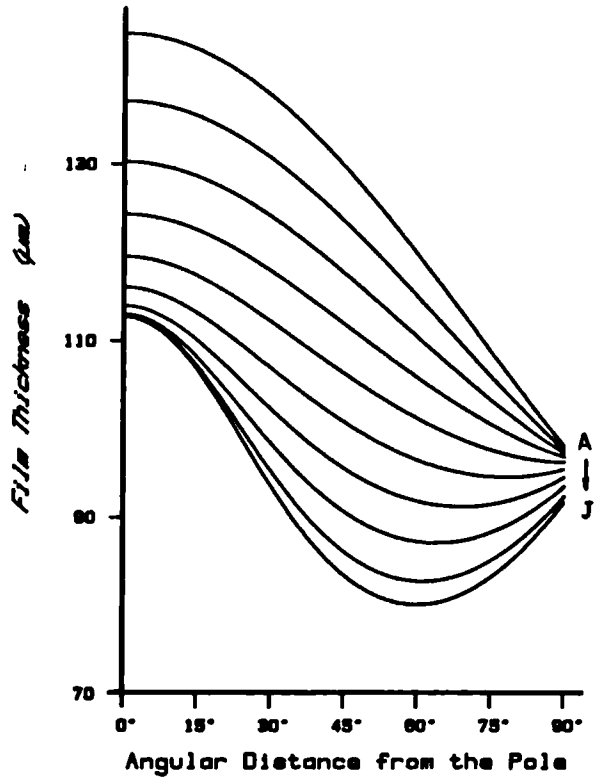

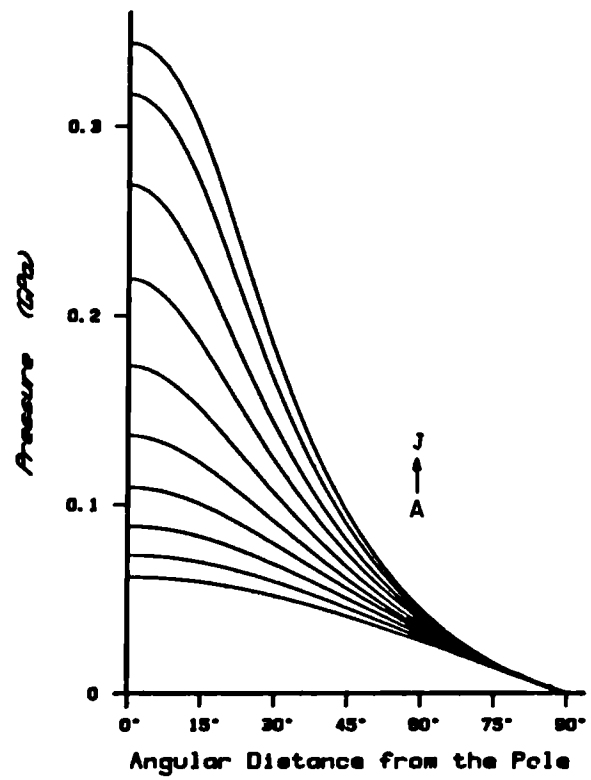

FIGURE 3.5

Results for Pressure dependent Viscosity

SPHERE
Radius = 0.03m
Poisson's Ratio = 0.3
Young's Modulus = 200GPa

SPHERE CENTRE VELOCITY = 1m/s

SEAT
Radius = 0.0301m
Thickness = ∞
Poisson's Ratio = 0.3
Young's Modulus = 200GPa

LUBRICANT
Viscosity = 0.01Pas
Pressure-Viscosity
coefficient = 1.842GPa^{-1}

	ECCENTRICITY (μm)	INSTANTANEOUS LOAD CAPACITY (KN)	LUBRICANT OUTFLOW (dm^3/s)
A	-30	110.18	2.54
B	-20	123.35	2.49
C	-10	139.15	2.43
D	0	158.11	2.36
E	10	180.77	2.27
F	20	207.61	2.18
G	30	239.98	2.08
H	40	275.05	1.98
I	50	315.81	1.87
J	56	342.48	1.81

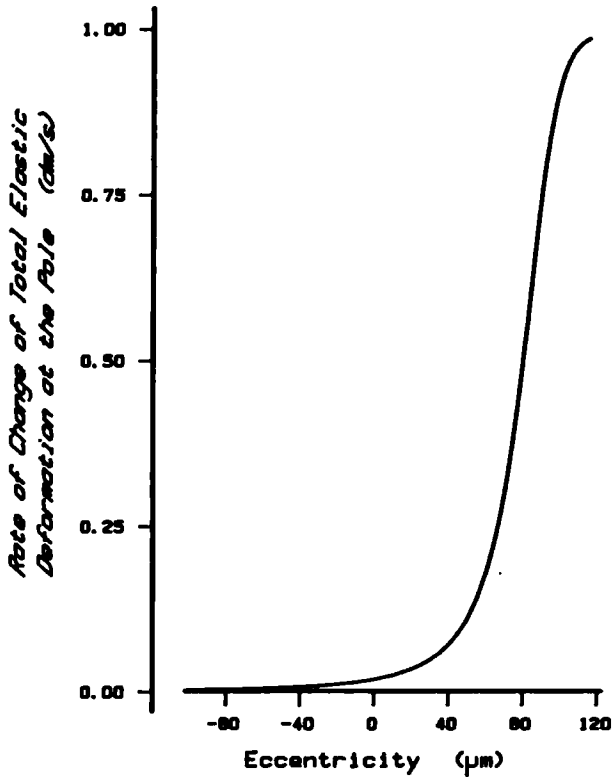

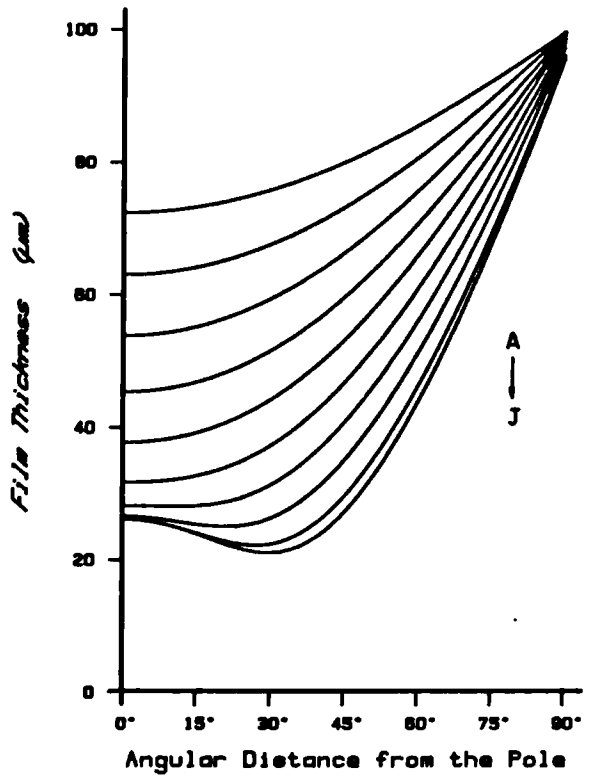

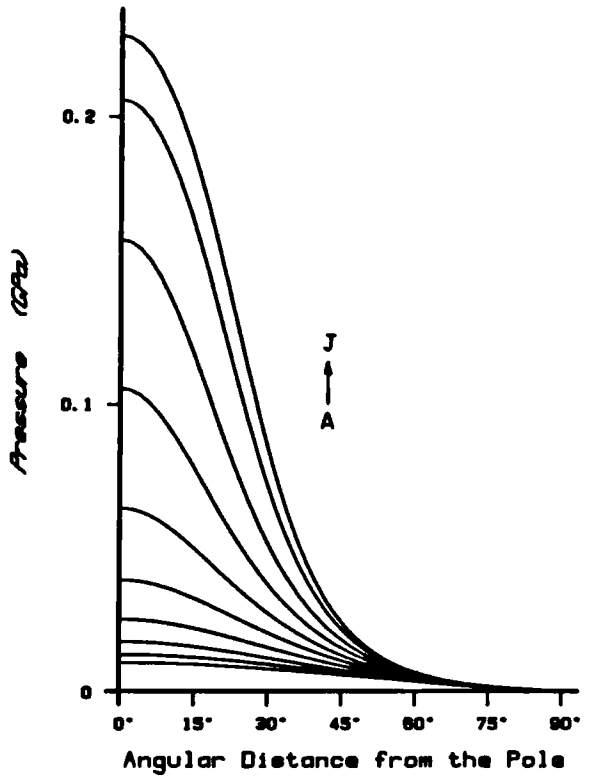

FIGURE 3.6

Results for Pressure dependent Viscosity

SPHERE
Radius = 0.03m
Poisson's Ratio = 0.3
Young's Modulus = 200GPa

SPHERE CENTRE VELOCITY = 1dm/s

SEAT
Radius = 0.0301m
Thickness = ∞
Poisson's Ratio = 0.3
Young's Modulus = 200GPa

LUBRICANT
Viscosity = 0.01Pas
Pressure-Viscosity
coefficient = 1.842GPa^{-1}

	ECCENTRICITY (μm)	INSTANTANEOUS LOAD CAPACITY (KN)	LUBRICANT OUTFLOW (dm^3/s)
A	30	15.87	0.277
B	40	19.01	0.275
C	50	23.22	0.272
D	60	29.30	0.267
E	70	38.34	0.259
F	80	51.95	0.248
G	90	71.65	0.234
H	100	99.14	0.218
I	110	133.99	0.201
J	115	154.13	0.193

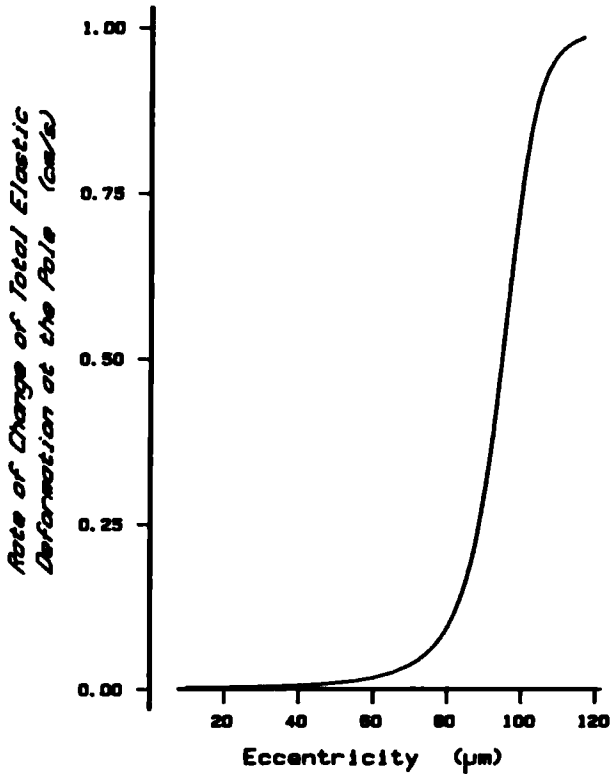

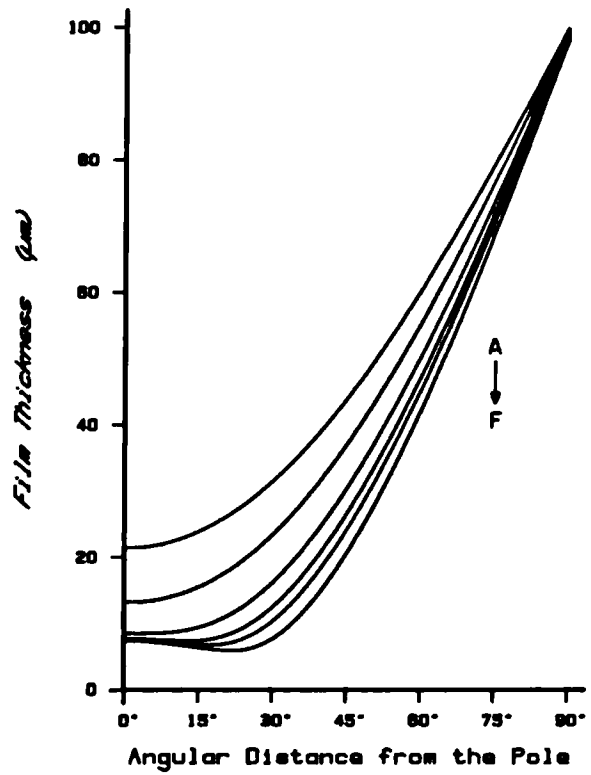

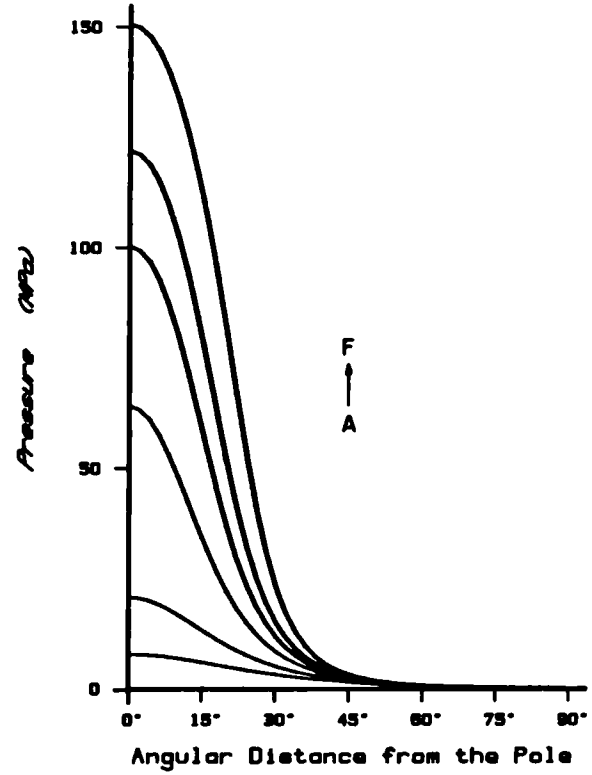

FIGURE 3.7

Results for Pressure dependent Viscosity

SPHERE
Radius = 0.03m
Poisson's Ratio = 0.3
Young's Modulus = 200GPa

SEAT
Radius = 0.0301m
Thickness = ∞
Poisson's Ratio = 0.3
Young's Modulus = 200GPa

SPHERE CENTRE VELOCITY = 1cm/s

LUBRICANT
Viscosity = 0.01Pas
Pressure-Viscosity
coefficient = 1.842GPa^{-1}

	ECCENTRICITY (μm)	INSTANTANEOUS LOAD CAPACITY (KN)	LUBRICANT OUTFLOW (cm^3/s)
A	80	5.96	27.66
B	90	10.70	26.80
C	100	22.40	24.91
D	106	34.65	23.51
E	110	45.09	22.59
F	116	63.95	21.26

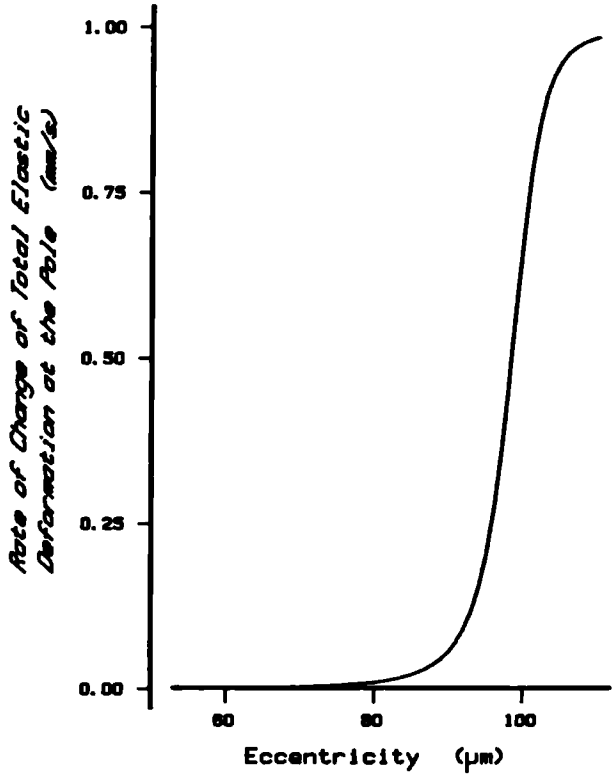

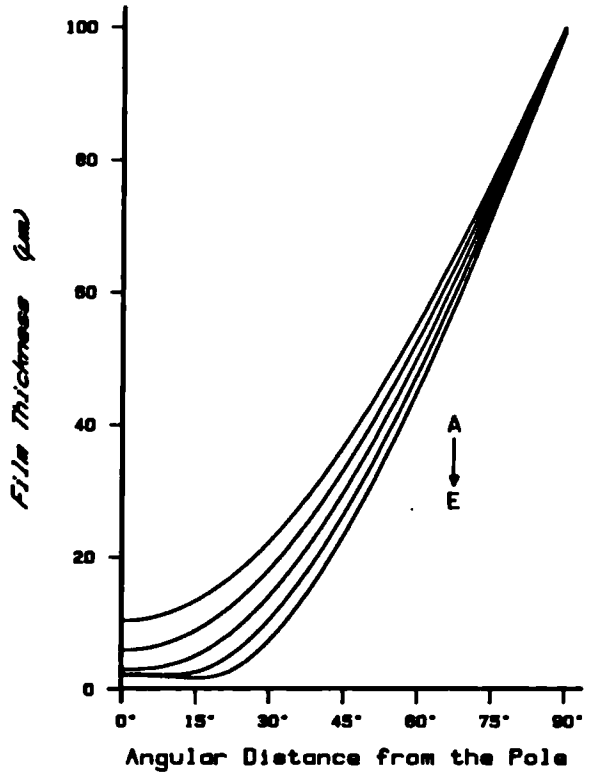

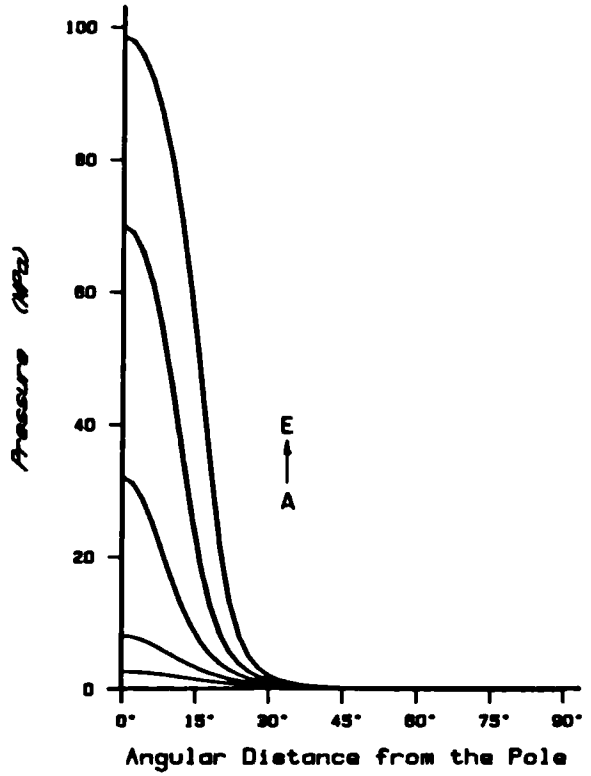

FIGURE 3.8

Results for Pressure dependent Viscosity

SPHERE
Radius = 0.03m
Poisson's Ratio = 0.3
Young's Modulus = 200GPa

SEAT
Radius = 0.0301m
Thickness = ∞
Poisson's Ratio = 0.3
Young's Modulus = 200GPa

SPHERE CENTRE VELOCITY = 1mm/s

LUBRICANT
Viscosity = 0.01Pas
Pressure-Viscosity
coefficient = 1.842GPa^{-1}

	ECCENTRICITY (μm)	INSTANTANEOUS LOAD CAPACITY (KN)	LUBRICANT OUTFLOW (cm^3/s)
A	90	1.27	2.80
B	95	2.34	2.76
C	100	5.44	2.64
D	105	12.46	2.47
E	110	23.46	2.33

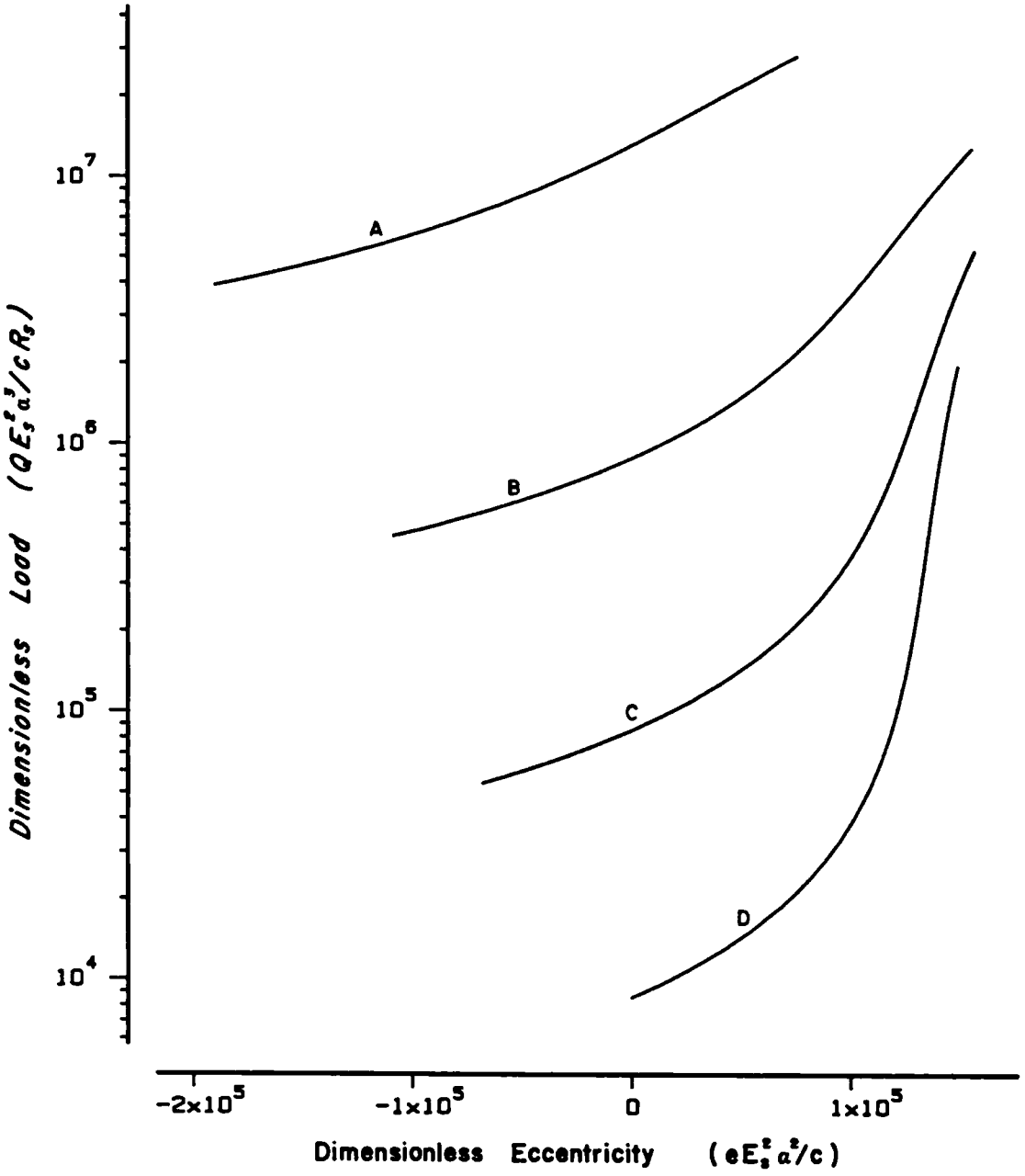

SPHERE
Radius = 0.03m
Poisson's Ratio = 0.3
Young's Modulus = 200GPa

SEAT
Radius = 0.0301m
Thickness = ∞
Poisson's Ratio = 0.3
Young's Modulus = 200GPa

LUBRICANT
Viscosity = 0.01Pas
Pressure-Viscosity
coefficient = $1.842GPa^{-1}$

	$\frac{\eta_o \dot{e} E_s^3 a^4}{R_s}$
A	3.07×10^{-2}
B	3.07×10^{-3}
C	3.07×10^{-4}
D	3.07×10^{-5}

FIGURE 3.9 : Comparison of Load Carrying Capacities

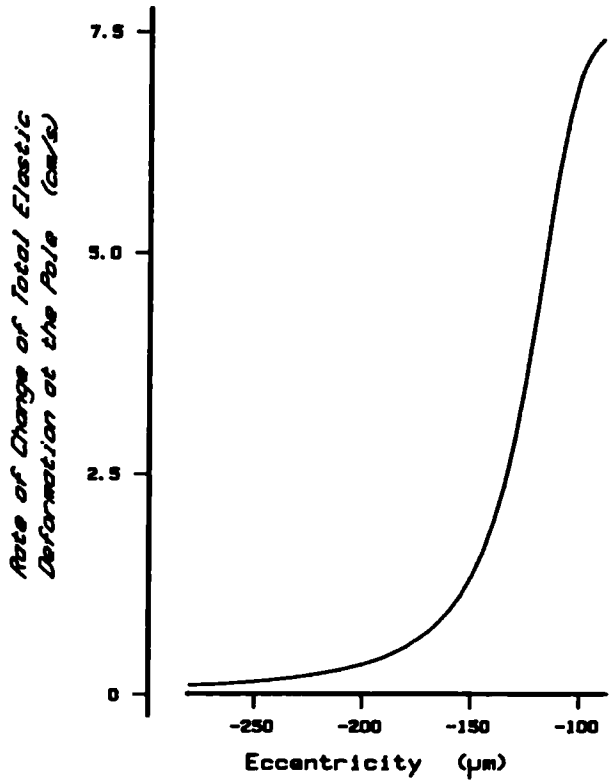

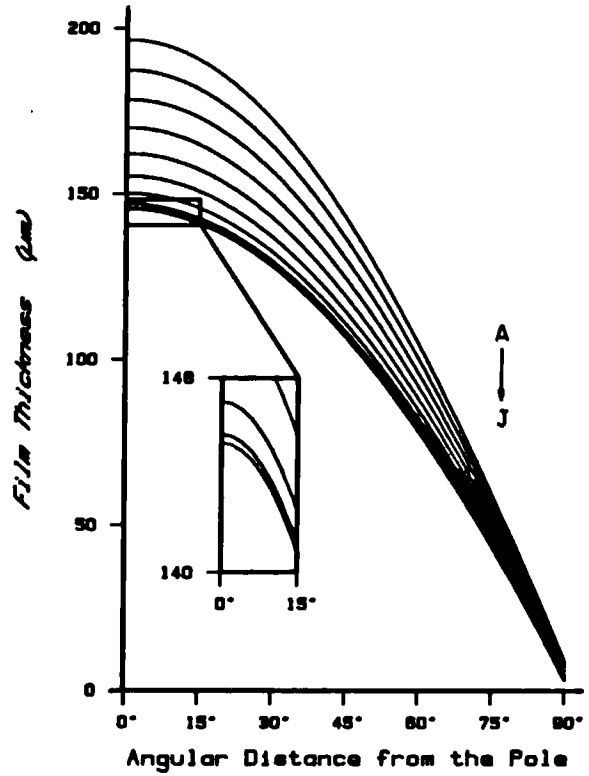

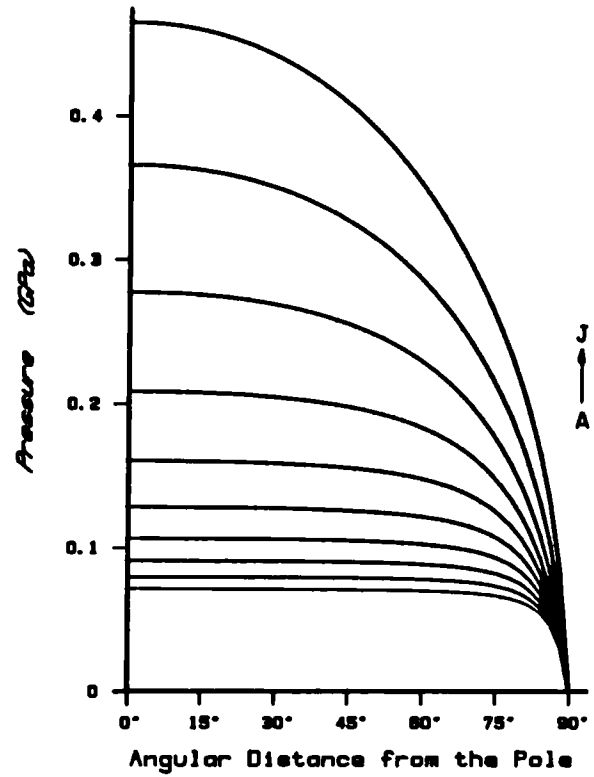

FIGURE 3.10

Results for Pressure dependent Viscosity

SPHERE
Radius = 0.016m
Poisson's Ratio = 0.3
Young's Modulus = 200GPa

SPHERE CENTRE VELOCITY = 7.5cm/s

SEAT
Radius = 0.01601m
Thickness = 0.015m
Poisson's Ratio = 0.3
Young's Modulus = 200GPa

LUBRICANT
Viscosity = 0.01Pas
Pressure-Viscosity
coefficient = 1.842GPa^{-1}

	ECCENTRICITY (μm)	INSTANTANEOUS LOAD CAPACITY (KN)	LUBRICANT OUTFLOW (cm^3/s)
A	-180	55.59	55.26
B	-170	62.11	53.87
C	-160	70.57	51.88
D	-150	81.95	48.98
E	-140	97.68	44.74
F	-130	119.92	38.62
G	-120	151.43	30.41
H	-110	194.42	20.93
I	-100	248.48	12.22
J	-90	310.44	5.99

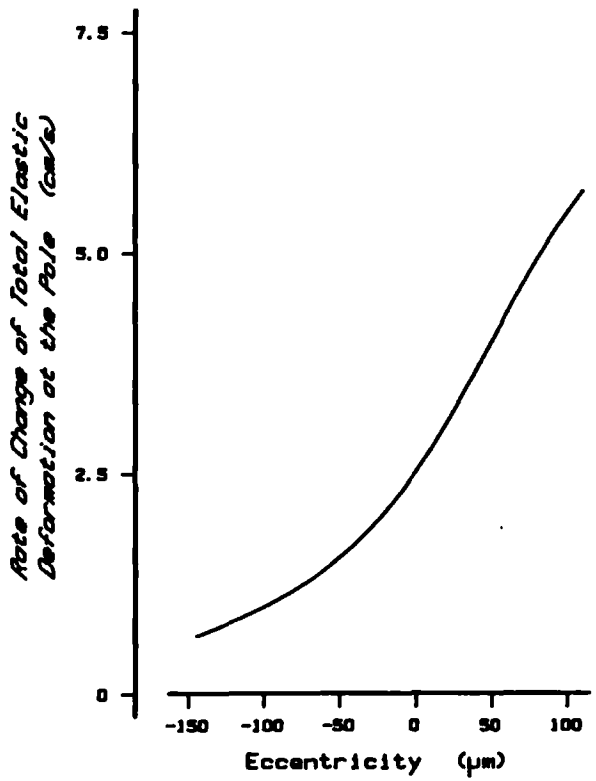

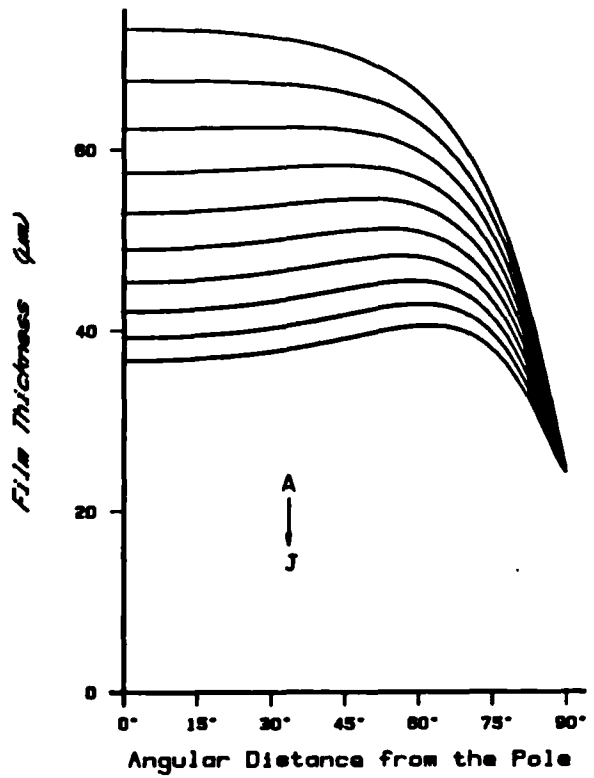

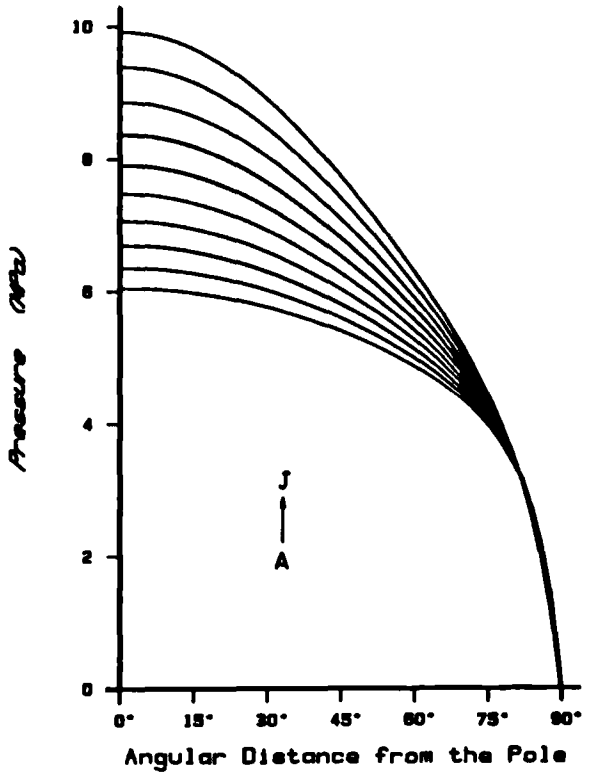

FIGURE 3.11

Results for Pressure dependent Viscosity

SPHERE
Radius = 0.016m
Poisson's Ratio = 0.3
Young's Modulus = 200GPa

SEAT
Radius = 0.01601m
Thickness = 0.015m
Poisson's Ratio = 0.38
Young's Modulus = 500MPa

SPHERE CENTRE VELOCITY = 7.5cm/s

LUBRICANT
Viscosity = 0.01Pas
Pressure-Viscosity coefficient = 1.842GPa^{-1}

	ECCENTRICITY (μm)	INSTANTANEOUS LOAD CAPACITY (KN)	LUBRICANT OUTFLOW (cm^3/s)
A	20	4.18	38.94
B	30	4.33	37.51
C	40	4.50	36.00
D	50	4.67	34.43
E	60	4.86	32.80
F	70	5.06	31.13
G	80	5.27	29.43
H	90	5.50	27.72
I	100	5.73	26.02
J	110	5.98	24.34

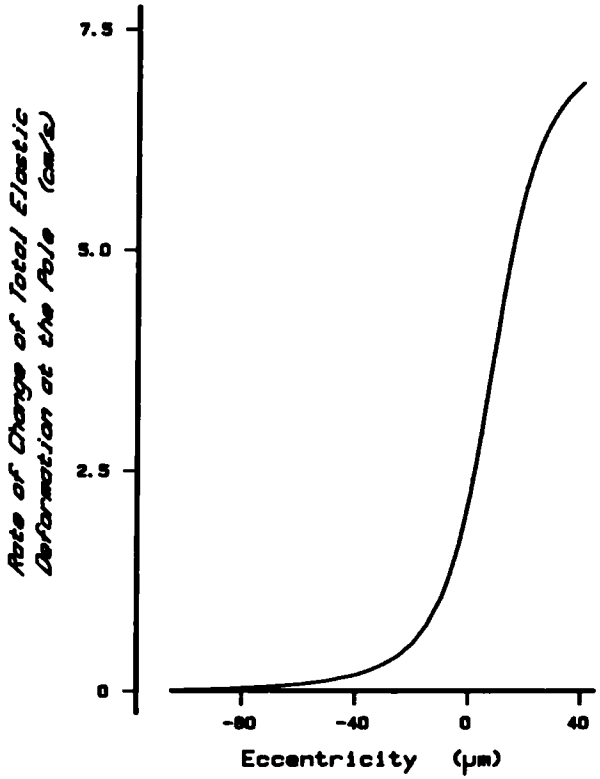

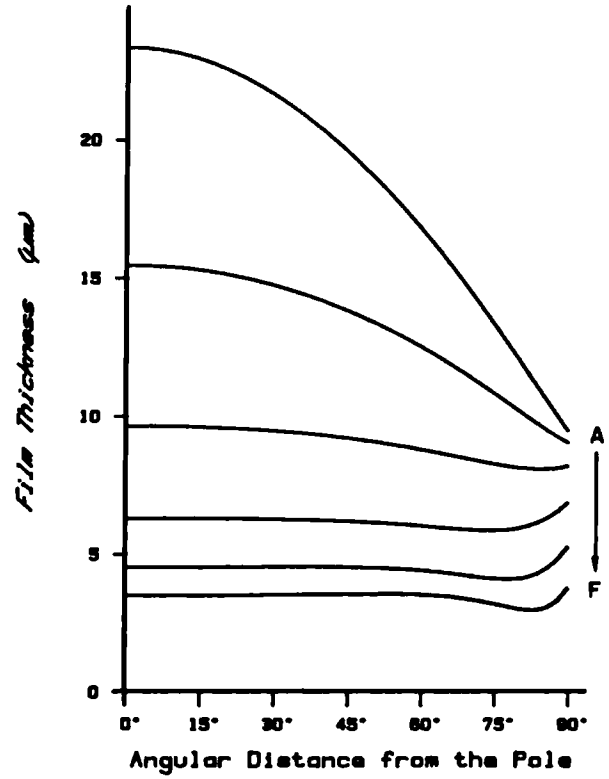

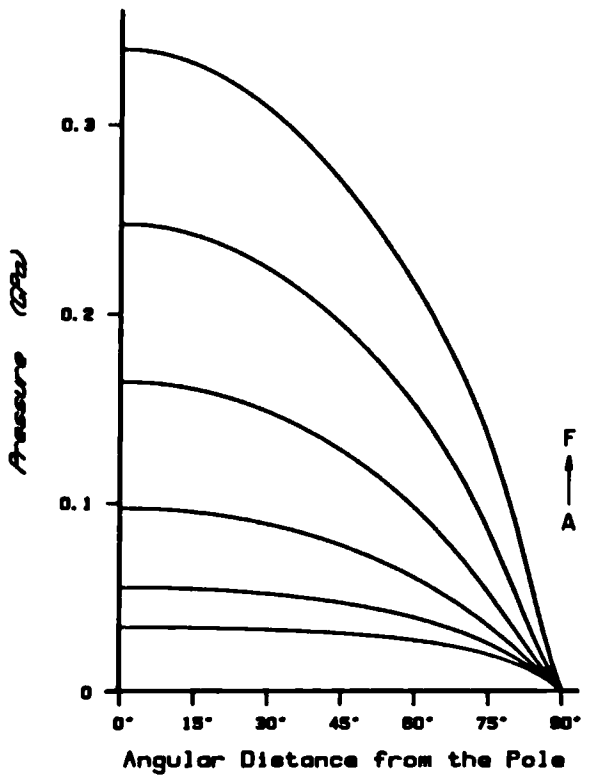

FIGURE 3.12

Results for Shear-Rate dependent Viscosity

SPHERE
Radius = 0.016m
Poisson's Ratio = 0.3
Young's Modulus = 200GPa

SEAT
Radius = 0.01601m
Thickness = 0.015m
Poisson's Ratio = 0.3
Young's Modulus = 200GPa

SPHERE CENTRE VELOCITY = 7.5cm/s

LUBRICANT VISCOSITY (Pas)

$\eta = 0.001 + 8.541(\dot{\gamma})^{-0.786}$

	ECCENTRICITY (μm)	INSTANTANEOUS LOAD CAPACITY (KN)	LUBRICANT OUTFLOW (cm^3/s)
A	-10	23.21	53.69
B	0	35.22	48.11
C	10	57.74	38.32
D	20	94.93	26.03
E	30	145.13	15.76
F	40	203.22	9.39

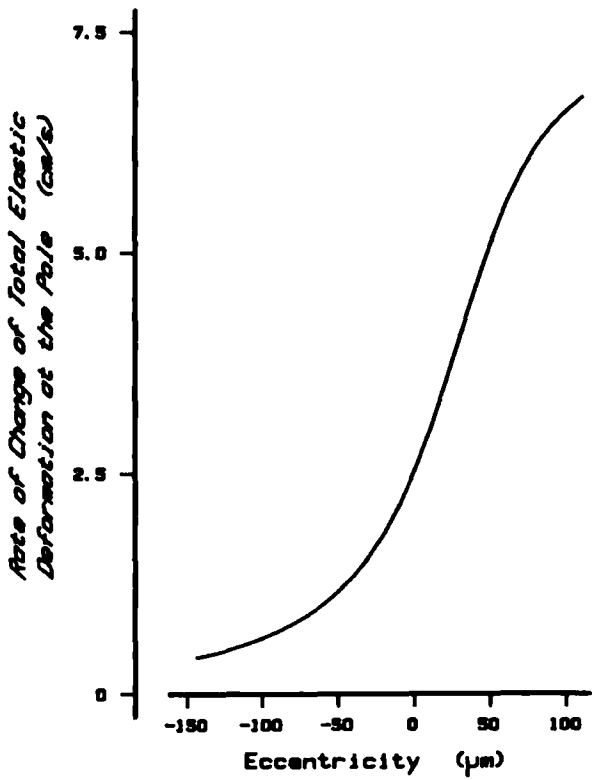

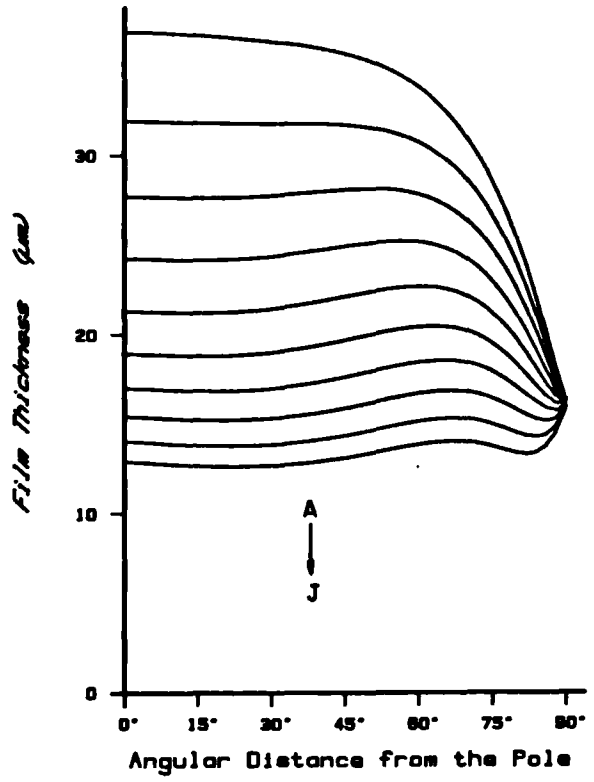

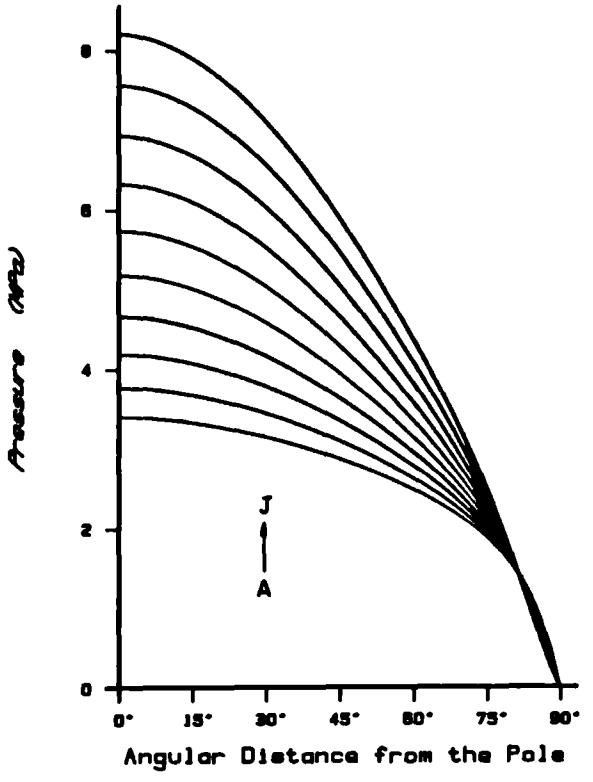

FIGURE 3.13

Results for Shear-Rate dependent Viscosity

SPHERE
Radius = 0.016m
Poisson's Ratio = 0.3
Young's Modulus = 200GPa

SEAT
Radius = 0.01601m
Thickness = 0.015m
Poisson's Ratio = 0.38
Young's Modulus = 500MPa

SPHERE CENTRE VELOCITY = 7.5cm/s

LUBRICANT VISCOSITY (Pas)

$$\eta = 0.001 + 8.541(\dot{\gamma})^{-0.795}$$

	ECCENTRICITY (μm)	INSTANTANEOUS LOAD CAPACITY (KN)	LUBRICANT OUTFLOW (cm^3/s)
A	20	2.22	36.75
B	30	2.39	34.01
C	40	2.59	31.08
D	50	2.81	28.09
E	60	3.04	25.08
F	70	3.30	22.19
G	80	3.58	19.47
H	90	3.87	16.99
I	100	4.18	14.76
J	110	4.50	12.82

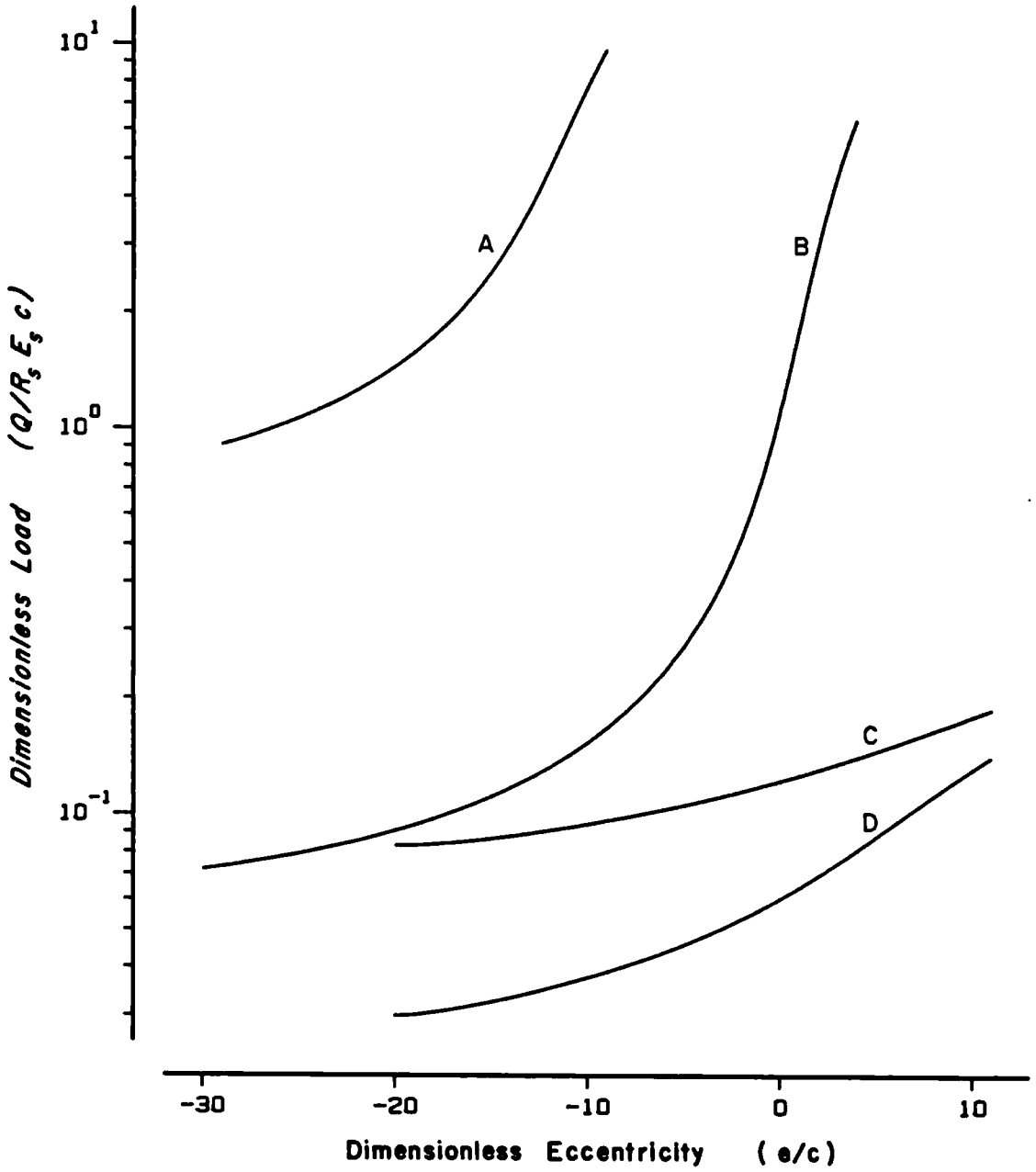

	SEAT		LUBRICANT
	Young's Modulus (GPa)	Poisson's Ratio	
A	200	0.3	Oil
B	200	0.3	Synovial Fluid
C	0.5	0.38	Oil
D	0.5	0.38	Synovial Fluid

SPHERE
Radius = 0.016m
Poisson's Ratio = 0.3
Young's Modulus = 200GPa

SEAT
Radius = 0.01601m
Thickness = 0.015m

FIGURE 3.14 : Comparison of Two Types of Lubricant

References

REFERENCES

1) BECKENBACH E.F.
Modern Mathematics for the Engineer
McGraw-Hill, 1961.

2) BONDAREVA V.F.
"Contact Problems for an Elastic Sphere"
PMM Vol. 35, No. 1, p. 61-70, 1971.

3) BOUSSINESQ M.J.
Application des Potentiels
Gauthier-Villars; Paris,1885.

4) CAMERON A.
Principles of Lubrication
Longmans, 1966.

5) CONSTANTINESCU V.N.
Gas Lubrication
ASME, New York, 1969.

6) CURREY J. , UNSWORTH A. , HALL D.A.
"Properties of Bone, Cartrilage and Synovial Fluid"
In: Introduction to the Biomechanics of Joints and Joint Replacement.
Edited by: DOWSON D. and WRIGHT V.
Mechanical Engineering Publications; London, 1981.

7) DOWSON D.
"Modes of Lubrication in Human Joints"
Proc. Inst. Mech. Eng., Vol. 181, p.45-54, 1966-67.

8) FEIN R.S.
"Are Synovial Joints Squeeze-Film Lubricated?"
Proc. Inst. Mech. Eng. Vol. 181, p. 125-128, 1966-67

9) FORD H. and ALEXANDER J.M.
Advanced Mechanics of Materials
John Wiley & Sons, 1977

10) FRANCAVILLA A. and ZIENKIEWICZ O.C.
"A Note on Numerical Computation of Elastic Contact Problems"
Int. J. for Num. Meth. in Eng., Vol. 9, p. 913-924, 1975.

11) GOODMAN L.E. and KEER L.M.
"The Contact Stress Problem for an Elastic Sphere Indenting an Elastic Cavity"
Int. J. Sol. Struct., Vol. 1, p. 407-415, 1965.

12) HERRENBRUCH K.
"Elastohydrodynamic Squeeze Films between Two Cylinders in Normal Approach"
J. of Lub. Tech., Vol. 92, No. 2, p.292-302, April 1970.

13) HERTZ H.
Miscellaneous Papers
Macmillan & Co. ; London, 1896.

14) HIGGINSON G.R.
"Elastohydrodynamic Lubrication in Human Joints"
Proc. Inst. Mech. Eng., Vol. 191, p. 217-223, 1977.

15) HOBSON E.W.
Spherical and Ellipsoidal Harmonics
Cambridge University Press, 1931.

16) HUSSAIN M.A. and PU S.L.
"Non-Hertzian Contact of an Elastic Sphere Identing an Elastic Spherical Cavity"
Devel. in Mech., Vol. 6, p. 647-658
Proc. 12th Midwest Mech. Conf.,
Notre Dame, i11, August 1971,
Univ. NOtre Dame Press, 1971.

17) JAEGER J.C. and STARFIELD A.M.
An Introduction to Applied Mathematics
Oxford University Press, 1974.

18) JOHNSON K.L.
"One Hundred Years of Hertz Contact"
Proc. Inst. Mech. Eng., Vol. 196, p. 363-378, 1982.

19) KALKER J.J. and van RANDEN Y.A.
"A Minimum Principle for Frictionless Elastic Contact with Application to Non-Hertzian Halfspace Contact Problems"
J. Eng. Math., Vol. 6, No. 2, p. 193-206, April 1972.

20) KARPENKO V.A.
"On the Closed Solution of the First Boundary Value Problem of Elasticity Theory for a Space with a Spherical Cavity"
PMM Vol. 39, No. 5, p. 951-955, 1975.

21) LEE K.M. and CHENG H.S.
"The Pressure and Deformation Profiles Between Two Normally Approaching Lubricated Cylinders"
J. of Lub. Tech., Vol. 95, No. 3, p. 308-320, July 1973.

22) LOVE A.E.H.
A Treatise on the Mathematical Theory of Elasticity
Dover Publications; New York, 1944.

23) LUR'E A.I.
Three-Dimensional Problems of the Theory of Elasticity
Interscience Publishers; New York, 1964.

24) MALIK M., DASS B., SINHASAN R.
"The Analysis of Hydrodynamic Journal Bearings Using Non-Newtonian Lubricants by Viscosity Averaging Across the Film"
ASLE Trans. Vol. 26, No. 1, p. 125-131, January 1983.

25) MOSTOFI A.
Oil Film Thickness and Pressure Distribution in Elastohydrodynamic Elliptical Contacts
PhD Thesis, Imperial College, London University, 1981.

26) NEUBER H.
"Ein neuer Ansatz zur Lösung räumlicher Probleme der Elastizitätstheorie"
Z. angew. Math. Mech., Vol. 14, No. 4, p. 203-212, 1934.

27) PAPKOVICH P.F.
"An Expression for a General Integral of the Equations of the Theory of Elasticity in Terms of Harmonic Functions"
Izvest. Akad. Nauk S.S.S.R., Ser. matem. i estestv. nauk, No. 10, 1932

28) PAUL B. and HASHEMI J.
"Contact Pressures on Closely Conforming Elastic Bodies"
J. of App. Mech., Vol. 48, No. 3, p. 543-548, 1981.

29) PAUL G.R.
Optical Determination of the High Pressure Refracture Index and Viscosity of Liguids Entrapped in Point Contacts
PhD Thesis, Imperial College, London University, 1971.

30) PINKUS O. and STERNLICHT B.
Theory of Hydrodynamic Lubrication
McGraw-Hill, 1961.

31) SCHOWALTER W.R.
Mechanics of Non-Newtonian Fluids
Pergamon Press, 1978.

32) SKELLAND A.H.
Non-Newtonian Flow and Heat Transfer
John Wiley & Sons, 1967.

33) SOMMERFIELD A.
Partial Differential Equations in Physics
Academic Press Inc.; New York, 1949.

34) STENBERG E., EUBANKS R.A., SADOWSKY M.A.
"On the Stress-Function Approaches of Boussinesq and Timple to the Axisymmetric Problem of Elasticity Theory"
J. of App. Physics, Vol. 22, No. 9, p. 1121-1124, 1951.

35) STENBERG E. and ROSENTHAL F.
"The Elastic Sphere Under Concentrated Loads"
J. of App. Mech., Vol. 19, No.4, p.413-421, December 1952.

36) STEPHENSON G.
Mathematical Methods for Science Students
Longmans, 1961.

37) TAYAL S.P., SINHASAN R., SINGH D.V.
a) "Analysis of Hydrodynamic Journal Bearings Having Non-Newtonian Lubricants by a Finite Element Method"
J. Mech. Eng. Sci., Vol. 23, No. 2, p. 63-68, 1981.
b) "Analysis of Hydrodynamic Journal Bearings Having Non-Newtonian Lubricants"
Tribology Int., Vol. 15, No. 2, p. 17-21, 1982.

38) TIMOSHENKO S.P. and GOODIER J.N.
Theory of Elasticity
McGraw-Hill, 1951.

39) TIMPLE A.
"Achsensymmetrische Deformation von Umdrehungskörpen"
Z. angew. Math. Mech., Vol. 4, No. 5, p. 361-376, 1924.

40) TIPEI N.
Theory of Lubrication
Oxford University Press, 1962.

41) WADA S. and HAYASHI H.
"Hydrodynamic Lubrication of Journal Bearings by
Pseudoplastic Lubricants (Part 2, Experimental Studies)
Bull. JSME, Vol. 14, No. 69, p.279-286, 1971.

42) van WAZER J.R., LYONS J.W., KIM K.Y., COLWELL R.E.
Viscosity and Flow Measurement
A Laboratory Hadbook of Reology
Interscience, 1963.

43) WEBER C.
a) "Achsensymmetrische Deformation von Umdrehungskörpen"
Z. angew. Math. Mech., Vol. 5, No. 6,p. 466-468, 1925.
b) "Kugel mit normalgerichteten Einzelkräften"
Z. angew. Math. Mech., Vol. 32, No. 6, p.186-195, 1952.

44) WHITTAKER E.T. and WATSON G.N.
Modern Analysis
Cambridge University Press, 1950.